Aus dem Rudolf-Zenker-Institut für Experimentelle Chirurgie
Direktorin: Univ.-Prof. Dr. med. Brigitte Vollmar

Die Rolle von FGF21 in der hepatisch-zerebralen Kommunikation

Kumulative Dissertation
zur
Erlangung des akademischen Grades
Doktorin der Medizinwissenschaften (Dr. rer. hum.)
der Universitätsmedizin Rostock

vorgelegt von
Nicole Christine Power Guerra, geboren am 13.02.1992 in Illertissen
aus Rostock

https://doi.org/10.18453/rosdok_id00004045

Gutachter:

Apl. Prof. Dr. rer. nat. Angela Kuhla, Rudolf-Zenker-Institut für Experimentelle Chirurgie, Universitätsmedizin Rostock

Apl. Prof. Dr. med. Martin Witt, Institut für Anatomie, Universitätsmedizin Rostock

Prof. Dr. med. Hans Jörgen Grabe, Klinik und Poliklinik für Psychiatrie und Psychotherapie, Universitätsmedizin Greifswald

Jahr der Einreichung: 2022

Jahr der Verteidigung: 2022

Tanzt, tanzt, sonst sind wir verloren
-Pina Bausch-

INHALTSVERZEICHNIS

I. Der kumulativen Arbeit zugrundeliegende Studien

Studie I: **Power Guerra, N.**; Müller, L.; Pilz, K.; Glatzel, A.; Jenderny, D.; Janowitz, D.; Vollmar, B.; Kuhla, A. Dietary-induced low-grade inflammation in the liver. *Biomedicines* **2020**, 8(12). https://doi.org/10.3390/biomedicines8120587.

Studie II (in Vorbereitung): **Power Guerra, N.**; Müller, L.; Schild, A.; Lindner, T.; Stenzel, J.; Behrangi, N.; Pilz, K.; Bühler, D.; Bergner, C.; Alberts, T.; Kurth, J.; Janowitz, D.; Vollmar, B.; Kuhla, A. Tentative title: Longitudinal characterisation of HFD-induced neuroinflammation by multimodal imaging.

Studie III: Müller, L.; **Power Guerra, N.**; Stenzel, J.; Rühlmann, C.; Lindner, T.; Krause, B. J.; Vollmar, B.; Teipel, S.; Kuhla, A. Long-term caloric restriction attenuates β-amyloid neuropathology and is accompanied by autophagy in APPswe/PS1delta9 mice. *Nutrients* **2021**, 13(3). https://doi.org/10.3390/nu13030985.

Studie IV (in Vorbereitung): Leyens, K.; **Power Guerra, N.**; Glatzel, A.; Müller, L.; Kuhla, A. Tentative title: Dietary change and treadmill exercise against obesity in mice rescue liver inflammation and FGF21 resistance.

Studie V: **Power Guerra, N.**; Parveen, A.; Bühler, D.; Brauer, D.L.; Müller, L.; Pilz, K.; Witt, M.; Glass, Ä.; Bajorat, R.; Janowitz, D.; Wolkenhauer, O.; Vollmar, B.; Kuhla, A. Fibroblast growth factor 21 as a potential biomarker for improved locomotion and olfaction detection ability after weight reduction in obese mice. *Nutrients* **2021**, 13(9), 2916. https://doi.org/10.3390/nu13092916.

Alle Studien sind im Anhang ab Seite 47 zu finden.

II. Zusammenfassung

25 % der Menschen weltweit leiden unter Übergewicht oder Adipositas, was pandemische Ausmaße angenommen hat. Neben einer erhöhten Prävalenz für das metabolische Syndrom und der nichtalkoholischen Fettlebererkrankung (NAFLD), welche als hepatische Manifestation der Adipositas angesehen wird, werden zentralnervöse Erkrankungen beschrieben. So zeigen Studien, dass adipöse Patienten ein bis zu 70 % erhöhtes Risiko haben, eine Demenz zu entwickeln. Auf der Suche nach Biomarkern in der hepatisch-neuronalen Kommunikation bei Adipositas ist der Fibroblast Growth Factor 21 (FGF21) ein prominenter Kandidat, der den Stoffwechsel sowohl bei gesunden, als auch bei adipösen Individuen moduliert. Das Ziel der zugrundeliegenden Mausstudien war, die Rolle von FGF21 in der hepatisch-neuronalen Achse in verschiedenen energetischen Zuständen — bei Adipositas *per se* oder bei therapiertem Übergewicht — zu charakterisieren.

Zuerst wurde der Zusammenhang zwischen einer Adipositas, einer NAFLD, der daraus resultierenden Low-Grade Inflammation und FGF21 untersucht. Zu diesem Zwecke wurden weibliche C57BL/6J Mäuse mit einer Hoch-Fett-Diät sechs Monate gefüttert. Dabei konnte gezeigt werden, dass sich zum einen der Grad der hepatischen Steatose und Entzündungsmarkern wie Tumor-Nekrose-Faktor alpha erhöhte (Studie I) und zum anderen, dass eine hepatische FGF21-Resistenz, die sich durch eine Zunahme der FGF21 mRNA Konzentration und der Reduktion des FGF21 Ko-Rezeptors (β-Klotho) ausdrückt (Studie IV), induziert wurde.

Weiterhin wurden neuroinflammatorische Prozesse bedingt durch eine Amyloidose analysiert, um ggf. Parallelitäten zwischen dem metabolischen Syndrom und der Demenz aufzuzeigen. Zunächst wurde eine Adipositas-induzierte Neuroinflammation longitudinal untersucht (Studie II), wobei gezeigt werden konnte, dass das [^{18}F]-Translokatorprotein Signal — ein Radiopharmakon für aktivierte Mikroglia — signifikant nach 6 monatiger Hoch-Fett-Diät erhöht war, was mit einer signifikanten Zunahme der zerebralen Interleukin-1β Expression einherging. Zum Studium der Amyloidose-bedingten Neuroinflammation (Studie III) wurden weibliche 68 Wochen alte transgene APP/PS1 Mäuse verwendet, die durch die Aggregation von Amyloid-β eine Erhöhung der aktivierten Mikroglia aufwiesen. Mittels [^{18}F]–Fluordesoxyglukose -PET-CT konnte eine erniedrigte Glukoseaufnahme gezeigt werden, die mit verschlechterter Kognition einherging. In der Summe ist es gelungen, sowohl durch eine Adipositas (Studie II), als auch durch eine Amyloidose (Studie III) eine Neuroinflammation zu induzieren und longitudinal zu evaluieren.

Weiterhin konnten die Kognitionsdefizite in der Amyloidose-bedingten Neuroinflammation durch eine Kalorienrestriktion (68 Wochen lang) therapiert werden. Die Kalorienrestriktion ging mit einem Amyloid-β-Abbau einher und war mit einer erhöhten Autophagie assoziiert. In Kombination führte dies zu einer verbesserten neuronalen Aktivität, Integrität und letztendlich

zu einer besseren kognitiven Leistung (Studie III). Bei der Adipositas-induzierten Neuroinflammation wurden translationale Therapiemaßnahmen verwendet, um den *circulus vitiosus* der Adipositas und (Low-Grade) Inflammation zu durchbrechen und um neue Erkenntnisse zur Rolle von FGF21 — bei Adipositas und nach erfolgter Therapie — zu gewinnen. Nach der Induktion der Adipositas wurden für weitere sechs Monate eine Ernährungsumstellung, Laufbandtraining und Intervallfasten durchgeführt (Studie IV und V). Die Gewichtsreduktion, ausgelöst durch einen Diätwechsel und Laufbandaktivität, ging mit einer verbesserten Riechleistung und Lokomotion sowie erniedrigte FGF21 Konzentrationen einher. Anhand von Verhaltensparametern konnte durch Machine Learning-basierende Ansätze FGF21 als ein potentieller Biomarker nach therapierter Adipositas klassifiziert werden (Studie V). In der Leber bewirkte ein Diätwechsel *per se* eine Reduktion der Low-Grade Inflammation durch die Abnahme der hepatischen Steatose, der NAFLD und Tumor-Nekrose-Faktor alpha mit einer gleichzeitigen Reduktion der hepatischen FGF21 Resistenz (Studie IV). Mit der vorgelegten Arbeit ist es gelungen, sowohl neurodegenerative - (Studie III), als auch Adipositas-induzierte (neuro-)inflammatorische Prozesse (Studie V und IV) durch verschiedene „Lifestyle“ Faktoren zu modulieren. Im Fokus stand dabei FGF21 — ein potentieller Biomarker für Adipositas, dessen regulatorisches Potential bei Stoffwechselprozessen peripher (Studie I) aber auch zentral (Studie II) durch inflammatorische Stimuli gestört aber auch moduliert wird.

III. Einleitung

Die weltweite Prävalenz von Adipositas hat sich zwischen 1975 und 2016 fast verdreifacht, wobei mehr als 1,9 Milliarden Erwachsene ab 18 Jahren übergewichtig sind und 13 % davon adipös. Global gesehen ist dabei Übergewicht und Adipositas mit einer höheren Mortalität assoziiert als Untergewicht. Adipositas ist laut WHO definiert als „abnorme Fettansammlung mit einem Body-Mass-Index ≥ 30, die sich negativ auf die Gesundheit auswirken kann“.[1] Bereits 1989 beschrieb Kaplan das "Tödliche Quartett" aus abdominaler Adipositas, Hypertonie, Hyperglykämie und Hypertriglyceridämie,[2] welches heutzutage als metabolisches Syndrom bezeichnet wird, das weitere kardiovaskuläre Risikofaktoren zusammenfasst.[3,4]

Das metabolische Syndrom ist mit der nichtalkoholischen Fettlebererkrankung (NAFLD) assoziiert, welche als die hepatische Manifestation dieser Erkrankung angesehen wird.[5–7] Ein vermuteter Grund für die Prävalenz der NAFLD und vieler anderer Begleit- und Folgeerkrankungen der Adipositas ist die Persistenz der systemischen Low-Grade Inflammation. Im Allgemeinen handelt es sich bei der ernährungsbedingten Low-Grade Inflammation um eine sterile Entzündung, die auch als Metaflammation (metabolisch ausgelöste Inflammation) bezeichnet wird,[7] die stark mit dem Immunstoffwechsel verwoben ist.[8] Während die infektiöse Inflammation in ihrer physiologischen Funktion eine Immunantwort des Organismus auslöst, hat die sterile Entzündung überwiegend pathologische Folgen, z. B. über die Veränderung homöostatischer Checkpoints und die damit einhergehende Entwicklung autoinflammatorischer Störungen.[9] Interessanterweise wird eine enge Korrelation zwischen Stoffwechselerkrankungen und abnormalen Immunreaktionen wie der Low-Grade Inflammation beobachtet.[7,10] In diesem Kontext ist das weiße Fettgewebe in der Lage, sowohl metabolische als auch immunologische Mediatoren zu exprimieren,[11] welche lokal wirken, aber systemische Auswirkungen haben können und andere Organe wie die Leber betreffen. Dies zeigt sich in einer Hochregulierung von proinflammatorischen Zytokinen wie Interleukin (IL)-1β, IL-6 und Tumor-Nekrose-Faktor alpha (TNFα).[8,12,13] Alle genannten Mediatoren sind an gut orchestrierten und streng regulierten Signalkaskaden beteiligt. Entgleisung dieser Mediatoren könnten für eine Low-Grade Inflammation-vermittelte Interaktion zwischen Adipositas und NAFLD verantwortlich sein.[14,15]

Des Weiteren wird davon ausgegangen, dass die hepatische Low-Grade Inflammation bei der Adipositas auch eine Inflammation im Zentralnervensystem induziert.[10,16] In diesem Zusammenhang kommt dem Hypothalamus eine besondere Bedeutung zu, da diese Struktur den Nucleus arcuatus beherbergt, in dem zwei unterschiedliche Neuronenpopulationen (NPY/AgRP-Neuronen und POMC/CART-Neuronen) an der Regulation des Körpergewichts und der Energiebalance beteiligt sind.[17] Das Monitoring des Energiestatus gelingt aufgrund der räumlichen Position des Hypothalamus, welche eine Nähe zum dritten Ventrikel, den zirkumventrikulären Organen und der mediobasalen Eminenz hat und somit periphere Signale

wie Insulin, Leptin oder Ghrelin verarbeiten kann.[18,19] Die Gabe einer Hoch-Fett-Diät (HFD) aktiviert, zum einen, Gliazellen (Mikroglia und Astrozyten) und induziert damit eine Gliose, die das endokrine Gleichgewicht im Hypothalamus stört.[10,20] Zum anderen bewirkt die HFD eine Aktivierung der JNK- und NF-κB-Signalwege mit anschließender Freisetzung von proinflammatorischen Zytokinen (TNFα, IL-6) im mediobasalen Hypothalamus.[21–24] Als Konsequenz der gestörten Signaltransduktion könnte ein Verlust von anorexigenen POMC-Neuronen im Hypothalamus entstehen, die zu einer erniedrigten Sättigung, einem erhöhtem Appetit und erhöhtem Nahrungsmittelkonsum führt und somit den Zustand der Adipositas verschärft.[25] Es wird davon ausgegangen, dass neuroinflammatorische und neuromodulatorische Prozesse ein gestörtes Essverhalten und eine gestörte Kognition hervorrufen oder *vice versa*. So zeigte eine retrospektive Zwillingstudie von Xu et al.,[26] dass die Patienten ein um bis zu 70 % erhöhtes Risiko für die Entwicklung einer Demenz hatten. Es wird weiter angenommen, dass ein hoher Body-Mass-Index mit einer Verringerung des Hirnvolumens korreliert und daher mit der Entstehung der Adipositas-assoziierten Neurodegeneration in Verbindung gebracht wird.[27] Auf der Basis dieses Wissens lag ein Schwerpunkt dieser Arbeit in longitudinalen Studien zu untersuchen, inwieweit eine fettreiche Diät die Kognition beeinflusst. Wir kombinierten diese Analysen mit bildgebenden Verfahren, welche uns die Möglichkeit mit Radiopharmaka, wie [^{18}F]-Translokatorprotein (Marker für aktivierte Mikroglia)[28] und [^{18}F]–Fluordesoxyglukose (Marker für Glukoseaufnahme)[29] geben, Störungen der Kognition mit neuroinflammatorischen Prozessen direkt zu korrelieren. Weiterhin wurden neuroinflammatorische Prozesse bedingt durch Amyloidose analysiert, um ggf. Parallelitäten zwischen dem metabolischen Syndrom und der Demenz aufzuzeigen. Um die Kausalität Adipositas-bedingter inflammatorischer Prozesse in der Peripherie sowie im Zentralnervensystem besser zu verstehen, ist die Betrachtung einzelner Organe aber auch das Zusammenspiel von Organsystem, reguliert über (neuro-)modulatorische Hormone, notwendig.

Ein vielversprechendes Hormon, das bei der hepatisch-neuronalen Kommunikation in der Adipositas-induzierten Low-Grade Inflammation eine Schlüsselrolle einnehmen könnte, ist der Fibroblast Growth Factor 21 (FGF21). Allgemein wird das endokrine Hormon mit der Fettsäureoxidation, der Lipolyse und einer erhöhten Energiedissipation in Verbindung gebracht.[30,31] Zudem konnte die Expression des Rezeptorkomplexes von FGF21 (Fibroblast Growth Factor Receptor 1c und β-Klotho) -neben Fettgewebe und Leber- auch im Gehirn und dort vorwiegend im Kortex [32] und Hypothalamus nachgewiesen werden.[30,33] Bemerkenswerterweise ist FGF21 einerseits bei Fastenzuständen und bei Kalorienrestriktion durch die Leber verstärkt exprimiert,[34,35] aber andererseits treten bei adipösen Menschen und Mäusen außerordentlich hohe zirkulierende FGF21-Plasmakonzentrationen auf.[36,37] Dies wird als FGF21 Paradoxon bezeichnet und wurde von Fisher et al.[37] ähnlich einer

hypothalamischen Leptin-Resistenz[25] als eine FGF21-Resistenz beschrieben, wobei bei einer Adipositas erhöhte FGF21 Konzentrationen mit einer gleichzeitigen Reduktion des FGF21 Rezeptorkomplexes assoziiert waren.[37] Eine direkte Kausalität zwischen FGF21 und Inflammation konnten Diaz-Delfin und Mitarbeiter in Maus-Adipozyten zeigen, die durch die Applikation von TNFα die β-Klotho Expression inhibierten.[38] Weiterhin konnte in einer Langzeitstudie im Fettgewebe von adipösen Mäusen nachgewiesen werden, dass die Expression von Fibroblast Growth Factor Receptor 1c und β-Klotho deutlich erniedrigt war und mit einer begrenzten Wirkung von exogen-applizierten FGF21 einherging, sodass eine Erniedrigung der FGF21 Sensitivität geschlussfolgert wurde.[39] Auf der Grundlage dieses Wissens wurde in der vorliegenden Arbeit untersucht, inwieweit ein solches Szenario auch in der hepatischen-neuronalen Achse zu finden ist. Im Detail wurde analysiert, ob inflammatorische Prozesse —ausgelöst durch Adipositas — eine FGF21 Resistenz, welche mit erhöhter FGF21 Konzentration bei gleichzeitiger reduzierter ß-Klotho Expression einhergeht, verursachen können. Eine damit verbundene geringere FGF21 Sensitivität, insbesondere im hypothalamischen Bereich, könnte analog zu der Leptin- oder Insulinresistenz eine Dysregulation der endokrinen Balance induzieren und das Ungleichgewicht der Ernährungsregulation weiter verschärfen.[25]

FGF21 ist zudem ein Regulator des Glukosetransporters 1,[40] welcher auch von den Endothelzellen der Blut-Hirn-Schranke exprimiert wird. Bei Adipositas wurde eine Reduktion der Glukosetransporter 1-Expression in den Endothelzellen beobachtet, die zu einer verminderten Glukoseaufnahme und folglich zu einer geringeren Konzentration von Glukose im Gehirn führte. Die Abnahme der Glukose im zentralnervösen Gewebe trägt zu einer Neuroinflammation und zu kognitiven Defiziten bei,[41] welche letztendlich zu Verhaltensänderungen führen.[42] Demnach begünstigte die Gabe einer HFD und die damit verbundene Neuroinflammation bei adoleszenten Mäusen olfaktorische Dysfunktionen und ängstliches Verhalten, welches wiederrum zu einer reduzierten Aktivität *per se* führen kann.[43,44] In diesem Zusammenhang ist beschrieben, dass die Adipositas im heranwachsenden Alter körperliche Inaktivität verschärft und *vice versa*, was folglich wiederrum das Risiko für allgemeine und abdominale Adipositas im Jugendalter erhöht.[45] Mögliche Therapiemaßnahmen, um den *circulus vitiosus* der Adipositas zu durchbrechen, sind Interventionsansätze wie Laufbandtraining, eine Ernährungsumstellung, Intervallfasten oder Kalorienrestriktion, um das Körpergewicht zu senken.[46] Dabei führte eine Reduktion des Körpergewichtes bei adipösen Mäusen zu einer Normalisierung der FGF21 Konzentration mit einer gleichzeitigen Erhöhung der FGF21-Sensitivität.[39,47] Ob nun Adipositas-bedingte neuromodulatorische Prozesse FGF21 vermittelt sind und ob FGF21 als möglicher Biomarker für den Erfolg einer Therapie klassifiziert werden kann, war ein weiterer Schwerpunkt dieser Arbeit. Außerdem wurde untersucht, ob neben der physikalischen Aktivität als Intervention für

kognitive Defizite, auch eine Kalorienrestriktion neuroprotektive Effekte hat. Kalorienrestriktion kann eine gliale Autophagie auslösen[48–50], indem Autophagy-Gene-Related Proteins LC3BII zusammen mit dem Sequestosom-1 exprimiert werden und ein Autophagosom bilden.[51] Ausgelöst durch eine Kalorienrestriktion könnte die Induktion der Autophagie die Amyloidose und damit eine Neuroinflammation senken und die Kognition verbessern.

In der Gesamtschau war das Ziel der Arbeit, zuerst die Adipositas-induzierte hepatische und zentralnervöse Inflammation zu charakterisieren und dabei die Regulationswege von FGF21 zu evaluieren. Um die Mechanismen von FGF21 besser zu verstehen, wurden Interventionen genutzt, um den *circulus vitiosus* aus „Adipositas + Low-Grade Inflammation + Verhaltensstörungen“ zu durchbrechen und um neue Erkenntnisse zur Rolle von FGF21 — bei Adipositas und nach erfolgter Therapie — zu gewinnen. Infolgedessen wurden fünf Hypothesen formuliert und evaluiert:

(i) Eine fettreiche Diät induziert eine nichtalkoholische Fettlebererkrankung und damit einhergehend eine hepatische Low-Grade Inflammation (Studie I) sowie eine Neuroinflammation (Studie II).

(ii) Eine Neuroinflammation und die damit verbundenen Kognitionsdefizite können durch eine Kalorienrestriktion reduziert werden (Studie III).

(iii) Um den *circulus vitiosus* aus Adipositas, nichtalkoholischer Fettlebererkrankung und Low-Grade Inflammation zu durchbrechen, stehen verschiedene Interventionen, wie Diätwechsel, Laufbandtraining und Intervallfasten zur Verfügung (Studie IV, Teil I).

(iv) Eine fettreiche Diät induziert eine hepatische FGF21 Resistenz, welche durch einen Diätwechsel und Laufbandtraining therapiert werden kann (Studie IV, Teil II).

(v) Adipositas-induzierte Verhaltensänderungen können durch Diätwechsel und Laufbandtraining nivelliert werden, wobei FGF21 als Biomarker für den Therapieerfolg klassifiziert werden kann (Studie V).

IV. Methoden

Alle verwendeten Methoden und Analysen der Studien I, III und V sind detailliert in den entsprechenden Publikationen im Anhang ab Seite 47 gelistet. Im Folgenden ist nur das experimentelle Design der Studien I - V beschrieben, welches für das Verständnis der Arbeit notwendig ist, sowie die detaillierten Methoden der Studien II und IV.

4.1. Tiermodelle und experimentelles Design

Für die Studien I, II und IV wurden weibliche C57BL/6J Mäuse (Charles River Laboratories, Sulzfeld, Deutschland) im Alter von 4 Wochen verwendet (siehe Power Guerra et al.[52]). Die Mäuse wurden zufällig in drei Gruppen eingeteilt, die über einen Zeitraum von 6 Monaten mit unterschiedlichen Diäten gefüttert. Die erste Gruppe erhielt eine Hoch-Fett-Diät (HFD; D12492; Research Diets, Lane, USA[53]) und wurde als HFD Gruppe bezeichnet (*n* = 31). Die zweite Gruppe erhielt die empfohlene Kontrolldiät (D12450J; Research Diets, Lane, USA;[53]) und wurde als KD Gruppe bezeichnet (*n* = 16). Die dritte Gruppe erhielt eine Standarddiät (ssniff® R/M-H, ssniff Spezialdiäten GmbH, Soest, Deutschland) und wurde als SD Gruppe bezeichnet (*n* = 15).

Für Studie III wurden weibliche APP/PS1 (tg)-Mäuse verwendet, die das humane Amyloid-β-Vorläuferprotein (APP) K594N und M595L-Mutation sowie das humane Presenilin (PS) 1, eine L166P-Mutation unter der Kontrolle des Mausprionprotein-Promotors ko-exprimieren (siehe Müller et al.[54]).[55,56] und eine Neuroinflammation und kognitive Defizite ausbilden.[57] Wurfgeschwister (B6xC3H) sowie C57BL6-Mäuse dienten als Kontrollmäuse (Wildtyp; wt). Die Mäuse wurden im Alter von 4 Wochen entweder *ad libitum* (AL) oder kalorienrestriktiv (KR, 60 % von *ad libitum*) für 16 Wochen (16 Wochen oder kurzfristig, *n* = 5-10 für jede Gruppe) oder 68 Wochen (68 Wochen oder langfristig, *n* = 5-10 für jede Gruppe) gefüttert.

Für die Studien IV und V wurden weitere 90 weibliche C57BL/6J Mäuse im Alter von 4 Wochen mit einer HFD für sechs Monate gefüttert (siehe Power Guerra et al.[58]). Nach der Manifestation der Adipositas wurden die Mäuse für weitere sechs Monate verschiedenen Interventionen mit je *n* = 15 Mäusen pro Gruppe unterzogen. Die erste Gruppe blieb auf einer HFD und wurde als HFD/HFD Gruppe bezeichnet. Die zweite Gruppe erhielt neben einer weiterführenden Fett-Diät Laufbandtraining (LB) und wurde als HFD/HFD+LB Gruppe bezeichnet. Für die bessere Translation wurde bei der dritten Gruppe statt einer KR ein Intervallfasten (time-restricted-feeding; TRF) eingeführt und als HFD/HFD+LB+TRF Gruppe bezeichnet. Die vierte Gruppe wechselte auf eine Niedrig-Fett Diät (NFD, D12450J) und wurde als HFD/NFD Gruppe gekennzeichnet. Die fünfte Gruppe erhielt die Interventionen Diätwechsel und LB und wurde als HFD/NFD+LB bezeichnet. Die letzte Gruppe erhielt alle drei Interventionen und wurde als HFD/NFD+LB+TRF bezeichnet. Nachdem die Ernährung auf eine NFD umgestellt wurde, wurde das LB für *n* = 60 Mäuse etabliert. Das Protokoll wurde nach Marinho et al.[59] mit

folgender Änderung durchgeführt: Das LB Training wurde zweimal die Woche in 5-Gruppen durchgeführt. Mäuse in der TRF Gruppe wurden zwischen 7 Uhr morgens bis 23 Uhr abends (16 h) gefastet. Die Futteraufnahme fand in der nachtaktiven Phase statt. Alle Mäuse hatten *ad libitum* Zugang zu Wasser.

4.2. Verhaltensexperimente

Da die Zelldynamik im Bulbus olfactorius bei Adipositas verändert ist, könnte auch das Riechvermögen beeinflusst sein.[60] Daher wurde ein Buried Pellet Test und Surface Pellet Test nach Dragotto et al.[61] und Lehmkuhl et al.[62] durchgeführt, bei dem die Latenzzeit gemessen wird, die ein Tier braucht, um eine verborgene Nahrungsquelle zu finden. Nach einer Erholungszeit von mindestens 24 h vom Surface Pellet Test wurde der Elevated Plus Maze-Test nach Komada et al [63] durchgeführt. Das EPM ist ein weit verbreitetes Labyrinth mit offenen und geschlossenen Armen, das Informationen über angstbedingtes Verhalten bei Nagern liefert, da Mäuse eine natürliche Aversion gegen offene Bereiche haben.[64,65] Ergänzend wurde der Open Field-Test nach Seibenhener et al. [66] etabliert, mit dessen Hilfe die lokomotorische und explorative Aktivität untersucht wird. Für die Messung des räumlichen Referenzgedächtnisses wurde der Morris-Water-Maze Test nach Müller et al.[54] durchgeführt.

4.3. Multimodale Bildgebungsanalysen

Alle Kleintier PET-CT Scans von [^{18}F]–Fluordesoxyglukose ([^{18}F]-FDG), Magnetresonanztomographie Analysen sowie spektroskopischen Analysen wurden nach Müller et al.[54] durchgeführt. Um eine Neuroinflammation zu untersuchen, wurde das Radiopharmakon GE-180 verwendet, welches ein Analogon zum [^{18}F]-Translokator Protein (TSPO) ist. Ähnlich zu den Analysen mit dem [^{18}F]-FDG Radiopharmakon (Müller et al.[54]), wurden die GE-180 Messungen mit folgenden Abweichungen ausgeführt: Die Mäuse erhielten 15.8 ± 1.45 MBq GE180 i.v. mit einer Aufnahmezeit von 30 min. Im Kleintier-PET/CT-Scanner (Inveon PET/CT Siemens, Knoxville, TN, USA) wurden dynamische Scans in Kopflage für 60 min aufgenommen. Die letzten 15 min wurden für eine statistische Auswertung gemittelt. Um adipöse und normalgewichtige Mäuse miteinander zu vergleichen, wurde der Standard Uptake Value (SUV) auf das metabolische Gewicht (SUV_c) nach Kleiber et al.[67] korrigiert.[68] Bei [^{18}F]-FDG wurde der SUV_c mit der Blutglukosekonzentration korrigiert ($SUV_{c,\,glc}$).[69] Daraus ergaben sich folgende Formeln:

$$\mathrm{SUV_c} = \%\frac{\mathrm{ID}}{\mathrm{g}} \cdot \text{ body weight } [\mathrm{g}]^{\frac{3}{4}} \qquad \mathrm{SUV_{c,\ glc}} = \%\frac{\mathrm{ID}}{\mathrm{g}} \cdot \text{ body weight } [\mathrm{g}]^{\frac{3}{4}} \cdot \text{blood glucose } [\frac{\mathrm{mmol}}{\mathrm{L}}]$$

4.4. Histologie, Immunhistochemie und Bildanalysen

Die histologischen Färbungen und die immunhistochemischen Reaktionen bei der Leber, sowie deren Auswertung, wurde nach Studie I durchgeführt. Die Methoden der Studie I sind in Power Guerra et al.[52] beschrieben.

4.5. Molekulare Analysen

4.5.1. Western Blot

Das hepatische Gewebe wurde im Lysepuffer homogenisiert (10 mM Tris pH 7.5, 10 mM NaCl, 0.1 mM EDTA, 0.5% Triton-X 100, 0.02% NaN3 und 0.2 mM PMSF, Protease Inhibitor Cocktail), für 30 min auf Eis inkubiert und anschließend für 10 min bei 4°C und 10 000 x g zentrifugiert. Die Proteinbestimmung erfolgte nach der Bicinchoninsäure Methode (Thermo Fisher Scientific, Rockford, USA) und mit 2.5 % BSA (Pierce Biotechnology, Rockford, IL, USA). Für die Analyse der β-Klotho Expression wurden 10 %ige Mini-PROTEAN® TGX Stain-Free™ Precast Gele (Bio-Rad Laboratories, Hercules, USA) verwendet und mit 10 µg beladen. Nach 60 min Elektrophorese wurde in den Mini-PROTEAN Gele das gesamte Protein mittels UV Licht in der ChemiDoc™ XRS+ Imager (Bio-Rad Laboratories, Hercules, CA, USA) aufgenommen. Anschließend wurde das Protein auf eine Polyvinyldifluoridmembran (Immobilon-P; Millipore, Burlington, MA, USA) transferiert und mit 2.5% BSA bei 4°C blockiert. Die Membran wurde mit rabbit-anti-β-Klotho (1:1000; LifeSpan BioSciences) über Nacht bei 4°C inkubiert und anschließend mit mouse-anti-rabbit-IgG-HRP-linked (1:10000; Sigma) versetzt. Die Proteinexpression wurde mittels Luminol-verstärkter Chemilumineszenz (ECL plus; Amersham Pharmacia Biotech, Amersham, UK) visualisiert und mit dem ChemiDoc™ XRS+ System digitalisiert. Die Signale wurden densitometrisch ausgewertet (Quantity One; Bio-Rad Laboratories, Hercules, CA, USA) und auf das Gesamtprotein normiert.

4.5.2. Real-time PCR

Die Fibroblast Growth Factor 21 (FGF21) mRNA Analyse wurde nach Power Guerra et al.[52] mit folgender Sequenz durchgeführt: Forward: 5'-GCTGTCTTCCTGCTGGG-3'; Reverse: 5'-CCTGGTTTGGGGAGTCCTTC-3'. Alle anderen Sequenzen sind bei Power Guerra et al.[52] zu finden.

4.5.3. Blutplasmanalysen

Der FGF21-ELISA wurde nach der Beschreibung des Herstellers durchgeführt (ab212160, abcam, Berlin, Deutschland; siehe Power Guerra et al.[58]).

4.6. Datenanalyse und Machine Learning Ansatz

Die Pipeline der Datenanalyse (Pearson's Correlation und Hauptkomponentenanalyse) sowie der Machine Learning Ansatz ist detailliert bei Power Guerra et al.[58] beschrieben.

V. Ergebnisse

5.1. Studie I

In der ersten Studie wurde der Einfluss der Hoch-Fett-Diät (HFD) auf die Adipositas-assoziierte Low-Grade Inflammation in der Leber untersucht. Dafür wurden für sechs Monate alte weibliche Mäuse entweder mit einer HFD oder mit zwei verschiedenen Kontrolldiäten (im weiteren als KD und SD bezeichnet) gefüttert. Eine Kontrolldiät war reich an Kohlenhydraten (KD), die andere zeigte eine ausgewogenere Nährstoffzusammensetzung (SD). Bei beiden Kontrollen (KD + SD) war das Gewicht der Mäuse nach sechs Monaten gegenüber der HFD (KD und SD ca. 23g, HFD ca. 40 g, Daten in der Publikation gezeigt) signifikant reduziert. Bei der Präparation der Leber wurde eine visuelle Abweichung sowohl der HFD- als auch der KD Gruppe zu einer gesund aussehenden Leber festgestellt, wie es sich in der SD Gruppe darstellte. Um den Status der Diät-induzierten Lebersteatose zu analysieren, wurde der Leberfettgehalt histologisch anhand von Hämatoxylin & Eosin (H&E) gefärbten Gewebeschnitten bestimmt (Abbildung 1, A). Als weiterer Parameter wurde histologisch der nichtalkoholische Fettlebererkrankung (NAFLD) Activity Score (NAS) in der Leber analysiert (Daten in der Publikation gezeigt). Als Hauptbefund zeigte die HFD eine makrovesikuläre Verfettung sowie einen signifikant höheren NAS mit 3.2 gegenüber den Kontrollen (KD mit 0.8 und SD mit 0.1). Als Nebenbefund zeigten die Mäuse, die mit einer KD gefüttert wurden, eine mikrovesikuläre Verfettung. Weiterhin wurden die inflammmatorischen Merkmale einer NAFLD evaluiert. Durch die Quantifizierung von Naphthol-AS-D-Chloracetat-Esterase $(CAE)^+$ Zellen (neutrophile Granulozyten) sowie $F4/80^+$ Zellen (Kupfferzellen) konnte festgestellt werden, dass eine HFD eine signifikant erhöhte Anzahl an inflammatorischen Zellen aufwies (A, B, C; $p \leq 0.01$). Zusätzlich zur zellulären wurde auch die humorale Immunantwort in der Leber mittels real-time PCR untersucht. Die HFD Gruppe zeigte die höchste Expression des proinflammatorischen Zytokins TNFα (D). Als Nebenbefund war in der KD Gruppe auch eine Erhöhung des inflammatorischen Potentials sowohl auf zellulärer Ebene (A, B, C; $p \leq 0.01$), als auch auf humoraler Ebene (D, $p = 0.005$) zu erkennen. Obwohl die KD ein erhöhtes Entzündungspotential zeigte, so war über den Versuchszeitraum kein signifikanter Anstieg der NAS zu beobachten. Somit blieb bei der KD Gruppe eine Low-Grade Inflammation-induzierte Leberschädigung aus. Zusammenfassend zeigen die Ergebnisse eine durch HFD und die damit verbundene Adipositas hepatische Low-Grade Inflammation, welche zu einer organischen Manifestation der Leberschädigung führte.

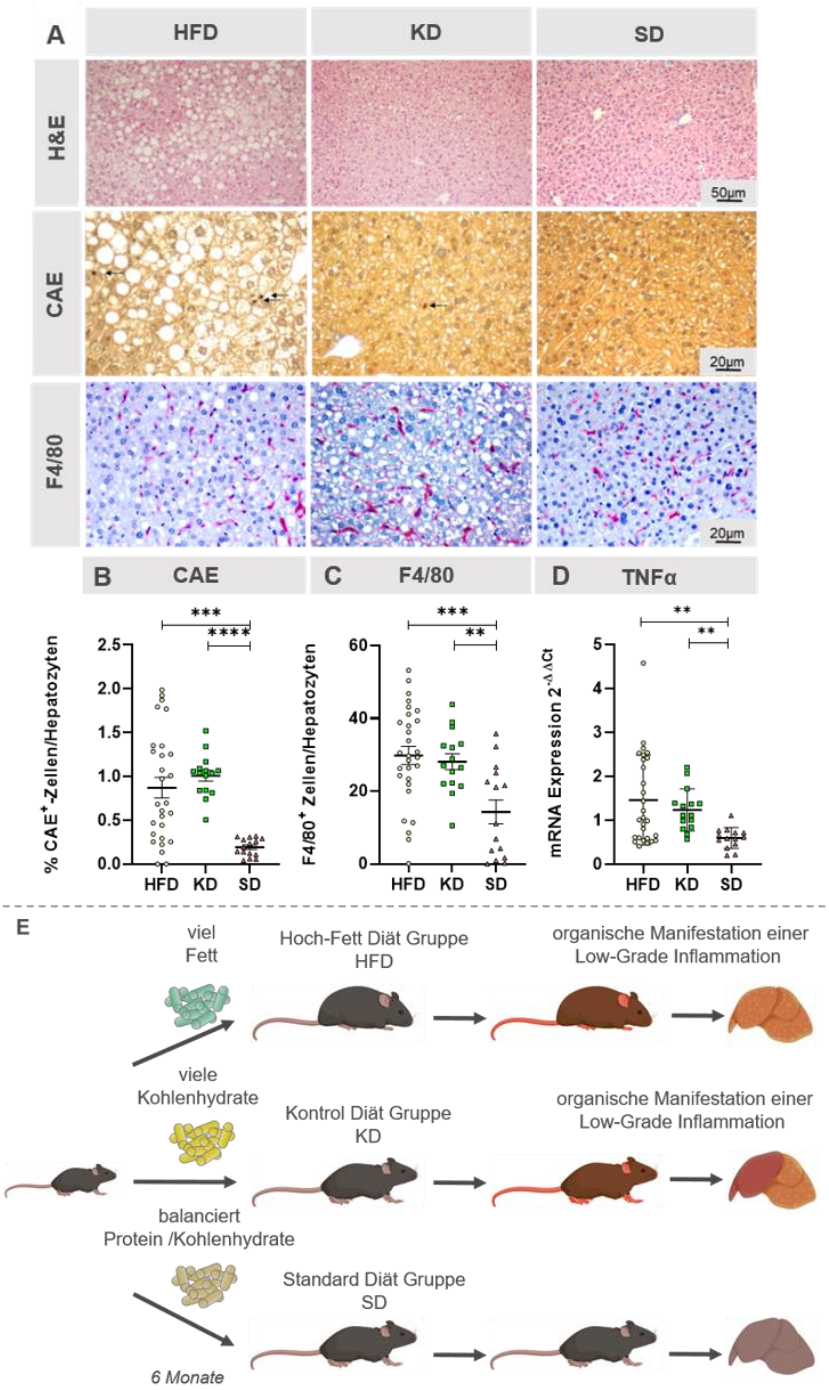

Abbildung 1: Diätisch induzierte Low-Grade Inflammation in der Leber. A: Repräsentative Aufnahmen der Leber im low-power-field entweder mit H&E Färbung (4x Objektiv, Maßstabbalken mit 50 µm), mit CAE-Färbung bzw. immunhistochemischer F4/80 Färbung (beide mit 20x Objektiv, Maßstabbalken mit 20 µm). Pfeile zeigen CAE^+ Zellen an. **B:** Relative Anzahl von Granulozyten (CAE^+) (HFD: *n* = 28; KD: *n* = 15, SD: *n* = 15). **C**: Relative Anzahl von Makrophagen ($F4/80^+$) (HFD: *n* = 28; KD: *n* = 15, SD: *n* = 15). **D:** Hepatische mRNA Expression von TNFα mittels real-time PCR (HFD: *n* = 28; KD: *n* = 15, SD: *n* = 14). Die Signifikanz der Unterschiede wurde entweder mittels Kruskal–Wallis gefolgt von Dunn's post hoc test für mehrfache Vergleiche getestet (**B**) oder mit einem Ordinary One-Way ANOVA gefolgt von Tukey's post hoc Test für mehrfache Vergleiche (**C, D**). Zahlen sind als Mittelwerte ± Standardabweichung (*sd)* dargestellt mit: **** $p < 0.0001$, *** $p < 0.001$ und ** $p < 0.01$. **E:** Graphical Abstract der Studie I.

5.2. Studie II

Nach der Evaluierung der hepatischen Inflammation wurde in Studie II eine Inflammation im Zentralnervensystem evaluiert. Dabei wurde untersucht, ob eine HFD eine Neuroinflammation induzieren und ob diese longitudinal mittels multimodaler Bildgebung dargestellt werden kann. Dafür wurden jeweils nach drei und sechs Monaten Magnetresonanztomographie (MRT), Massenspektroskopie (MR) und PET-CT – Analysen bei weiblichen C57BL/6J Mäusen durchgeführt. Nach der letzten Analyse wurde das räumliche Gedächtnis der Mäuse mittels Morris-Water-Maze (MWM) getestet (Abbildung 2, A). Die anschließenden zerebralen mRNA Analysen zeigten, dass - im Gegensatz zu der Leber - die IL-1β Expression ($p = 0.0224$, B) bei der HFD signifikant erhöht war, und nicht die TNFα Expression. Für die longitudinale Analyse der Neuroinflammation wurde das Radiopharmakon GE-180 verwendet. Dabei zeigte sich ein signifikant höherer Standard Uptake Value (normiert auf das metabolische Gewicht; SUV_c) im Cortex, Hippocampus und Hypothalamus bei der HFD im Vergleich zur Kontrolle nach sechs, jedoch nicht nach drei Monaten Fütterung ($p < 0.0001$; C). Als zweites Radiopharmakon wurde [^{18}F]-Fluordesoxyglukose (FDG) verwendet, welches direkt den Glukosemetabolismus darstellen kann. Dabei war der $SUV_{c,\ glc}$ (normiert auf die Blutzuckerkonzentration) ebenfalls erst nach 6-monatiger HFD signifikant erhöht ($p < 0.0001$; E). Die MR-spektroskopischen Untersuchungen des Metaboliten N-Acetyl-Aspartat ergaben keine Änderung zwischen den beiden Gruppen (E). Auch das Arbeitsgedächtnis, evaluiert durch den MWM, blieb durch eine HFD unverändert (repräsentative Bilder dargestellt, F). Obwohl weitere Verifizierungen wie immunhistochemische Analysen in Bearbeitung sind, deuten die GE-180 Analyse und auch die zerebrale IL-β Analyse auf eine Neuroinflammation hin. Die [^{18}F]-FDG Analysen suggerieren, dass eine hohe metabolische Aktivität im Gehirn nach sechs Monaten HFD vorherrscht, die vermutlich auf eine erhöhte Aktivierung der Mikroglia zurückzuführen ist.

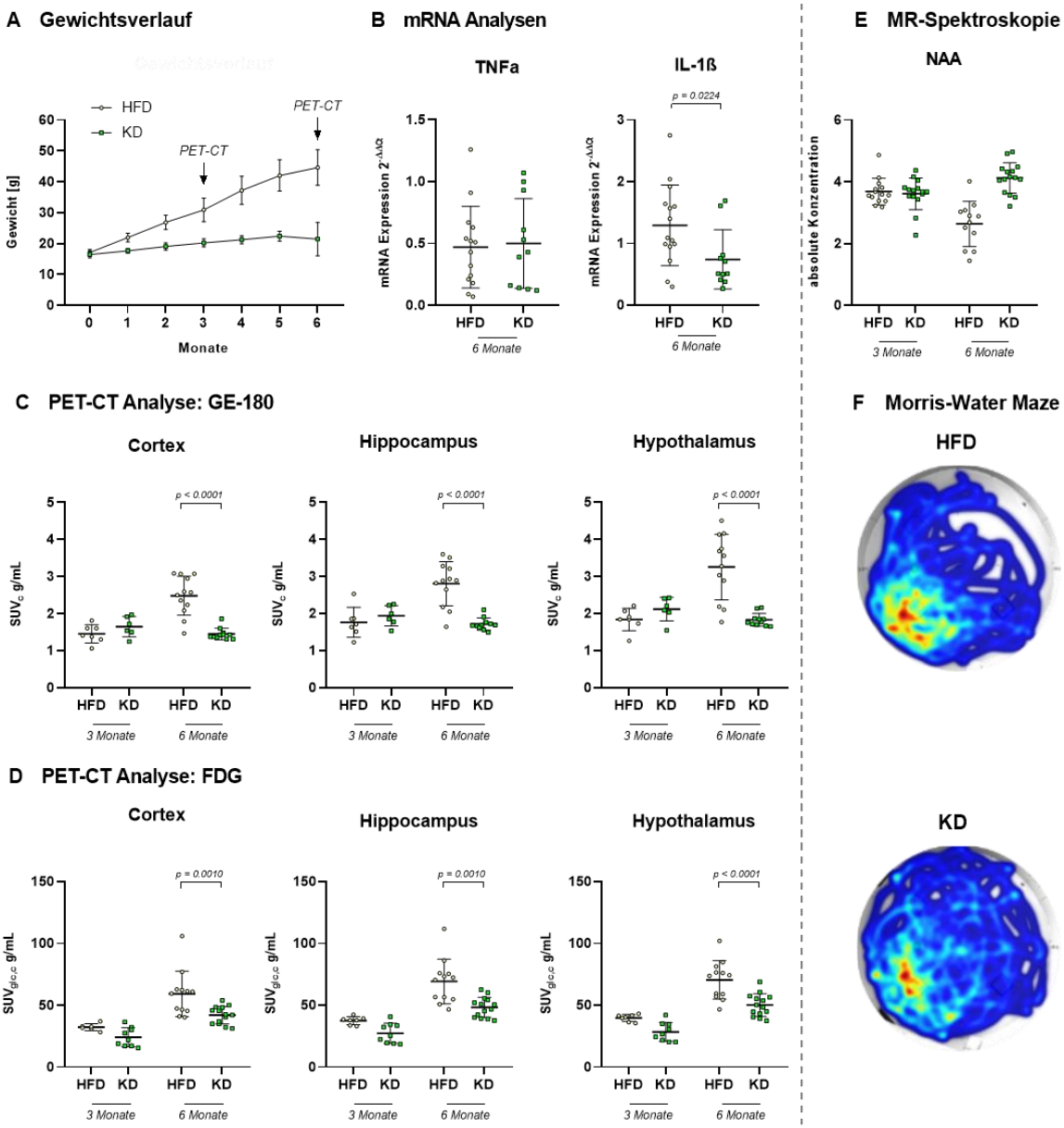

Abbildung 2: Longitudinale Charakterisierung einer HFD-induzierten Neuroinflammation. A: Monatlicher Gewichtsverlauf über den experimentellen Zeitraum mit *n* = 16 Mäusen pro Gruppe zum Beginn und *n* = 14 bei der HFD Gruppe und *n* = 15 bei der KD Gruppe zum Endzeitpunkt. Pfeile zeigen MRT, MR-Spektroskopie und PET-CT Messzeitpunkte an. **B**: Zerebrale mRNA Expression von TNFα und IL-1β. Daten sind als $2^{-\Delta\Delta Ct}$ Werte dargestellt und wurden mittels real-time PCR bestimmt; HFD: n = 14, KD: n = 11. **C:** Quantifizierung der GE-180 Aufnahme im Cortex, Hippocampus und Hypothalamus. SUV wurde auf das metabolische Gewicht normiert (SUV_c). Drei Monate: HFD: *n* = 7; KD: *n* = 6. Sechs Monate: HFD: *n* = 12; KD: *n* = 11. **D:** Quantifizierung der [^{18}F]-FDG Aufnahme im Cortex, Hippocampus und Hypothalamus. SUV wurde auf die Blutglukosekonzentration und auf das metabolische Gewicht genormt ($SUV_{c, glc}$). Drei Monate: HFD: *n* = 6-7; KD: *n* = 9. Sechs Monate: HFD: *n* = 12; KD: *n* = 14. **E:** MR-Spektroskopie von N-Acetyl-Aspartat (NAA) als absolute Konzentration dargestellt. Drei Monate: HFD: *n* = 14; KD: *n* = 15. Sechs Monate: HFD: *n* = 12; KD: *n* = 15. **F:** Repräsentative Heatmap Darstellung im MWM der Tierpräsenz von der HFD und KD Gruppe im MWM über 180 s, wobei die rote Farbe die höchste Aufenthaltsdauer anzeigt und die blaue Farbe die niedrigste Aufenthaltsdauer. Die Signifikanz der Unterschiede wurde mittels two-tailed unpaired t-Test (B) getestet oder mittels Mixed-Effects Analysis gefolgt von Sidak's post hoc Test für mehrfache Vergleiche (C-E). Zahlen sind als Mittelwerte ± *sd* dargestellt und die statistische Signifikanz wurde auf $p < 0.05$ gesetzt.

5.3. Studie III

Neben der Fett-induzierten Neuroinflammation[70] wird mit der APP/PS1 Maus eine Neuroinflammation durch die Akkumulation von Amyloid (A)β Plaques und kognitive Defizite dargestellt. Diese Pathologie beschreibt ein Modell für die Alzheimer'sche Erkrankung.[57]

Eine geeignete Intervention, um die Neuroinflammation zu reduzieren, ist die Kalorienrestriktion (KR),[71] die in der Lage ist, autophagische Prozesse zu induzieren, und aggregierte Proteine wie Aβ Plaques abzubauen.[48–50] Inwieweit eine KR eine Autophagie induziert und damit einhergehend eine Neuroinflammation reduziert und somit die Kognition verbessert, war Gegenstand der Untersuchungen in Studie III. Dafür wurden APP/PS1 (tg) Mäuse und ihre Wurfgeschwister (wt) für 16 oder 68 Wochen einer KR unterzogen oder *ad libitum* (AL) gefüttert. Während eine kurzfristige KR für 16 Wochen keine nennenswerten Veränderungen des Phänotyps der Alzheimer'schen Erkrankung in tg-Mäusen ergab, zeigte eine langfristige KR für 68 Wochen positive Effekte. So führte eine langfristige KR- vs. AL-Fütterung in tg-Mäusen zu einem signifikanten Anstieg der [^{18}F]-FDG-Aufnahme im Hippocampus (Abbildung 3, A, $p = 0.0035$), verbesserte die Arbeitsgedächtnisleistung (B, $p = 0.0161$) und erhöhte die Expression der Autophagie-assoziierten Proteine LC3BII und p62 signifikant (C, Daten von p62 in der Publikation gezeigt). Auch in der immunhistochemischen Analyse zeigte die KR- vs. AL-Fütterung in tg-Mäusen eine Reduktion positiver Iba1 Zellen (F, $p = 0.0329$), der Plaquefläche (D, $p < 0.0001$) und der Plaqueanzahl (E, $p < 0.0001$). Zusammenfassend spricht ein erhöhtes [^{18}F]-FDG Signal und die damit einhergehende gesteigerte Glukoseaufnahme eher für eine gesteigerte neuronale Aktivität, als für eine Neuroinflammation. Die KR kann die Akkumulation von Aβ-Plaques vermutlich über autophagische Prozesse abbauen, somit eine Neuroinflammation reduzieren und damit die Kognition verbessern.

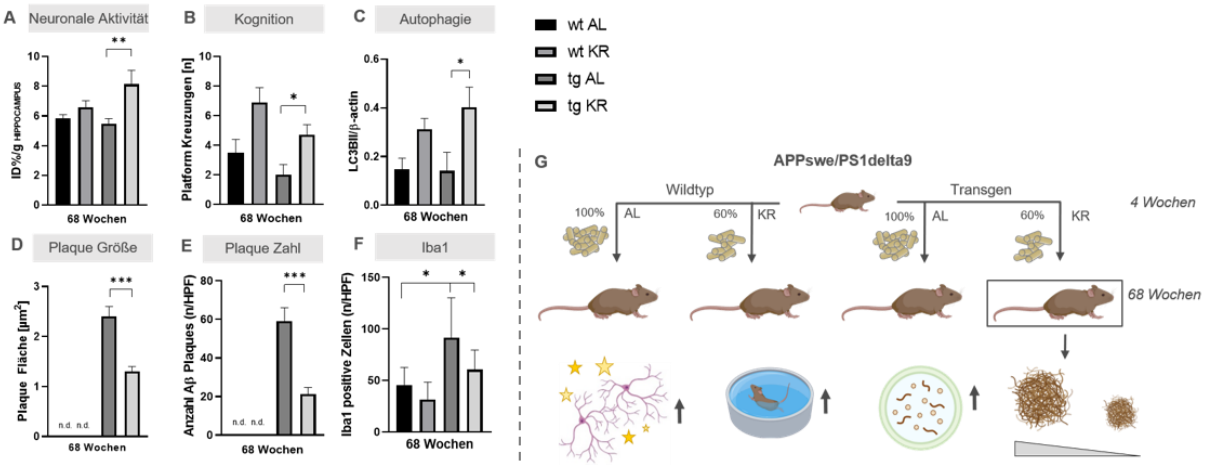

Abbildung 3: Langzeit Kalorienrestriktion ist von Autophagie begleitet und verringert damit die β-Amyloid Neuropathologie in APP/PS1 Mäusen. APP/PS1 Mäuse (wt und tg) wurden jeweils entweder AL oder KR (60 % von AL) gefüttert. **A:** Quantifizierung der [^{18}F]-FDG Aufnahme im Hippocampus. Werte sind als %ID/g dargestellt. **B:** Anzahl der Plattform Kreuzungen beim MWM. **C:** Densitometrische Analyse der zerebralen LC3BII

Proteinexpression (normiert auf β-Actin). **D, E:** Quantitative Analyse der hippocampalen Aβ Plaque Fläche (D) und der Plaque Anzahl (E). **F:** Quantitative Analyse der hippocampalen Iba1-positiven Zellen pro high power field (HPF). **G:** Graphical Abstract der Studie IV. Die Signifikanz der Unterschiede wurde mittels unpaired Students t-Test getestet gefolgt von einer Bonferroni Korrektur mit Threshold = 0.0166. Zahlen sind als Mittelwerte ± Standardfhler des Mittelwertes dargestellt mit *p < 0.05, **p < 0.005 oder ***$p \leq 0.001$ vs. AL.

5.4. Studie IV

Im ersten Part der Studie IV wurde untersucht, ob die Auswirkungen der hepatischen Low-Grade Inflammation aus Studie I durch Interventionen wie Diätwechsel (zu einer Niedrig-Fett-Diät (NFD)), Laufbandtraining (LB) oder Intervallfasten (TRF) moduliert werden können. Die kontinuierliche Gabe einer HFD führte zu einer starken Körpergewichtszunahme in den ersten sechs Monaten (Abbildung 4, A). Nach Einführung der Interventionen ergab nur die Ernährungsumstellung eine Gewichtsreduktion (gelb vs. blau, A). Die diätische Umstellung führte außerdem zu einer Reduktion der hepatischen Steatose (HFD vs. HFD/NFD, HFD/NFD+LB und HFD/NFD+LB+TRF mit $p < 0.005$, B), jedoch nicht zu einer Reduktion der Plasma Triglyceridkonzentration (C). Die Cholesterolkonzentration im Plasma war in den Gruppen HFD/NFD und HFD/NFD+LB reduziert ($p < 0.05$, D). Ein zusätzliches Laufbandtraining führte zu einer Erhöhung der hepatischen Steatose ($p < 0.05$ vs. HFD/HFD+LB+TRF), der Plasma Triglyceridkonzentration ($p < 0.05$ vs. HFD/NFD+LB+TRF) und der Cholesterolkonzentration ($p < 0.005$ vs. alle Gruppen bis auf HFD/HFD). Die Reduktion der Verfettung in Kombination „Diätwechsel+Laufbandtraining“ ist demnach der Ernährungsumstellung zuzuschreiben. Interessanterweise führte die Einführung von Intervallfasten zu einer signifikanten Reduktion der hepatischen Steatose ($p < 0.05$ HFD/HFD+LB+TRF vs. HFD/HFD+LB) und der Cholesterolkonzentration ($p < 0.05$ vs. HFD/HFD). Ein Diätwechsel (HFD/NFD+LB+TRF) führte jedoch nicht zu einer weiteren Reduktion der Cholesterolkonzentration. Betrachtet man nun die Inflammation in der Leber, gemessen durch die TNFα mRNA Expression, führte hauptsächlich der Diätwechsel zu einer signifikanten Reduktion der Inflammation ($p < 0.05$, gelb vs. blau, E). Als Zwischenergebnis zeigt die Studie IV, dass nach der Manifestation der Adipositas für sechs Monate die Kombination aus einer HFD, Laufbandtraining und Intervallfasten protektiv sein kann, aber auch dass vor allem ein Diätwechsel zu einer NFD *per se* vor einer NAFLD schützt und den *circulus vitiosus* aus Adipositas und Low-Grade Inflammation durchbrechen kann.

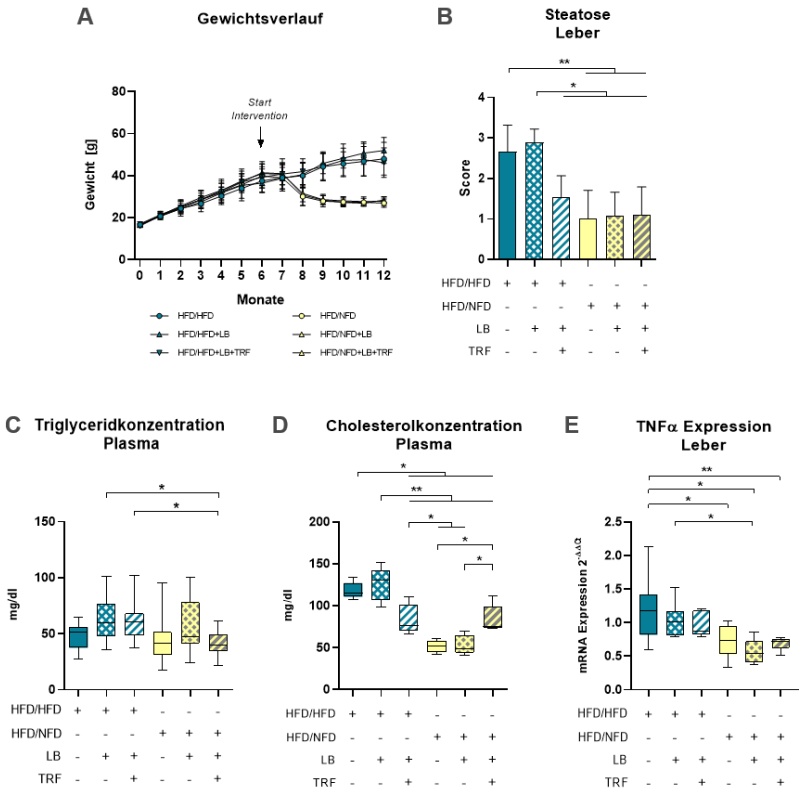

Abbildung 4: Die Interventionen Diätwechsel und Laufbandtraining führen bei Mäusen zu einer Reduktion des Gewichtes, der Verfettung und der hepatischen Inflammation **A**: Monatlicher Gewichtsverlauf über die experimentelle Zeit mit *n* = 90 zu anfangs und *n* = 84 Mäusen beim finalen Zeitpunkt. **B**: Auswertung des Steatose-Scores in der Leber über histologische H&E-Färbungen nach 12 Monaten (4x Objektiv, Bilder im Anhang). HFD/HFD: *n* = 12, HFD/HFD+LB: *n* = 9, HFD/HFD+LB+TRF: *n* = 11, HFD/NFD: *n* = 13, HFD/NFD+LB: *n* = 15, HFD/NFD+LB: *n* = 15, HFD/NFD+LB+TRF: *n* = 11; HFD/NFD+LB: *n* = 15, HFD/NFD+LB+TRF: *n* = 11; insgesamt *n* = 71. **C**, **D**: Plasma Triglycerid- und Cholesterolkonzentration nach 12 Monaten mit: HFD/HFD: *n* = 13, HFD/HFD+LB: *n* = 13, HFD/HFD+LB+TRF: *n* = 15, HFD/NFD: *n* = 14, HFD/NFD+LB: *n* = 15, HFD/NFD+LB+TRF: *n* = 14; insgesamt *n* = 84. **E**: Hepatische mRNA Expression von TNFα nach 12 Monaten. Daten sind als $2^{-\Delta\Delta Ct}$ Werte dargestellt und wurden mittels real-time PCR bestimmt. HFD/HFD: *n* = 7, HFD/HFD+LB: *n* = 7, HFD/HFD+LB+TRF: *n* = 7, HFD/NFD: *n* = 7, HFD/NFD+LB: *n* = 7, HFD/NFD+LB+TRF: *n* = 6; insgesamt *n* = 41. Die Signifikanz der Unterschiede wurde entweder mittels Kruskal–Wallis gefolgt von Dunn's post hoc Test für mehrfache Vergleiche getestet (B) oder mit einem Ordinary One-Way ANOVA gefolgt von Tukey's post hoc Test für mehrfache Vergleiche (C-E). Zahlen sind als Mittelwerte ± *sd* dargestellt mit *p < 0.05, **p < 0.005 oder ***p ≤ 0.001.

Im Weiteren wurde der Fibroblast Growth Factor 21 (FGF21) Metabolismus zum einem bei Adipositas und zum anderen nach Gewichtsreduktion betrachtet. Eine fettreiche Ernährung induzierte eine signifikante Erhöhung der hepatischen TNFα Expression (vgl. Studie I), was eine hepatische Low-Grade Inflammation widerspiegelte. Außerdem bewirkte die HFD einen Anstieg der hepatischen FGF21 Plasma Konzentrationen ($p \leq 0.001$, Abbildung 5, A; analoge Gruppen zu Studie I), die mit einer Reduktion der Proteinexpression des FGF21 Ko-Rezeptors β-Klotho ($p < 0.005$, B) einherging. Die zugrundeliegende Inflammation, bei gleichzeitiger FGF21 Zunahme und β-Klotho Abnahme, weisen auf eine hepatische FGF21 Resistenz hin.

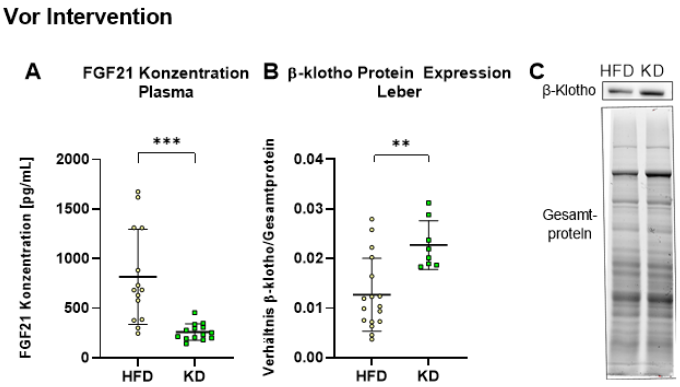

Abbildung 5: Eine HFD induziert eine hepatische FGF21 Resistenz. A: Plasmakonzentration von FGF21. HFD: *n* = 14, KD: *n* = 14. **B:** Densitometrische Analyse der hepatischen Proteinexpression von β-Klotho (normiert auf das Gesamtprotein; HFD: *n* = 14, KD: *n* = 8). **C**: Repräsentative Western Blots. Die Signifikanz der Unterschiede wurde mittels two-tailed unpaired t-Test (**A**, **B**) getestet. Zahlen sind als Mittelwerte ± *sd* dargestellt mit *p < 0.05, **p < 0.005 oder ***p ≤ 0.001

Anschließend wurde die hepatische FGF21 Resistenz mit einem Diätwechsel, Laufbandtraining und Intervallfasten therapiert. Nach der Intervention konnte vor allem durch den Diätwechsel die hepatische TNFα (vgl. Abbildung 5, E) und die FGF21 mRNA Expression signifikant reduziert (Abbildung 6; $p < 0.05$, A) und zeitgleich die β-Klotho Proteinexpression erhöht werden ($p < 0.05$, B). Die Ergebnisse deuten darauf hin, dass die HFD-induzierte hepatische FGF21 Resistenz hauptsächlich durch einen Diätwechsel erfolgreich therapiert werden konnte. Interessanterweise bewirkt das Intervallfasten analog zur hepatischen Steatose eine Reduktion der FGF21 mRNA Expression und womöglich auch eine Aufhebung der Resistenz.

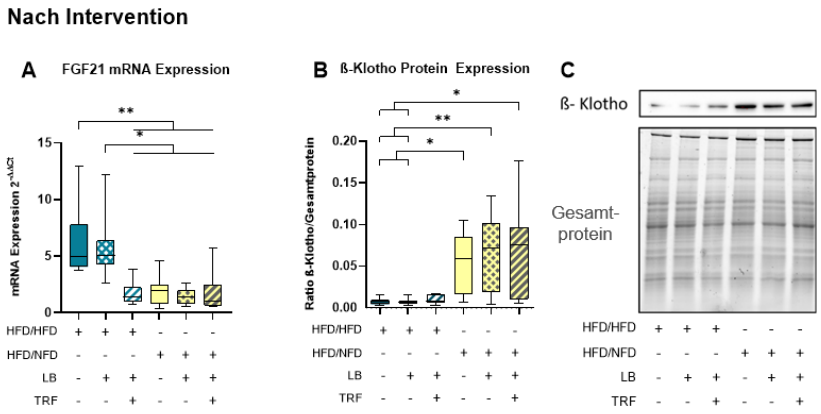

Abbildung 6: Ein Diätwechsel restauriert nach Gewichtsreduktion eine FGF21 Resistenz bei Mäusen. A, B: Densitometrische Analyse der hepatischen Proteinexpression von β-Klotho (normiert auf das Gesamtprotein). **G:** HFD/HFD: *n* = 13, HFD/HFD+LB: *n* = 12, HFD/HFD+LB+TRF: *n* = 13, HFD/NFD: *n* = 10, HFD/NFD+LB: *n* = 11, HFD/NFD+LB+TRF: *n* = 12; insgesamt *n* = 71. **H:** HFD/HFD: *n* = 13, HFD/HFD+LB: *n* = 11, HFD/HFD+LB+TRF: *n* = 13, HFD/NFD: *n* = 13, HFD/NFD+LB: *n* = 15, HFD/NFD+LB+TRF: *n* = 14; insgesamt *n* = 79. **C**: Repräsentative Western Blots. Die Signifikanz der Unterschiede wurde mittels Kruskal–Wallis gefolgt von Dunn's post hoc Test für mehrfache Vergleiche getestet (**B**) oder mit einem Ordinary One-Way ANOVA gefolgt von Tukey's post hoc Test für mehrfache Vergleiche (**A**). Zahlen sind als Mittelwerte ± *sd* dargestellt mit *p < 0.05, **p < 0.005 oder ***p ≤ 0.001.

5.5. Studie V

Anknüpfend an Studie IV wurde mit den beschriebenen Interventionen (Diätwechsel, Laufbandtraining, Intervallfasten), die sich protektiv auf eine NAFLD auswirken, untersucht, ob auch reduzierte Lokomotion, schlechtere olfaktorische Identifikation und ängstliches Verhalten moduliert werden können. In diesem Kontext wurde auch analysiert, inwieweit FGF21 als ein

potentieller Biomarker für Verhaltensänderungen nach erfolgreicher therapierter Adipositas angesehen werden kann. Nach der HFD-induzierten Adipositas für sechs Monate, wurden für weitere sechs Monate, die zuvor beschriebenen Interventionen durchgeführt. Am Ende des Experimentes zeigte sich (wie bereits bei Studie IV, Teil I gezeigt), dass das Körper- und das Fettgewicht aufgrund der Diätumstellung um etwa 50 % reduziert wurden (Abbildung 7, A $p \leq 0.0012$ für HFD/HFD Gruppen (blau) vs. HFD/NFD Gruppen (gelb); B: $p < 0.0001$ für HFD/HFD (blau) vs. HFD/NFD Gruppen (gelb)). Weiterhin war in diesen Gruppen neben der hepatischen FGF21 Konzentration (Studie IV) auch die systemische FGF21 Konzentration signifikant reduziert, wobei ein zusätzliches Laufbandtraining die FGF21 Konzentration noch weiter sinken ließ (C, $p < 0.0001$ für HFD/NFD+LB vs. HFD/HFD). Diese Kombination aus Ernährungsumstellung und physikalischer Aktivität verbesserte die Verhaltensparameter signifikant, die beim Buried Pellet Test, Elevated Plus Maze (EPM) oder Open Field (OF) erhoben wurden. Die Geruchserkennung war bei diesen Mäusen verbessert (E), die Ängstlichkeit war reduziert (F) und die Aktivität (G) war im Vergleich zu den adipösen Gruppen (nicht aber in Kombination mit Intervallfasten) erhöht. Um mögliche Zusammenhänge zwischen den erhobenen Beobachtungen und den Interventionsgruppen zu finden, wurde eine Hauptkomponentenanalyse durchgeführt (Daten in der Publikation). Dabei haben vor allem die Gruppen geclustert, welche neben dem Diätwechsel auch Laufbandtraining bekommen haben. Dieses Ergebnis wurde auch durch die Daten der Verhaltensexperimente bestätigt. Um in diesem Kontext, da ebenfalls Diätwechsel und Laufbandtraining die stärkste FGF21 Reduktion zeigte, die Rolle von FGF21 als potentiellen Biomarker zu evaluieren, wurde ein supervised Machine Learning-Ansatz durchgeführt. Drei unterschiedlich arbeitende Feature Selection (FS)-Algorithmen wurden angewendet (Chi-Square, Recursive Feature Elimination und Ridge Regularization), um die Schlüssel-Features auszuwählen (G). Unter den acht ausgewählten Features waren die Features FGF21, Körpergewicht, Lokomotion und olfaktorische Identifikation enthalten. Um die Leistung der FS-Algorithmen zu validieren, wurden acht verschiedene Machine Learning-Algorithmen implementiert, die entweder auf den nicht-Feature-selektierten Daten (Originaldaten oder Nicht-FS) oder auf FS-Daten basierten. Diejenigen Modelle, denen ein FS-Datensatz (dunkelgrau) zugrunde lag, waren in der Summe robustere Modelle als die Modellen, die auf dem nicht-FS-Datensatz (hellgrau) basierten, mit jeweils $p = 0.0078$ (H). Zusammenfassend unterstützen diese Beobachtungen, dass FGF21, auf Basis der Verhaltensparameter, neben den anderen ausgewählten Features, als ein Biomarker für verbesserte Lokomotion und olfaktorische Erkennungsfähigkeit nach therapierter Adipositas angesehen werden kann.

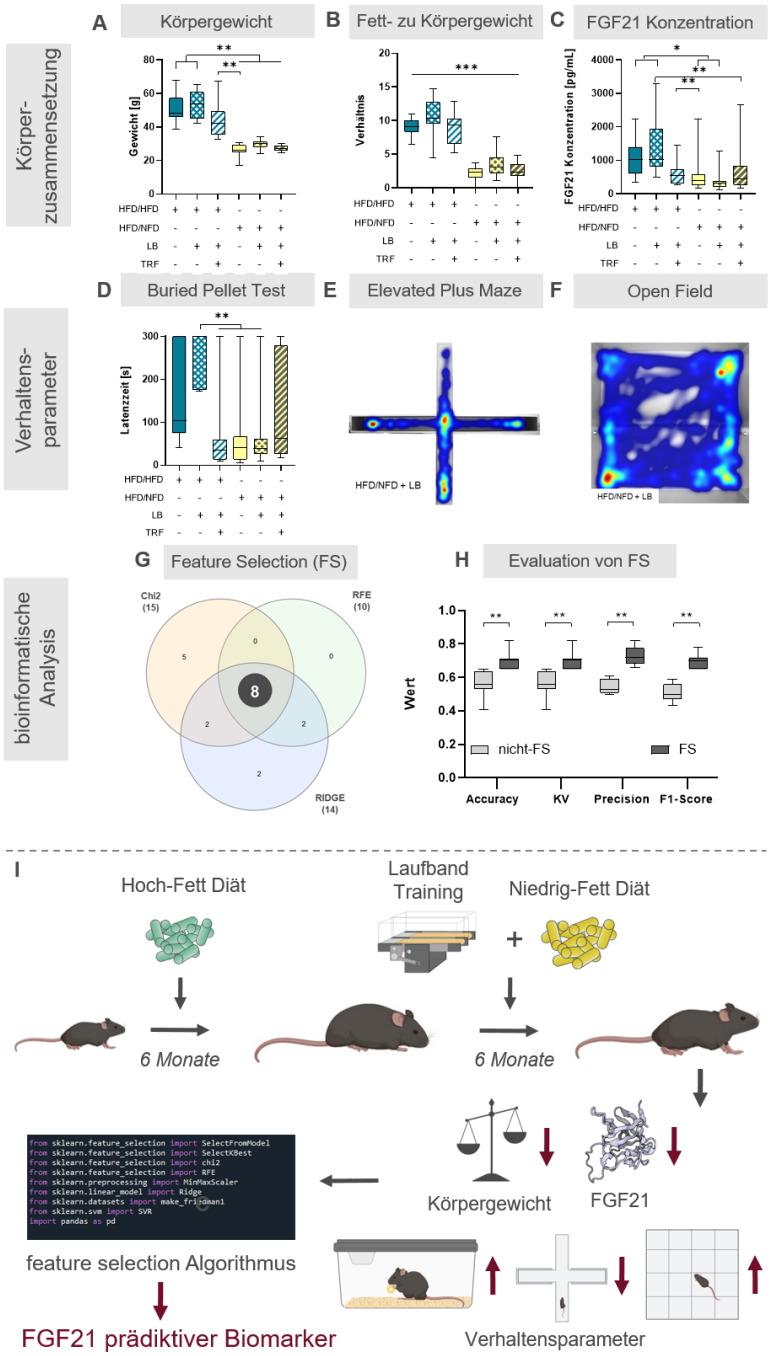

Abbildung 7: FGF21 ist ein prädiktiver Biomarker für verbesserte Lokomotion und olfaktorische Identifikationsleistung nach Gewichtsreduktion in Mäusen. Die Mäuse wurden sechs Monate mit einer HFD gefüttert und anschließend für die Interventionen in sechs Gruppen aufgeteilt: HFD/HFD (keine Intervention), HFD/HFD+LB, HFD/HFD+LB+TRF, HFD/NFD, HFD/NFD+LB, HFD/NFD+LB+TRF. **A:** Finale Körpergewichte [g] vor Euthanasie. **B:** Verhältnis vom viszeralen Fett zu Körpergewicht. **C:** FGF21 Plasmakonzentrationen [pg/mL] der letzten Blutentnahme. **D:** Latenzzeit [s] um das vergrabene Pellet zu essen. **A-D:** HFD/HFD: n = 13, HFD/HFD+LB: n = 13, HFD/HFD+LB+TRF: n = 15, HFD/NFD: n = 13, HFD/NFD+LB: n = 15, HFD/NFD+LB+TRF: n = 13-14, insgesamt n = 82-83. **E, F:** Heatmap Darstellung der Tierpräsenz von der HFD/NFD+LB Gruppe im EPM und OF über 300 s, wobei die rote Farbe die höchste Aufenthaltsdauer anzeigt und die blaue Farbe die niedrigste Aufenthaltsdauer. Beim EPM zeigten n = 12/15 und OF n = 5/10 dieses Muster. **G:** Drei verschiedene FS Algorithmen (Chi-Square, Recursive Feature Elimination und Ridge Regularization) wurden angewendet um die gewichteten Features zu extrahieren. Generierte Features sind als Mengendiagramm dargestellt, wobei FGF21 und das Körpergewicht unter den acht Features zählten. **H:** Evaluierung der Modelle basierend auf den nicht-FS-Datensatz (hellgrau) und den FS-Datensatz (Dunkelgrau). **I:** Graphical Abstract der Studie V. Die Signifikanz der Unterschiede wurde entweder mittels Kruskal–Wallis gefolgt von Dunn's post hoc Test für mehrfache Vergleiche getestet (**A, D**), Brown-Forsythe und Welch's ANOVA gefolgt von Tamhane T2 post hoc Test für mehrfache Vergleiche (**B**) oder mit einem Ordinary One-Way ANOVA gefolgt von Tukey's post hoc Test für mehrfache Vergleiche (**C**). Bei **H** wurde die Signifikanz der Unterschiede mit dem Wilcoxon Signed Rank Test getestet, wobei die theoretischen Mediane (*tm*) auf den Mittelwert der entsprechenden nicht-FS-Daten gesetzt wurden: *tm* der Accuracy = 0.56; *tm* der Kreuzvalidierung = 0.56; *tm* der Precision = 0.54; und *tm* des F1-Scores = 0.51. Zahlen sind als Mittelwerte ± *sd* dargestellt und die statistische Signifikanz wurde auf $p < 0.05$ gesetzt.

VI. Diskussion

In der vorliegenden Arbeit wurden die Adipositas-induzierte hepatische und zentralnervöse Inflammation in der Maus charakterisiert und dabei die Regulationswege von Fibroblast Growth Factor 21 (FGF21) evaluiert. Die Gabe einer fettreichen Diät führte zu einer hepatischen Low-Grade Inflammation und zu einer Neuroinflammation. In einem anderen Modell für eine Neuroinflammation — ausgelöst durch eine Amyloid-β Aggregation — konnte eine Kalorienrestriktion als Therapiemaßnahme mit einer glialen Autophagie assoziiert werden und somit zu einem Rückgang der Neuroinflammation beitragen. Weitere Interventionen wie Laufbandtraining und eine Ernährungsumstellung konnten die Adipositas-induzierte hepatische und zentralnervöse Inflammation erfolgreich therapieren, was durch einen Rückgang der nichtalkoholischen Fettlebererkrankung (NAFLD) und Verhaltensänderungen dargestellt werden konnte. Ebenfalls konnte die Adipositas-induzierte FGF21 Resistenz sowie die Adipositas-induzierten Verhaltensdefizite durch Laufbandtraining und einer Ernährungsumstellung nivelliert werden. Anhand des Therapieerfolges von Verhaltensparametern konnte durch Künstliche Intelligenz-basierende Ansätze FGF21 als ein potentieller Biomarker klassifiziert werden.

Adipositas ist nicht nur *per se* ein Gesundheitsrisiko, sondern oft mit anderen Begleit- und Folgeerkrankungen verbunden.[6,7,72] Ein Mechanismus, von dem angenommen wird, dass er zur Krankheitsprogression beiträgt, ist die ernährungsbedingte Low-Grade Inflammation, die vom Fettgewebe ausgeht, später systemisch wird und sich in anderen Organen wie der Leber manifestiert.[73] Studie I untersuchte, ob eine fettreiche Diät eine Low-Grade Inflammation in der Leber auslösen kann. Die im Rahmen der Auswertung erstellten NAFLD Activity Scores zeigten durch die Hoch-Fett-Diät (HFD) im Vergleich gegenüber einer Kontrolldiät einen mehr als vierfachen Anstieg des Scores, der hauptsächlich auf eine Steatose zurückzuführen war. Die Gabe der fettreichen Diät deutete auf eine beginnende und fortschreitende NAFLD hin, die in der Literatur als eine organische Manifestation des metabolischen Syndroms beschrieben wird.[5] Eine persistierende Low-Grade Inflammation könnte ein mechanistisches Bindeglied zwischen Adipositas und verschiedenen Komorbiditäten, wie z. B. der NAFLD, darstellen. Es gibt überzeugende Hinweise aus der Literatur, dass Adipositas einen Einfluss auf das Immunsystem ausübt und sich als Zustand der chronischen Low-Grade Inflammation manifestiert.[8,74] Neben den Entzündungsherden in der Leber nahm die Anzahl der neutrophilen Granulozyten und der Makrophagen durch eine fettreiche Diät signifikant zu. Es wanderten nicht nur reife Makrophagen aus der Blutbahn in die Leber ein, sondern auch myeloische Vorläuferzellen, die durch ein eng reguliertes Zusammenspiel von Genen für Chemokine, Chemokinrezeptoren, Adhäsionsmoleküle, myeloische Marker und inflammatorische Zytokine abgebildet werden.[75] Daher wurde als weiterer Schritt die hepatische Expression

verschiedener Zytokine bestimmt. In Anlehnung an die von anderen Arbeitsgruppen gezeigten TNFα-Erhöhungen bei Adipositas[12,74,76] konnte auch in Studie I eine solche Erhöhung in der HFD Gruppe gezeigt werden. Zusammenfassend konnte die Hypothese bestätigt werden, (i) dass eine fettreiche Ernährung eine hepatische NAFLD und eine Low-Grade Inflammation auslöst (Studie I).

Nach der Evaluierung der hepatischen Inflammation wurde eine zentralnervöse Inflammation in zwei verschiedenen Mausmodellen evaluiert. Dabei wurde eine Adipositas-induzierte Neuroinflammation (Studie II) mit neuroinflammatorischen Prozessen bedingt durch eine Amyloidose (Studie III) parallel untersucht, um ähnliche Pathomechanismen aufzuzeigen. Durch die Amyloid (A)β Aggregation in den transgenen Mäusen konnte eine Neuroinflammation durch die signifikante Zunahme an Iba1 gefärbter Mikroglia dargestellt werden, was bei Brendel und Mitarbeiter[77] ebenfalls gezeigt werden konnte. Neben immunhistochemischer Charakterisierung kann eine Amyloidose-induzierte Neuroinflammation auch durch einen Anstieg des [^{18}F]- Translokatorprotein (TSPO) Signals abgebildet werden, was die Möglichkeit gibt, longitudinale Untersuchungen durchzuführen.[29] So wurden in der Studie von Barron et al.[78] adipöse Mäuse, welche mit Aβ intrazerebroventrikulär infundiert wurden, longitudinal mittels den Radiopharmaka [^{18}F]-TSPO und [^{18}F]-Fluordesoxyglukose (FDG, für den zerebralen Glukosemetabolismus über Glukosetransporters 1 (GLUT1)) für drei Monate analysiert. Barron und Mitarbeiter zeigten, dass es nach drei Monaten zu einem Anstieg des [^{18}F]-TSPO und [^{18}F]-FDG Signals kam, welcher mit ergänzenden Methoden als Neuroinflammation und zerebraler Hypermetabolismus interpretiert wurde. HFD gefütterte Mäuse ohne Aβ-Infusion zeigten hingegen keine Veränderung des Signals gegenüber normalgewichtigen Mäusen.[78] In der eigenen Studie konnte dieses Ergebnis bestätigt werden, denn auch hier zeigten sich nach dreimonatiger HFD keine Unterschiede im [^{18}F]-TSPO und [^{18}F]-FDG Signal. Eine longitudinale Beobachtung über weitere drei Monate hinaus zeigte sich — im Gegensatz zu Baron et al. — eine Erhöhung des [^{18}F]-TSPO und [^{18}F]-FDG Signals. Dies zeigt, dass die Dauer einer HFD entscheidend für die Ausbildung einer Neuroinflammation ist. Es muss aber beachtet werden, dass die fettreiche Diät die Permeabilität der Blut-Hirn-Schranke beeinflussen kann.[20] Nerurkar et al.[79] fanden unter Verwendung des Evans-Blau-Farbstoffs eine erhöhte Passage des Farbstoffs in das Zentralnervensystem von Mäusen, die 16 Wochen lang mit einer HFD gefüttert wurden.[20] Inwieweit nun auch mehr Radiopharmaka ([^{18}F]-TSPO und [^{18}F]-FDG) die Blut-Hirn-Schranke passieren könnten und somit das Gleichgewicht zugunsten des Liganden verschieben würden, kann momentan nur spekuliert werden. Dem entgegen würde sprechen, dass eine HFD zu einer Verringerung der Expression von GLUT1 in vaskulären Endothelzellen an der Blut-Hirn-Schranke und damit zu einer geringeren Glukoseaufnahme, u.a. angezeigt

durch ein niedrigeres [^{18}F]-FDG Signal im Gehirn, führt.[41] Jedoch konnten Jais et al. auch zeigen, dass eine fettreiche Ernährung über längere Zeit zu einer kompensatorischen Hochregulierung von GLUT1 durch verstärkte Entzündungssignale von perivaskulären Makrophagen führt.[41] In diesem Kontext konnte in der eigenen Studie auch eine Inflammation mit einem signifikanten Anstieg der kortikalen IL-1β mRNA Expression beobachtet werden, welche mit einem erhöhten [^{18}F]-FDG Signal einherging. Ob nun die beobachtete Steigerung des [^{18}F]-FDG Signals bei einer sechsmonatigen HFD auf eine kompensatorische Hochregulierung des GLUT1 als Folge inflammatorischer Signale (Inflammation) oder als erhöhte Glukoseaktivität von vermehrter aktivierter Mikroglia (Neuroinflammation) zurückzuführen ist, ist derzeit Gegenstand immunhistochemischer Analysen. Bei der Aβ-induzierten Neuroinflammation konnte die Summe aus Aggregation von Aβ, Zunahme von aktivierter Mikroglia, niedrigerer Glukoseaufnahme durch eine Reduktion des [^{18}F]-FDG Signals und schlechterer Performance im Morris-Water-Maze als verschlechterte Kognition interpretiert werden. Bei der Adipositas-induzierten Neuroinflammation hingegen konnte keine Abnahme der Kognition durch den Morris-Water-Maze festgestellt werden. Eine verschlechterte Kognition in Form von Verhaltensstörungen konnte erst nach zwölfmonatiger HFD (Studie V) gezeigt werden. Bei einer fettreichen Ernährung erweist sich ein längerer Zeitraum (> sechs Monate) als entscheidende Voraussetzung, um einen kognitiven Verlust zu beobachten. In der Summe ist es gelungen (i) sowohl durch die Adipositas (Studie II), als auch durch eine Amyloidose (Studie III) eine Neuroinflammation zu induzieren.

In der Aβ-Plaque-induzierten Neuroinflammation wurde weiterhin untersucht, ob eine Kalorienrestriktion - mechanistisch über autophagische Prozesse — eine Therapiemaßnahme ist. Es konnte gezeigt werden, dass die Kalorienrestriktion die Aβ-Plaques reduzierte, somit eine Neuroinflammation senkte und folglich zu einem messbaren Anstieg der Glukoseaufnahme, dargestellt durch eine Erhöhung des [^{18}F]-FDG Signals, führte. In Kombination mit einer besseren Performance im Morris-Water-Maze wurde die Summe der Ergebnisse als kognitive Verbesserung interpretiert. Dong et al.[80] berichten, dass die Kalorienrestriktion *per* se die Zelldichte in der CA3-Region im Hippocampus signifikant erhöht und somit zu einer gesteigerten neuronalen Aktivität führt. Inwieweit nun die gesteigerte neuronale Aktivität einen Anstieg des [^{18}F]-FDG Signals widerspiegelt, ist noch offen. Auf der anderen Seite ist die Kalorienrestriktion in der Lage, eine Autophagie zu induzieren,[81] die die Anzahl der Plaques reduzierte, was wiederrum die Mikroglia-Aktivierung im Hippocampus abschwächte.[82] Zudem ist bekannt, dass die Autophagie positiv die Glukoseaufnahme über die Hochregulierung der GLUT1-Proteinexpression moduliert.[83] Daher kann auch gefolgert werden, dass die erhöhte [^{18}F]-FDG-Aufnahme bei Kalorienrestriktion in den transgenen Mäusen eine Folge der erhöhten Autophagie-Aktivität, dargestellt durch erhöhte LCB3II

Proteinexpressionen, ist. Aus den Ergebnissen der Aβ-induzierten Neuroinflammation lässt sich zusammenfassen, (ii) dass die Kalorienrestriktion eine Therapiemaßnahme ist, um eine Neuroinflammation durch Aβ-Abbau-assoziierte Prozesse zu reduzieren (Studie III).

Anders als bei Amyloidose-induzierter Neuroinflammation wurde bei der Adipositas-induzierten Inflammation (zentralnervös und hepatisch) translationale Therapieansätze gewählt, wie eine Ernährungsumstellung (Wechsel von einer fettreichen Diät zu einer Niedrig-Fett-Diät), Laufbandtraining oder Intervallfasten (Studie IV). Wird zuerst der Therapieerfolg der Interventionen anhand der Gewichtsreduktion der adipösen Mäuse evaluiert, so können die Daten aus Studie IV und V zusammen betrachtet werden, da diese Studien auf denselben Experimenten beruhen. Dabei wurde gezeigt, dass ein Diätwechsel zu einer Reduktion des Körpergewichtes, der viszeralen und subkutanen Fettdepots (Studie IV und V) führte, was ebenfalls von Astrup et al.[84] gezeigt werden konnte. Obwohl eine physikalische Aktivität in Form von Laufbandtraining in mehreren Studien auch eine Gewichtsreduktion verursachte,[39,85,86] zeigten eine andere[87] und die eigene Studie keine Gewichtsreduktion. Es wird vermutet, dass unterschiedliche Laufbandintensitäten die Ursache dieser unterschiedlichen Ergebnisse sind.[88] Weiterhin konnte in Studie IV gezeigt werden, dass durch einen Diätwechsel die hepatische Steatose erniedrigt wird, welche vergleichbar mit einer Langzeitfütterung der Mäuse mit einer Niedrig-Fett-Diät[89,90] ist (unpublizierte Daten). Die Analyse der hepatischen Inflammation zeigte, dass durch eine Ernährungsumstellung TNFα signifikant reduziert werden konnte. Ein ähnlicher Befund konnte im Fettgewebe nachgewiesen werden, da dort eine Gewichtsabnahme zu einem Rückgang der proinflammatorischen Biomarker wie TNFα und zu einem Anstieg des antiinflammatorischen Biomarkers Adiponektin führte.[91,92] Da die Low-Grade Inflammation in der Leber (Studie I) und im Fettgewebe durch einen Anstieg von proinflammatorischen Markern gekennzeichnet ist,[93] kann gefolgert werden, dass eine Reduktion von TNFα auch zu einer Verringerung der Low-Grade Inflammation in beiden Geweben führt. Abschließend ist festzuhalten, (iii) dass eine Adipositas-induzierte hepatische Low-Grade Inflammation hauptsächlich durch einen Diätwechsel therapierbar war (Studie IV).

Im Weiteren wurde in Studie IV der FGF21 Metabolismus in zwei energetisch verschiedenen Zuständen (bei Adipositas und nach Intervention) betrachtet. Eine HFD-induzierte FGF21 Resistenz geht analog zum weißen Fettgewebe auch mit einer verschlechterten Energieregulierung einher.[94–96] In diesem Kontext konnte FGF21 in einer Studie bei einer fettreichen Diät unter Verwendung von uncoupling protein 1 (ein thermogenes fettspezifisches Protein) und FGF21 Doppel-knock out-Mäusen als Hauptregulator identifiziert werden, wobei FGF21 vor einer Diät-induzierten Adipositas schützte und den Umbau von weißem

Fettgewebe in Abwesenheit von uncoupling protein 1 vermittelte.[97] Außerdem zeigte eine andere Studie, dass eine Überexpression des Ko-Rezeptors β-Klotho in Adipozyten wahrscheinlich endogenes FGF21 sensitiviert,[98] und somit die Ratio von Ligand/Rezeptor entscheidend für die metabolische Aktivität von FGF21 ist. In eigenen Vorarbeiten korrelierte — hauptsächlich durch den Diätwechsel ausgelöst — die Reduktion der hepatischen Inflammation (TNFα) mit der Erhöhung des hepatischen β-Klotho (unpublizierte Daten) und FGF21, was einen Hinweis auf eine Modulation von FGF21 durch eine therapierte Low-Grade Inflammation und ggf. eine NAFLD gibt. Unter der Einbeziehung der zirkulierenden FGF21 Plasmakonzentration aus Studie V ist die metabolische Aktivität von FGF21 in den Gruppen mit Kombination aus einem Diätwechsel und Laufbandtraining oder mit allen drei Interventionen erhöht. Dies zeichnete sich durch einen markanten Rückgang der hepatischen und zirkulierenden FGF21 Expression und durch einen Anstieg des β-Klotho aus. Geng et al.[39] zeigten, dass durch körperliche Aktivität die FGF21-Expression gesenkt werden kann, und dass die FGF21-Sensitivität bei adipösen Mäusen wiederhergestellt und die metabolische Interaktion zwischen Fettgewebe, Leber und Skelettmuskel wieder ins Gleichgewicht gebracht wird.[39] Ein Rückgang der hepatischen FGF21 Resistenz deutet sich auch in Kombination mit einer HFD, Laufbandtraining und Intervallfasten an. Es wurde beschrieben, dass das Intervallfasten vor Folgen der Adipositas schützen kann.[99,100] Eine Folge der Adipositas ist beispielsweise eine FGF21-Resistenz, die durch hohe zirkulierende FGF21-Konzentrationen und stark erhöhtes Körpergewicht beschrieben wird.[37] Da FGF21 einen zirkadianen Rhythmus aufweist, der durch eine fettreiche Diät gestört wird, wird davon ausgegangen, dass Intervallfasten die Oszillation von FGF21 wieder ins Gleichgewicht bringt, indem es die Nahrungsaufnahme in einer tageszeitabhängigen Weise koppelt.[46,101] Basierend auf der erhobenen Datenlage wird spekuliert, dass die Abnahme von zirkulierenden FGF21 in der Gruppe mit HFD, Laufbandtraining und Intervallfasten ein Hinweis auf den positiven Effekt des Fastens sein könnte, da die physikalische Aktivität allein nicht zu einer Abnahme der zirkulierenden FGF21-Konzentrationen führte. In der vorliegenden Studie konnte gezeigt werden, dass (iv) eine fettreiche Ernährung eine hepatische FGF21-Resistenz induziert, die durch einen Diätwechsel therapiert werden konnte (Studie IV).

Abschließend wurde mittels Verhaltensparametern untersucht, ob FGF21 ein prädiktiver Biomarker für verbesserte Riechleistung und Lokomotion nach therapierter Adipositas ist (Studie V). Die Ernährungsumstellung auf eine Niedrig-Fett-Diät führte im Vergleich zu adipösen Mäusen zu einer Reduktion der Neuroinflammation, die mittels dem Radiopharmakon [^{18}F]-TSPO gemessen wurde (unpublizierte Daten). Darüber hinaus führte der Diätwechsel in Kombination mit physikalischer Aktivität zu weniger Angst-bedingtem Verhalten, zu einer insgesamt höheren Aktivität und zu besseren olfaktorischen Fähigkeiten.

Inwieweit eine reduzierte Neuroinflammation zur Verbesserung der Verhaltensparameter führt kann nur spekuliert werden. Es ist beschrieben, dass Bewegungstraining die Angstsensitivität reduziert, indem Stressoren der Hypothalamus-Hypophysen-Nebenniere-(HPA)–Achse moduliert werden.[102,103] Zu den Stressoren gehört die HFD, die zu erhöhten FGF21-Konzentrationen führt. FGF21 ist wiederum an metabolischen Stressprozessen beteiligt und wurde ebenfalls als Stressor beschrieben.[104] Es wird postuliert, dass FGF21 den Hypothalamus direkt beeinflussen und damit die HPA–Achse stimulieren könnte.[105] Wahrscheinlich wird durch den stressinduzierten Anstieg der FGF21-Konzentration, ausgelöst durch eine HFD, die HPA–Achse negativ moduliert. Diese Modulation wird durch das Laufbandtraining kompensiert, was sich in einer Reduktion des angstbedingten Verhaltens äußert. Offensichtlich ist der positive Effekt auf das Verhalten nicht allein auf die Laufbandaktivität zurückzuführen, sonst wäre dieser positive Effekt auch in der Gruppe aus HFD und Laufbandtraining präsent. Vielmehr ist die Kombination von einer Niedrig-Fett-Diät mit physikalischer Aktivität entscheidend, d.h. die Kombination aus einer Reduktion des Ernährungsstresses - die mit einer Reduktion der Entzündung und FGF21 einhergeht - und dem positiven Effekt durch die Laufbandaktivität, für eine erfolgversprechende Intervention gegen Verhaltensstörungen bei Adipositas. Mithilfe von Machine Learning wurden FGF21, Körpergewicht, Riechleistung und das Aktivitätsmuster im Open Field als stark gewichtete Features identifiziert. Es wird davon ausgegangen, dass die höhere Genauigkeit der Machine Learning Modelle, die auf dem Feature Selection Datensatz basieren, die ausgewählten Features, hauptsächlich FGF21 und Körpergewicht, als relevante Biomarker bestätigt. Die Ergebnisse untermauern die Hypothese, dass (v) FGF21 als möglicher Biomarker für verbesserte Riechleistung und Lokomotion nach Gewichtsreduktion angesehen werden kann (Studie V).

Mit der vorgelegten Arbeit ist es gelungen, neben Adipositas-assoziierten Erkrankungen, wie einer NAFLD und Neurodegeneration und die daraus abgeleiteten Demenzerkrankungen, die inflammatorischen Prozesse besser zu verstehen und durch verschiedene „Lifestyle“ Faktoren, wie Ernährung und Bewegung, zu modulieren. Im Fokus stand dabei ganz wesentlich das Hormon FGF21 -ein potentieller Biomarker für Adipositas-, dessen regulatorisches Potential bei Stoffwechselprozessen peripher aber auch zentral durch inflammatorische Stimuli gestört wird. Die Verwendung der PET-CT (und MRT) Technik ermöglichte longitudinale Untersuchungen neuroinflammtorischer sowie neurodegenerativer Prozesse, was zur Generierung neuer Biomarker beitrug und damit den Grad an Translationalität erhöhte. Mit KI-basierten Ansätzen gelang es, FGF21 bei Adipositas *per se* und nach der Behandlung der Adipositas als Biomarker zu klassifizieren, was im Sinne der Translation neue Optionen für die Diagnostik Adipositas-bedingter Erkrankungen ermöglicht.

VII. Literaturverzeichnis

(1) WHO. *Obesity and overweight*. https://www.who.int/en/news-room/fact-sheets/detail/obesity-and-overweight (accessed 2022-02-02).

(2) Kaplan, N. M. The Deadly Quartet. *Arch Intern Med* **1989**, *149* (7), 1514. DOI: 10.1001/archinte.1989.00390070054005.

(3) Beilby, J. Definition of Metabolic Syndrome: Report of the National Heart, Lung, and Blood Institute/American Heart Association Conference on Scientific Issues Related to Definition. *Clin. Biochem. Rev.* **2004**, *25* (3), 195–198.

(4) Gogia, A.; Agarwal, P. K. Metabolic syndrome. *Indian J. Med. Sci.* **2006**, *60* (2), 72–81. DOI: 10.4103/0019-5359.19918.

(5) Marchesini, G.; Brizi, M.; Bianchi, G.; Tomassetti, S.; Bugianesi, E.; Lenzi, M.; McCullough, A. J.; Natale, S.; Forlani, G.; Melchionda, N. Nonalcoholic fatty liver disease: a feature of the metabolic syndrome. *Diabetes* **2001**, *50* (8), 1844–1850. DOI: 10.2337/diabetes.50.8.1844.

(6) Schattenberg, J. M.; Schuppan, D. Nonalcoholic steatohepatitis: the therapeutic challenge of a global epidemic. *Curr. Opin. Lipidol.* **2011**, *22* (6), 479–488. DOI: 10.1097/MOL.0b013e32834c7cfc.

(7) Hotamisligil, G. S. Inflammation and metabolic disorders. *Nature* **2006**, *444*, 860 EP -. DOI: 10.1038/nature05485.

(8) Wellen, K. E.; Hotamisligil, G. S. Obesity-induced inflammatory changes in adipose tissue. *J. Clin. Invest.* **2003**, *112* (12), 1785–1788. DOI: 10.1172/JCI200320514.

(9) Medzhitov, R. Origin and physiological roles of inflammation. *Nature* **2008**, *454* (7203), 428–435. DOI: 10.1038/nature07201.

(10) Lumeng, C. N.; Saltiel, A. R. Inflammatory links between obesity and metabolic disease. *J. Clin. Invest.* **2011**, *121* (6), 2111–2117. DOI: 10.1172/JCI57132. Published Online: Jun. 1, 2011.

(11) Juge-Aubry, C. E.; Henrichot, E.; Meier, C. A. Adipose tissue: a regulator of inflammation. *Best Pract. Res. Clin. Endocrinol. Metab.* **2005**, *19* (4), 547–566. DOI: 10.1016/j.beem.2005.07.009.

(12) Kim, K.-A.; Gu, W.; Lee, I.-A.; Joh, E.-H.; Kim, D.-H. High fat diet-induced gut microbiota exacerbates inflammation and obesity in mice via the TLR4 signaling pathway. *PLoS One* **2012**, *7* (10), e47713. DOI: 10.1371/journal.pone.0047713.

(13) Wu, Z.; Xu, J.; Tan, J.; Song, Y.; Liu, L.; Zhang, F.; Zhang, Y.; Li, X.; Chi, Y.; Liu, Y. Mesenteric adipose tissue B lymphocytes promote local and hepatic inflammation in non-alcoholic fatty liver disease mice. *J. Cell. Mol. Med*. **2019.** DOI: 10.1111/jcmm.14232.

(14) Koyama, Y.; Brenner, D. A. Liver inflammation and fibrosis. *J. Clin. Invest.* **2017**, *127* (1), 55–64. DOI: 10.1172/JCI88881.

(15) Saltiel, A. R.; Olefsky, J. M. Inflammatory mechanisms linking obesity and metabolic disease. *J. Clin. Invest.* **2017**, *127* (1), 1–4. DOI: 10.1172/JCI92035.

(16) Miller, A. A.; Spencer, S. J. Obesity and neuroinflammation: A pathway to cognitive impairment. *Brain Behav. Immun.* **2014**, *42*, 10–21. DOI: 10.1016/j.bbi.2014.04.001.

(17) Thaler, J. P.; Guyenet, S. J.; Dorfman, M. D.; Wisse, B. E.; Schwartz, M. W. Hypothalamic inflammation: marker or mechanism of obesity pathogenesis? *Diabetes* **2013**, *62* (8), 2629–2634. DOI: 10.2337/db12-1605.

(18) Williams, K. W.; Elmquist, J. K. From neuroanatomy to behavior: central integration of peripheral signals regulating feeding behavior. *Nat. Neurosci.* **2012**, *15* (10), 1350–1355. DOI: 10.1038/nn.3217. Published Online: Sep. 25, 2012.

(19) Sainsbury, A.; Zhang, L. Role of the arcuate nucleus of the hypothalamus in regulation of body weight during energy deficit. *Mol. Cell. Endocrinol.* **2010**, *316* (2), 109–119. DOI: 10.1016/j.mce.2009.09.025. Published Online: Oct. 12, 2009.

(20) Guillemot-Legris, O.; Muccioli, G. G. Obesity-Induced Neuroinflammation: Beyond the Hypothalamus. *Trends Neurosci.* **2017**, *40* (4), 237–253. DOI: 10.1016/j.tins.2017.02.005.

(21) De Souza, C. T.; Araujo, E. P.; Bordin, S.; Ashimine, R.; Zollner, R. L.; Boschero, A. C.; Saad, M. J. A.; Velloso, L. A. Consumption of a fat-rich diet activates a proinflammatory response and induces insulin resistance in the hypothalamus. *Endocrinology* **2005**, *146* (10), 4192–4199. DOI: 10.1210/en.2004-1520. Published Online: Jul. 7, 2005.

(22) Ziko, I.; Luca, S. de; Dinan, T.; Barwood, J. M.; Sominsky, L.; Cai, G.; Kenny, R.; Stokes, L.; Jenkins, T. A.; Spencer, S. J. Neonatal overfeeding alters hypothalamic microglial profiles and central responses to immune challenge long-term. *Brain Behav. Immun.* **2014**, *41*, 32–43. DOI: 10.1016/j.bbi.2014.06.014. Published Online: Jun. 27, 2014.

(23) Cano, V.; Valladolid-Acebes, I.; Hernández-Nuño, F.; Merino, B.; Del Olmo, N.; Chowen, J. A.; Ruiz-Gayo, M. Morphological changes in glial fibrillary acidic protein immunopositive astrocytes in the hippocampus of dietary-induced obese mice. *Neuroreport* **2014**, *25* (11), 819–822. DOI: 10.1097/WNR.0000000000000180.

(24) Hu, P.; Thinschmidt, J. S.; Caballero, S.; Adamson, S.; Cole, L.; Chan-Ling, T.; Grant, M. B. Loss of survival factors and activation of inflammatory cascades in brain sympathetic centers in type 1 diabetic mice. *Am. J. Physiol. Endocrinol. Metab.* **2015**, *308* (8), E688-98. DOI: 10.1152/ajpendo.00504.2014. Published Online: Feb. 24, 2015.

(25) Kälin, S.; Heppner, F. L.; Bechmann, I.; Prinz, M.; Tschöp, M. H.; Yi, C.-X. Hypothalamic innate immune reaction in obesity. *Nat. Rev. Endocrinol.* **2015**, *11* (6), 339–351. DOI: 10.1038/nrendo.2015.48. Published Online: Mar. 31, 2015.

(26) Xu, W. L.; Atti, A. R.; Gatz, M.; Pedersen, N. L.; Johansson, B.; Fratiglioni, L. Midlife overweight and obesity increase late-life dementia risk: a population-based twin study. *Neurology* **2011**, *76* (18), 1568–1574. DOI: 10.1212/WNL.0b013e3182190d09.

(27) Raji, C. A.; Ho, A. J.; Parikshak, N. N.; Becker, J. T.; Lopez, O. L.; Kuller, L. H.; Hua, X.; Leow, A. D.; Toga, A. W.; Thompson, P. M. Brain structure and obesity. *Hum. Brain Mapp.* **2010**, *31* (3), 353–364. DOI: 10.1002/hbm.20870.

(28) James, M. L.; Belichenko, N. P.; Shuhendler, A. J.; Hoehne, A.; Andrews, L. E.; Condon, C.; Nguyen, T.-V. V.; Reiser, V.; Jones, P.; Trigg, W.; Rao, J.; Gambhir, S. S.; Longo, F. M. 18FGE-180 PET Detects Reduced Microglia Activation After LM11A-31 Therapy in a Mouse Model of Alzheimer's Disease. *Theranostics* **2017**, *7* (6), 1422–1436. DOI: 10.7150/thno.17666. Published Online: Mar. 24, 2017.

(29) Brendel, M.; Probst, F.; Jaworska, A.; Overhoff, F.; Korzhova, V.; Albert, N. L.; Beck, R.; Lindner, S.; Gildehaus, F.-J.; Baumann, K.; Bartenstein, P.; Kleinberger, G.; Haass, C.; Herms, J.; Rominger, A. Glial Activation and Glucose Metabolism in a Transgenic Amyloid Mouse Model: A Triple-Tracer PET Study. *J. Nucl. Med.* **2016**, *57* (6), 954–960. DOI: 10.2967/jnumed.115.167858. Published Online: Feb. 18, 2016.

(30) Luo, Y.; Ye, S.; Li, X.; Lu, W. Emerging Structure-Function Paradigm of Endocrine FGFs in Metabolic Diseases. *Trends Pharmacol. Sci.* **2019**, *40* (2), 142–153. DOI: 10.1016/j.tips.2018.12.002. Published Online: Jan. 4, 2019.

(31) Laeger, T.; Baumeier, C.; Wilhelmi, I.; Würfel, J.; Kamitz, A.; Schürmann, A. FGF21 improves glucose homeostasis in an obese diabetes-prone mouse model independent of body fat changes. *Diabetologia* **2017**, *60* (11), 2274–2284. DOI: 10.1007/s00125-017-4389-x.

(32) Rühlmann, C.; Wölk, T.; Blümel, T.; Stahn, L.; Vollmar, B.; Kuhla, A. Long-term caloric restriction in ApoE-deficient mice results in neuroprotection via Fgf21-induced AMPK/mTOR pathway. *Aging* **2016**, *8* (11), 2777--2789. DOI: 10.18632/aging.101086.

(33) Bookout, A. L.; Groot, M. H. M. de; Owen, B. M.; Lee, S.; Gautron, L.; Lawrence, H. L.; Ding, X.; Elmquist, J. K.; Takahashi, J. S.; Mangelsdorf, D. J.; Kliewer, S. A. FGF21 regulates metabolism and circadian behavior by acting on the nervous system. *Nat. Med.* **2013**, *19* (9), 1147–1152. DOI: 10.1038/nm.3249. Published Online: Aug. 11, 2013.

(34) Domouzoglou, E. M.; Maratos-Flier, E. Fibroblast growth factor 21 is a metabolic regulator that plays a role in the adaptation to ketosis. *Am. J. Clin. Nutr.* **2011**, *93* (4), 901S-5. DOI: 10.3945/ajcn.110.001941. Published Online: Feb. 23, 2011.

(35) Zhang, Y.; Xie, Y.; Berglund, E. D.; Coate, K. C.; He, T. T.; Katafuchi, T.; Xiao, G.; Potthoff, M. J.; Wei, W.; Wan, Y.; Yu, R. T.; Evans, R. M.; Kliewer, S. A.; Mangelsdorf, D. J. The starvation hormone, fibroblast growth factor-21, extends lifespan in mice. *eLife* **2012**, *1*, e00065. DOI: 10.7554/eLife.00065. Published Online: Oct. 15, 2012.

(36) Gallego-Escuredo, J. M.; Gómez-Ambrosi, J.; Catalan, V.; Domingo, P.; Giralt, M.; Frühbeck, G.; Villarroya, F. Opposite alterations in FGF21 and FGF19 levels and disturbed expression of the receptor machinery for endocrine FGFs in obese patients. *Int. J. Obes.* **2015**, *39* (1), 121–129. DOI: 10.1038/ijo.2014.76. Published Online: May. 12, 2014.

(37) Fisher, F. M.; Chui, P. C.; Antonellis, P. J.; Bina, H. A.; Kharitonenkov, A.; Flier, J. S.; Maratos-Flier, E. Obesity is a fibroblast growth factor 21 (FGF21)-resistant state. *Diabetes* **2010**, *59* (11), 2781–2789. DOI: 10.2337/db10-0193. Published Online: Aug. 3, 2010.

(38) Díaz-Delfín, J.; Hondares, E.; Iglesias, R.; Giralt, M.; Caelles, C.; Villarroya, F. TNF-α represses β-Klotho expression and impairs FGF21 action in adipose cells: involvement of JNK1 in the FGF21 pathway. *Endocrinology* **2012**, *153* (9), 4238–4245. DOI: 10.1210/en.2012-1193.

(39) Geng, L.; Liao, B.; Jin, L.; Huang, Z.; Triggle, C. R.; Ding, H.; Zhang, J.; Huang, Y.; Lin, Z.; Xu, A. Exercise Alleviates Obesity-Induced Metabolic Dysfunction via Enhancing FGF21 Sensitivity in Adipose Tissues. *Cell Rep.* **2019**, *26* (10), 2738-2752.e4. DOI: 10.1016/j.celrep.2019.02.014.

(40) Ge, X.; Chen, C.; Hui, X.; Wang, Y.; Lam, K. S. L.; Xu, A. Fibroblast growth factor 21 induces glucose transporter-1 expression through activation of the serum response factor/Ets-like protein-1 in adipocytes. *J. Biol. Chem.* **2011**, *286* (40), 34533–34541. DOI: 10.1074/jbc.M111.248591. Published Online: Aug. 16, 2011.

(41) Jais, A.; Solas, M.; Backes, H.; Chaurasia, B.; Kleinridders, A.; Theurich, S.; Mauer, J.; Steculorum, S. M.; Hampel, B.; Goldau, J.; Alber, J.; Förster, C. Y.; Eming, S. A.; Schwaninger, M.; Ferrara, N.; Karsenty, G.; Brüning, J. C. Myeloid-Cell-Derived VEGF Maintains Brain Glucose Uptake and Limits Cognitive Impairment in Obesity. *Cell* **2016**, *165* (4), 882–895. DOI: 10.1016/j.cell.2016.03.033. Published Online: Apr. 28, 2016.

(42) Han, J.; Nepal, P.; Odelade, A.; Freely, F. D.; Belton, D. M.; Graves, J. L.; Maldonado-Devincci, A. M. High-Fat Diet-Induced Weight Gain, Behavioral Deficits, and Dopamine Changes in Young C57BL/6J Mice. *Front. Nutr.* **2020**, *7*, 591161. DOI: 10.3389/fnut.2020.591161. Published Online: Jan. 20, 2021.

(43) Tomiga, Y.; Yoshimura, S.; Ra, S.-G.; Takahashi, Y.; Goto, R.; Kugimoto, I.; Uehara, Y.; Kawanaka, K.; Higaki, Y. Anxiety-like behaviors and hippocampal nNOS in response to diet-induced obesity combined with exercise. *J. Physiol. Sci.* **2019**, *69* (5), 711–722. DOI: 10.1007/s12576-019-00686-5. Published Online: May. 23, 2019.

(44) Takase, K.; Tsuneoka, Y.; Oda, S.; Kuroda, M.; Funato, H. High-fat diet feeding alters olfactory-, social-, and reward-related behaviors of mice independent of obesity. *Obesity* **2016**, *24* (4), 886–894. DOI: 10.1002/oby.21441. Published Online: Feb. 18, 2016.

(45) Pietiläinen, K. H.; Kaprio, J.; Borg, P.; Plasqui, G.; Yki-Järvinen, H.; Kujala, U. M.; Rose, R. J.; Westerterp, K. R.; Rissanen, A. Physical inactivity and obesity: a vicious circle. *Obesity (Silver Spring)* **2008**, *16* (2), 409–414. DOI: 10.1038/oby.2007.72.

(46) Hatori, M.; Vollmers, C.; Zarrinpar, A.; DiTacchio, L.; Bushong, E. A.; Gill, S.; Leblanc, M.; Chaix, A.; Joens, M.; Fitzpatrick, J. A.J.; Ellisman, M. H.; Panda, S. Time-restricted feeding without reducing caloric intake prevents metabolic diseases in mice fed a high-fat diet. *Cell Metab.* **2012**, *15* (6), 848–860. DOI: 10.1016/j.cmet.2012.04.019.

(47) Kruse, R.; Vienberg, S. G.; Vind, B. F.; Andersen, B.; Højlund, K. Effects of insulin and exercise training on FGF21, its receptors and target genes in obesity and type 2 diabetes. *Diabetologia* **2017**, *60* (10), 2042–2051. DOI: 10.1007/s00125-017-4373-5. Published Online: Jul. 18, 2017.

(48) Mouton, P. R.; Chachich, M. E.; Quigley, C.; Spangler, E.; Ingram, D. K. Caloric restriction attenuates amyloid deposition in middle-aged dtg APP/PS1 mice. *Neurosci. Lett.* **2009**, *464* (3), 184–187. DOI: 10.1016/j.neulet.2009.08.038. Published Online: Aug. 20, 2009.

(49) Patel, N. V.; Gordon, M. N.; Connor, K. E.; Good, R. A.; Engelman, R. W.; Mason, J.; Morgan, D. G.; Morgan, T. E.; Finch, C. E. Caloric restriction attenuates Abeta-deposition in Alzheimer transgenic models. *Neurobiol. Aging* **2005**, *26* (7), 995–1000. DOI: 10.1016/j.neurobiolaging.2004.09.014. Published Online: Nov. 25, 2004.

(50) Schafer, M. J.; Alldred, M. J.; Lee, S. H.; Calhoun, M. E.; Petkova, E.; Mathews, P. M.; Ginsberg, S. D. Reduction of β-amyloid and γ-secretase by calorie restriction in female Tg2576 mice. *Neurobiol. Aging* **2015**, *36* (3), 1293–1302. DOI: 10.1016/j.neurobiolaging.2014.10.043. Published Online: Dec. 4, 2014.

(51) Moreira, P. I.; Santos, R. X.; Zhu, X.; Lee, H.-g.; Smith, M. A.; Casadesus, G.; Perry, G. Autophagy in Alzheimer's disease. *Expert Rev. Neurother.* **2010**, *10* (7), 1209–1218. DOI: 10.1586/ern.10.84.

(52) Power Guerra, N.; Müller, L.; Pilz, K.; Glatzel, A.; Jenderny, D.; Janowitz, D.; Vollmar, B.; Kuhla, A. Dietary-Induced Low-Grade Inflammation in the Liver. *Biomedicines* **2020**, *8* (12). DOI: 10.3390/biomedicines8120587. Published Online: Dec. 9, 2020.

(53) Ulman, E. A. *The "Original" High-Fat Diets for Diet Induced Obesity*. https://www.weizmann.ac.il/vet/sites/vet/files/uploads/diet_d12451_d12492.pdf.

(54) Müller, L.; Power Guerra, N.; Stenzel, J.; Rühlmann, C.; Lindner, T.; Krause, B. J.; Vollmar, B.; Teipel, S.; Kuhla, A. Long-Term Caloric Restriction Attenuates β-Amyloid Neuropathology and Is Accompanied by Autophagy in APPswe/PS1delta9 Mice. *Nutrients* **2021**, *13* (3). DOI: 10.3390/nu13030985. Published Online: Mar. 18, 2021.

(55) Jankowsky, J. L.; Younkin, L. H.; Gonzales, V.; Fadale, D. J.; Slunt, H. H.; Lester, H. A.; Younkin, S. G.; Borchelt, D. R. Rodent A beta modulates the solubility and distribution of amyloid deposits in transgenic mice. *J. Biol. Chem.* **2007**, *282* (31), 22707–22720. DOI: 10.1074/jbc.M611050200. Published Online: Jun. 7, 2007.

(56) Xiong, H.; Callaghan, D.; Wodzinska, J.; Xu, J.; Premyslova, M.; Liu, Q.-Y.; Connelly, J.; Zhang, W. Biochemical and behavioral characterization of the double transgenic mouse model (APPswe/PS1dE9) of Alzheimer's disease. *Neurosci. Bull.* **2011**, *27* (4), 221–232. DOI: 10.1007/s12264-011-1015-7.

(57) Malm, T.; Koistinaho, J.; Kanninen, K. Utilization of APPswe/PS1dE9 Transgenic Mice in Research of Alzheimer's Disease: Focus on Gene Therapy and Cell-Based Therapy Applications. *Int. J. Alzheimers. Dis.* **2011**, *2011*, 517160. DOI: 10.4061/2011/517160. Published Online: Oct. 30, 2011.

(58) Power Guerra, N.; Parveen, A.; Bühler, D.; Brauer, D. L.; Müller, L.; Pilz, K.; Witt, M.; Glass, Ä.; Bajorat, R.; Janowitz, D.; Wolkenhauer, O.; Vollmar, B.; Kuhla, A. Fibroblast Growth Factor 21 as a Potential Biomarker for Improved Locomotion and Olfaction Detection Ability after Weight Reduction in Obese Mice. *Nutrients* **2021**, *13* (9), 2916. DOI: 10.3390/nu13092916.

(59) Marinho, R.; Munõz, V. R.; Pauli, L. S.S.; Ropelle, E. C.C.; Moura, L. P. de; Moraes, J. C.; Moura-Assis, A.; Cintra, D. E.; da Silva, A. S.R.; Ropelle, E. R.; Pauli, J. R. Endurance training prevents inflammation and apoptosis in hypothalamic neurons of obese mice. *J. Cell. Physiol.* **2018**, *234* (1), 880–890. DOI: 10.1002/jcp.26909.

(60) Chelminski, Y.; Magnan, C.; Luquet, S. H.; Everard, A.; Meunier, N.; Gurden, H.; Martin, C. Odor-Induced Neuronal Rhythms in the Olfactory Bulb Are Profoundly Modified in ob/ob Obese Mice. *Front. Physiol.* **2017**, *8*, 2. DOI: 10.3389/fphys.2017.00002.

(61) Dragotto, J.; Palladino, G.; Canterini, S.; Caporali, P.; Patil, R.; Fiorenza, M. T.; Erickson, R. P. Decreased neural stem cell proliferation and olfaction in mouse models of Niemann-Pick C1 disease and the response to hydroxypropyl-β-cyclodextrin. *J. Appl. Genet.* **2019**, *60* (3-4), 357–365. DOI: 10.1007/s13353-019-00517-8.

(62) Lehmkuhl, A. M.; Dirr, E. R.; Fleming, S. M. Olfactory Assays for Mouse Models of Neurodegenerative Disease. *J. Vis. Exp.* **2014** (90), e51804. DOI: 10.3791/51804.

(63) Komada, M.; Keizo, T.; Miyakawa, T. Elevated plus maze for mice. *J. Vis. Exp.* **2008** (22), 1088. DOI: 10.3791/1088.

(64) Rodgers, R. J.; Dalvi, A. Anxiety, Defence and the Elevated Plus-maze. PII: S0149-7634(96)00058-9. *Neurosci. Biobehav. Rev.* **1997**, *21* (6), 801–810. DOI: 10.1016/s0149-7634(96)00058-9.

(65) Lister, R. G. The use of a plus-maze to measure anxiety in the mouse. *Psychopharmacology* **1987**, *92* (2). DOI: 10.1007/BF00177912.

(66) Seibenhener, M. L.; Wooten, M. C. Use of the Open Field Maze to Measure Locomotor and Anxiety-like Behavior in Mice. *J. Vis. Exp.* **2015** (96). DOI: 10.3791/52434.

(67) KLEIBER, M. Body size and metabolic rate. *Physiol. Rev.* **1947**, *27* (4), 511–541. DOI: 10.1152/physrev.1947.27.4.511.

(68) Drake, C.; Boutin, H.; Jones, M. S.; Denes, A.; McColl, B. W.; Selvarajah, J. R.; Hulme, S.; Georgiou, R. F.; Hinz, R.; Gerhard, A.; Vail, A.; Prenant, C.; Julyan, P.; Maroy, R.; Brown, G.; Smigova, A.; Herholz, K.; Kassiou, M.; Crossman, D.; Francis, S.; Proctor, S. D.; Russell, J. C.; Hopkins, S. J.; Tyrrell, P. J.; Rothwell, N. J.; Allan, S. M. Brain inflammation is induced by co-morbidities and risk factors for stroke. *Brain Behav. Immun.* **2011**, *25* (6), 1113–1122. DOI: 10.1016/j.bbi.2011.02.008.

(69) Deleye, S.; Waldron, A.-M.; Richardson, J. C.; Schmidt, M.; Langlois, X.; Stroobants, S.; Staelens, S. The Effects of Physiological and Methodological Determinants on 18F-FDG Mouse Brain Imaging Exemplified in a Double Transgenic Alzheimer Model. *Molecular imaging* **2016**, *15.* DOI: 10.1177/1536012115624919.

(70) Park, H. R.; Park, M.; Choi, J.; Park, K.-Y.; Chung, H. Y.; Lee, J. A high-fat diet impairs neurogenesis: involvement of lipid peroxidation and brain-derived neurotrophic factor. *Neurosci. Lett.* **2010**, *482* (3), 235–239. DOI: 10.1016/j.neulet.2010.07.046. Published Online: Jul. 27, 2010.

(71) Gregosa, A.; Vinuesa, Á.; Todero, M. F.; Pomilio, C.; Rossi, S. P.; Bentivegna, M.; Presa, J.; Wenker, S.; Saravia, F.; Beauquis, J. Periodic dietary restriction ameliorates amyloid pathology and cognitive impairment in PDAPP-J20 mice: Potential implication of glial autophagy. *Neurobiol. Dis.* **2019**, *132*, 104542. DOI: 10.1016/j.nbd.2019.104542. Published Online: Jul. 24, 2019.

(72) Singh-Manoux, A.; Czernichow, S.; Elbaz, A.; Dugravot, A.; Sabia, S.; Hagger-Johnson, G.; Kaffashian, S.; Zins, M.; Brunner, E. J.; Nabi, H.; Kivimäki, M. Obesity phenotypes in midlife and cognition in early old age: the Whitehall II cohort study. *Neurology* **2012**, *79* (8), 755–762. DOI: 10.1212/WNL.0b013e3182661f63.

(73) Sikaris, K. A. The Clinical Biochemistry of Obesity. *Clin. Biochem. Rev.* **2004**, *25* (3), 165–181.

(74) van der Heijden, Roel A.; Sheedfar, F.; Morrison, M. C.; Hommelberg, P. P.H.; Kor, D.; Kloosterhuis, N. J.; Gruben, N.; Youssef, S. A.; Bruin, A. de; Hofker, M. H.; Kleemann, R.; Koonen, D. P.Y.; Heeringa, P. High-fat diet induced obesity primes inflammation in adipose tissue prior to liver in C57BL/6j mice. *Aging* **2015**, *7* (4), 256–268. DOI: 10.18632/aging.100738.

(75) Obstfeld, A. E.; Sugaru, E.; Thearle, M.; Francisco, A.-M.; Gayet, C.; Ginsberg, H. N.; Ables, E. V.; Ferrante, A. W. C-C Chemokine Receptor 2 (CCR2) Regulates the Hepatic Recruitment of Myeloid Cells That Promote Obesity-Induced Hepatic Steatosis. *Diabetes* **2010**, *59* (4), 916–925. DOI: 10.2337/db09-1403.

(76) Marques, P.; Collado, A.; Martinez-Hervás, S.; Domingo, E.; Benito, E.; Piqueras, L.; Real, J. T.; Ascaso, J. F.; Sanz, M.-J. Systemic Inflammation in Metabolic Syndrome: Increased Platelet and Leukocyte Activation, and Key Role of CX3CL1/CX3CR1 and CCL2/CCR2 Axes in Arterial Platelet-Proinflammatory Monocyte Adhesion. *J. Clin. Med.* **2019**, *8* (5). DOI: 10.3390/jcm8050708.

(77) Brendel, M.; Focke, C.; Blume, T.; Peters, F.; Deussing, M.; Probst, F.; Jaworska, A.; Overhoff, F.; Albert, N.; Lindner, S.; Ungern-Sternberg, B. von; Bartenstein, P.; Haass, C.; Kleinberger, G.; Herms, J.; Rominger, A. Time Courses of Cortical Glucose Metabolism and Microglial Activity Across the Life Span of Wild-Type Mice: A PET Study. *J. Nucl. Med.* **2017**, *58* (12), 1984--1990. DOI: 10.2967/jnumed.117.195107.

(78) Barron, A. M.; Tokunaga, M.; Zhang, M.-R.; Ji, B.; Suhara, T.; Higuchi, M. Assessment of neuroinflammation in a mouse model of obesity and β-amyloidosis using PET. *J Neuroinflammation* **2016**, *13* (1), 1–14. DOI: 10.1186/s12974-016-0700-x.

(79) Nerurkar, P. V.; Johns, L. M.; Buesa, L. M.; Kipyakwai, G.; Volper, E.; Sato, R.; Shah, P.; Feher, D.; Williams, P. G.; Nerurkar, V. R. Momordica charantia (bitter melon) attenuates high-fat diet-associated oxidative stress and neuroinflammation. *J. Neuroinflammation* **2011**, *8*, 64. DOI: 10.1186/1742-2094-8-64. Published Online: Jun. 3, 2011.

(80) Dong, W.; Wang, R.; Ma, L.-N.; Xu, B.-L.; Zhang, J.-S.; Zhao, Z.-W.; Wang, Y.-L.; Zhang, X. Influence of age-related learning and memory capacity of mice: different effects of a high and low caloric diet. *Aging Clin. Exp. Res.* **2016**, *28* (2), 303–311. DOI: 10.1007/s40520-015-0398-0. Published Online: Jul. 3, 2015.

(81) Lilienbaum, A. Relationship between the proteasomal system and autophagy. *Int. J. Biochem. Mol. Biol.* **2013**, *4* (1), 1–26.

(82) Speakman, J. R.; Mitchell, S. E. Caloric restriction. *Mol. Aspects Med.* **2011**, *32* (3), 159–221. DOI: 10.1016/j.mam.2011.07.001. Published Online: Aug. 10, 2011.

(83) Lee, Y.-R.; Wu, S.-Y.; Chen, R.-Y.; Lin, Y.-S.; Yeh, T.-M.; Liu, H.-S. Regulation of autophagy, glucose uptake, and glycolysis under dengue virus infection. *Kaohsiung J. Med. Sci.* **2020**, *36* (11), 911–919. DOI: 10.1002/kjm2.12271. Published Online: Aug. 12, 2020.

(84) Astrup, A. The role of dietary fat in the prevention and treatment of obesity. Efficacy and safety of low-fat diets. *Int. J. Obes. Relat. Metab. Disord.* **2001**, *25 Suppl 1*, S46-50. DOI: 10.1038/sj.ijo.0801698.

(85) Laing, B. T.; Do, K.; Matsubara, T.; Wert, D. W.; Avery, M. J.; Langdon, E. M.; Zheng, D.; Huang, H. Voluntary exercise improves hypothalamic and metabolic function in obese mice. *J. Endocrinol.* **2016**, *229* (2), 109–122. DOI: 10.1530/JOE-15-0510.

(86) Yang, W.; Liu, L.; Wei, Y.; Fang, C.; Zhou, F.; Chen, J.; Han, Q.; Huang, M.; Tan, X.; Liu, Q.; Pan, Q.; Zhang, L.; Lei, X.; Li, L. Exercise ameliorates the FGF21-adiponectin axis impairment in diet-induced obese mice. *Endocr. Connect.* **2019**, *8* (5), 596–604. DOI: 10.1530/EC-19-0034.

(87) Ringseis, R.; Mooren, F.-C.; Keller, J.; Couturier, A.; Wen, G.; Hirche, F.; Stangl, G. I.; Eder, K.; Krüger, K. Regular endurance exercise improves the diminished hepatic carnitine status in mice fed a high-fat diet. *Mol. Nutr. Food Res.* **2011**, *55 Suppl 2*, S193-202. DOI: 10.1002/mnfr.201100040. Published Online: Jul. 19, 2011.

(88) Poole, D. C.; Copp, S. W.; Colburn, T. D.; Craig, J. C.; Allen, D. L.; Sturek, M.; O'Leary, D. S.; Zucker, I. H.; Musch, T. I. Guidelines for animal exercise and training protocols for cardiovascular studies. *Am. J. Physiol. Heart Circ. Physiol.* **2020**, *318* (5), H1100-H1138. DOI: 10.1152/ajpheart.00697.2019. Published Online: Mar. 20, 2020.

(89) Duval, C.; Thissen, U.; Keshtkar, S.; Accart, B.; Stienstra, R.; Boekschoten, M. V.; Roskams, T.; Kersten, S.; Müller, M. Adipose tissue dysfunction signals progression of hepatic steatosis towards nonalcoholic steatohepatitis in C57BL/6 mice. *Diabetes* **2010**, *59* (12), 3181–3191. DOI: 10.2337/db10-0224. Published Online: Sep. 21, 2010.

(90) Velázquez, K. T.; Enos, R. T.; Bader, J. E.; Sougiannis, A. T.; Carson, M. S.; Chatzistamou, I.; Carson, J. A.; Nagarkatti, P. S.; Nagarkatti, M.; Murphy, E. A. Prolonged high-fat-diet feeding promotes non-alcoholic fatty liver disease and alters gut microbiota in mice. *World J. Hepatol.* **2019**, *11* (8), 619–637. DOI: 10.4254/wjh.v11.i8.619.

(91) Forsythe, L. K.; Wallace, J. M. W.; Livingstone, M. B. E. Obesity and inflammation: the effects of weight loss. *Nutr. Res. Rev.* **2008**, *21* (2), 117–133. DOI: 10.1017/S0954422408138732.

(92) Gálvez, I.; Navarro, M. C.; Martín-Cordero, L.; Otero, E.; Hinchado, M. D.; Ortega, E. The Influence of Obesity and Weight Loss on the Bioregulation of Innate/Inflammatory Responses: Macrophages and Immunometabolism. *Nutrients* **2022**, *14* (3), 612. DOI: 10.3390/nu14030612.

(93) Hotamisligil, G. S. Inflammation, metaflammation and immunometabolic disorders. *Nature* **2017**, *542* (7640), 177–185. DOI: 10.1038/nature21363.

(94) Babaknejad, N.; Nayeri, H.; Hemmati, R.; Bahrami, S.; Esmaillzadeh, A. An Overview of FGF19 and FGF21: The Therapeutic Role in the Treatment of the Metabolic Disorders and Obesity. *Horm. Metab. Res.* **2018**, *50* (6), 441–452. DOI: 10.1055/a-0623-2909. Published Online: Jun. 8, 2018.

(95) Cantó, C.; Auwerx, J. Cell biology. FGF21 takes a fat bite. *Science (New York, N.Y.)* **2012**, *336* (6082), 675–676. DOI: 10.1126/science.1222646.

(96) Salminen, A.; Kaarniranta, K.; Kauppinen, A. Regulation of longevity by FGF21: Interaction between energy metabolism and stress responses. *Ageing Res. Rev.* **2017**, *37*, 79–93. DOI: 10.1016/j.arr.2017.05.004. Published Online: May. 25, 2017.

(97) Keipert, S.; Lutter, D.; Schroeder, B. O.; Brandt, D.; Ståhlman, M.; Schwarzmayr, T.; Graf, E.; Fuchs, H.; Angelis, M. H. de; Tschöp, M. H.; Rozman, J.; Jastroch, M. Endogenous FGF21-signaling controls paradoxical obesity resistance of UCP1-deficient mice. *Nat. Commun.* **2020**, *11* (1), 624. DOI: 10.1038/s41467-019-14069-2. Published Online: Jan. 31, 2020.

(98) Samms, R. J.; Cheng, C. C.; Kharitonenkov, A.; Gimeno, R. E.; Adams, A. C. Overexpression of β-Klotho in Adipose Tissue Sensitizes Male Mice to Endogenous FGF21 and Provides Protection From Diet-Induced Obesity. *Endocrinology* **2016**, *157* (4), 1467–1480. DOI: 10.1210/en.2015-1722. Published Online: Feb. 22, 2016.

(99) Chaix, A.; Zarrinpar, A.; Miu, P.; Panda, S. Time-restricted feeding is a preventative and therapeutic intervention against diverse nutritional challenges. *Cell Metab.* **2014**, *20* (6), 991–1005. DOI: 10.1016/j.cmet.2014.11.001.

(100) Chaix, A.; Lin, T.; Le, H. D.; Chang, M. W.; Panda, S. Time-Restricted Feeding Prevents Obesity and Metabolic Syndrome in Mice Lacking a Circadian Clock. *Cell Metab.* **2019**, *29* (2), 303-319.e4. DOI: 10.1016/j.cmet.2018.08.004. Published Online: Aug. 30, 2018.

(101) Chapnik, N.; Genzer, Y.; Froy, O. Relationship between FGF21 and UCP1 levels under time-restricted feeding and high-fat diet. *J. Nutr. Biochem.* **2017**, *40*, 116–121. DOI: 10.1016/j.jnutbio.2016.10.017. Published Online: Nov. 2, 2016.

(102) Anderson, E.; Shivakumar, G. Effects of exercise and physical activity on anxiety. *Front. Psychiatry* **2013**, *4*, 27. DOI: 10.3389/fpsyt.2013.00027. Published Online: Apr. 23, 2013.

(103) Droste, S. K.; Gesing, A.; Ulbricht, S.; Müller, M. B.; Linthorst, A. C. E.; Reul, J. M. H. M. Effects of long-term voluntary exercise on the mouse hypothalamic-pituitary-adrenocortical axis. *Endocrinology* **2003**, *144* (7), 3012–3023. DOI: 10.1210/en.2003-0097.

(104) Martínez-Garza, Ú.; Torres-Oteros, D.; Yarritu-Gallego, A.; Marrero, P. F.; Haro, D.; Relat, J. Fibroblast Growth Factor 21 and the Adaptive Response to Nutritional Challenges. *Int. J. Mol. Sci.* **2019**, *20* (19). DOI: 10.3390/ijms20194692. Published Online: Sep. 21, 2019.

(105) Hui, X.; Feng, T.; Liu, Q.; Gao, Y.; Xu, A. The FGF21-adiponectin axis in controlling energy and vascular homeostasis. *J. Mol. Cell Biol.* **2016**, *8* (2), 110–119. DOI: 10.1093/jmcb/mjw013. Published Online: Mar. 18, 2016.

VIII. Abkürzungsverzeichnis

AL	*ad libitum*
Aβ	Amyloid β
CAE	Naphthol-AS-D-Chloracetatesterase-Färbung
[^{18}F]–FDG	[^{18}F]–Fluordesoxyglucose
FGF21	fibroblast growth factor 21
FS	feature selection
GE-180	[^{18}F]-translocator protein (TSPO)
H&E	Hämatoxylin-Eosin
HFD	Hoch-Fett-Diät (engl. high-fat diet)
HPA	Hypothalamus-Hypophysen-Nebenniere (engl. hypothalamus-pituitary-adrenal)
IL-6	Interleukin 6
IL-1β	Interleukin 1β
KD	Kontroll Diät
KR	Kalorienrestriktion
LB	Laufband
MR	Massenspektroskopie
MRT	Magnetresonanztomographie
MWM	Morris-Water Maze
NAFLD	nichtalkoholische Fettlebererkrankung (engl. non-alcoholic fatty liver disease)
NAS	NAFLD Activity Score
NFD	Niedrig-Fett Diät (engl. low-fat diet, LFD)
SD	Standard Diät
sd	Standardabweichung (engl. standard deviation)
SUV	Standard Uptake Value
tg	transgen
tm	theoretical medians
TNFα	Tumornekrosefaktor α
TRF	time-restricted feeding
TSPO	translocator protein
wt	Wildtyp

X. Publikationsverzeichnis

peer-reviewed Publikationen

Power Guerra, N.; Parveen, A.; Bühler, D.; Brauer, D.L.; Müller, L.; Pilz, K.; Witt, M.; Glass, Ä.; Bajorat, R.; Janowitz, D.; Wolkenhauer, O.; Vollmar, B.; Kuhla, A. Fibroblast growth factor 21 as a potential biomarker for improved locomotion and olfaction detection ability after weight reduction in obese mice. *Nutrients* **2021**, 13(9), 2916. https://doi.org/10.3390/nu13092916.

Müller, L., **Power Guerra, N**., Stenzel, J., Rühlmann, C., Lindner, T., Krause, B. J., Vollmar, B., Teipel, S. y Kuhla, A. Long-term caloric restriction attenuates β-amyloid neuropathology and is accompanied by autophagy in APPswe/PS1delta9 mice. *Nutrients* **2021**, 13(3). https://doi.org/10.3390/nu13030985.

Power Guerra, N.; Müller, L.; Pilz, K.; Glatzel, A.; Jenderny, D.; Janowitz, D.; Vollmar, B.; Kuhla, A. Dietary-induced low-grade inflammation in the liver. *Biomedicines* **2020**, 8(12). https://doi.org/10.3390/biomedicines8120587

Schmale, O.; Krause, S.; Holtermann, P.; **Power Guerra, N.C.**; Umlauf, L. Dense bottom gravity currents and their impact on pelagic methanotrophy at oxic/anoxic transition zones. *Geophys. Res. Lett*. **2016**; 43, 5225–5232, https://doi.org/10.1002/2016GL069032.

XI. Danksagung

Ich bedanke mich aus tiefsten Herzen bei allen, die mich während meiner Promotion begleitet haben, sowohl beruflich als auch privat, denn eine Doktorarbeit bleibt doch immer eine Teamarbeit, die ohne euch nicht möglich gewesen wäre.

Allen voran möchte ich mich bei meiner Doktormutter Prof. Dr. Angela Kuhla (Angie) bedanken, die mir meine Doktorarbeit durch ihre innovativen und interessanten Projektideen überhaupt erst ermöglichte. Mit ihrer ständigen Hilfsbereitschaft, ihren wertvollen empathischen Fähigkeiten, ihrer Geduld und ihrem grenzenlosen Vertrauen in meine Fähigkeiten trug sie entscheidend zum Erfolg meiner Promotion bei. Dabei stand Angela nicht nur beratend für fachliche und persönliche Gespräche zur Seite, sondern formte mich zu jener Wissenschaftlerin, die ich heute voller Stolz sein kann. Vielen Dank für diesen wertvollen Lebensabschnitt, den ich mit ihr teilen durfte.

Ich bedanke mich von ganzem Herzen bei meinem Partner Friis Kock, der seit wir uns kennen, an meiner Seite war und für mich immer mein Ruhepol und mein Rückzugsort ist.

Ein besonderer Dank geht an Prof. Dr. Martin Witt, der mich erst an Angela vermittelte und mir die Möglichkeit bot, diesen Weg beschreiten zu können. Sein Vertrauen in meine Fähigkeiten, seine Unterstützung und sein offenes Ohr für mich ermöglichte mir den Abschluss dieser Promotionsarbeit. Durch sein Engagement nahm er mich am Ende meiner Promotionszeit herzlich in sein Team auf, wobei ich mich für meinen beruflichen Werdegang weiterentwickeln durfte.

Ein großer Dank geht an Prof. Dr. Brigitte Vollmar, die mir die Möglichkeit gab, am IEC zu promovieren und mich so herzlich in ihr Team aufgenommen hat. Dank ihrer konstruktiven und ehrlichen Kritik sowie ihrer ständigen Unterstützung habe ich mich während meiner Promotion nicht nur wissenschaftlich, sondern auch persönlich weiterentwickelt. Weiterhin bedanke ich mich bei Prof. Dr. Dr. Markus Kipp, der mich am Ende meiner Promotionszeit in der Anatomie beschäftigte und mich mit einem zukunftsorientierten Team unterstützte.

Außerdem möchte ich mich herzlichst beim gesamten Team des Instituts für Experimentelle Chirurgie, der Zentralen Versuchstierhaltung und der Multimodalen Kleintierbildgebung für die fachliche Unterstützung, das hervorragende Arbeitsklima und die vielen schönen Momente bedanken! Danke an Kerstin Abshagen und Dietmar Zechner für die zahlreichen Gespräche, aus denen viele gute Ideen hervorgegangen sind; an Tobias Lindner, Jan Stenzel, Anna Schildt, Joanna Förster und Anne Möller für die hervorragende Leistung, um die vielen Tiere bildgebungstechnisch aufzunehmen, zu betreuen und für die Expertise bei der Datenauswertung; an Berit Blendow, Dorothea Frenz, Eva Lorbeer, Maren Nerowski und Sabine Glaublitz für die hervorragende Unterstützung und Durchführung im Labor; an Anja

Gellert für ihre endlose Unterstützung bei allen Problemen (nicht nur die Arbeitsverträge), an Henrike Seydel für ihre Hilfsbereitschaft; an Andrea Wilhelm, Chantal von Hörsten, Ilona Klamfuß, Karin Gerber, Klaus Russow, Mareike Degner, Petra Wolff, Reinhard Schwärmer und Roland Gerber für die Pflege meiner Tiere, die Hilfe bei den tierexperimentellen Arbeiten und der Fastenexperimente. Meine Promotion wäre ohne euch und eure tatkräftige, fachkundige und professionelle Arbeit nicht möglich gewesen.

Ein großer Dank geht auch an alle gegenwärtigen und alten Mitglieder der AG Kuhla mit Theresa Renken, David Dannehl, Marcus Brodtrück, Mohammad Sreij, Alexander Kaiser, Franziska Eyo, Claire Rühlmann, Katarina Leyens und Annika Glatzel, die durch ihr Engagement maßgeblich zur erfolgreichen Bearbeitung der Projekte und zu den Veröffentlichungen der Ergebnisse beigetragen haben.

Ein großer Dank geht auch an das Team der Anatomie, die mich sehr herzlich in ihre Reihen aufgenommen haben.

Wie das mit der Arbeit so ist, werden Arbeitskolleg:innen zu Mitstreiter:innen und zu Freund:innen, sodass sich das nicht mehr trennen lässt. Daher möchte ich mich bei Marie Liebig, Simone Kumstel, Luisa Müller, Wiebke Nierath, Tim Schreiber, Benjamin Schulz, Wentao Xie, Sadaf (Sadi) Gill, Linda Frintrop, Daniel (David) Bühler, Lina Krysewski, Janett (Jette) Herold, Sebastian (Basti) Hoyer, Marcel (Celli) Behse, Jannis Reuter, Alessandra (Lexy) Noack, Marvin Blum, Marina Kalb, Theresa Proissl, Isabelle (Isi) Wochner, Fin Quante, Katrin Fender, Lilly und Venzi Petkov, Wolf Berger und Melissa Yunus bedanken. Ihr habt dazu beigetragen, dass meine Promotionszeit so wunderschön geworden ist, sei es durch schöne Städtetrips, durch Festivals, durch nächtliche Aktivitäten, durch stundenlange Spieletage, durch Filmabende oder einfach durch gemütliche Abende auf der Couch. Und dabei hattet ihr immer ein offenes Ohr für mich und habt mich immer unterstützt.

Ein wichtige Säule während meiner Promotionsarbeit war das Tanzen im Tanzland und im Ballettstudio Dance. Ich möchte mich bei den Lehrer:innen Lilly, Briddie, Anton, Daniele, Peter, Amrey und Josh bedanken, die durch ihre Herzlichkeit, ihr Können und ihren Witz immer wunderschöne Stunden gezaubert haben. Dabei habt ihr immer sehr tolerant meine Unpünktlichkeit hingenommen und mich tänzerisch sehr gefördert. Und ich möchte mich bei allen Tänzer:innen der beiden Tanzschulen bedanken. Ich hatte mit euch sehr viel Spaß.

Am Ende möchte ich mich von ganzem Herzen bei meiner Familie bedanken, die durch Friis Kock auch an Zuwachs gewonnen hat, nämlich bei George Power, Nelly und Rolly Dölling, Erika, Sebi, Josua und Elli Lingk; Christian, Maja, Lukas, Selina Power(-Quint); Tobi, Maria und Justus Dölling; bei Marita und Hajo (Willamowski-)Kock; Jenny Kock, Lasse, Fenja und Yannick Stahnke. Ich bedanke mich für eure Unterstützung, für euer offenes Ohr und für die tolle Gemeinschaft.

XII. Selbstständigkeitserklärung

Hiermit versichere ich, dass ich die vorliegende Dissertation selbstständig und ohne fremde Hilfe verfasst habe, keine anderen als die von mir angegeben Quellen und Hilfsmittel verwendet habe und die den benutzten Quellen wörtlich oder inhaltlich entnommenen Stellen als solche kenntlich gemacht habe.

Rostock, den _____

_____
Nicole Power Guerra

XIII. Anhang

Anhang1: Studie IV: Histologische Bilder

Anhang 2: Studie I

Anhang 3: Studie III

Anhang 4: Studie V

Anhang 1

Zu Studie IV: H&E-Färbungen der Leber, 4x Objektiv, Maßstabbalken 500 µm

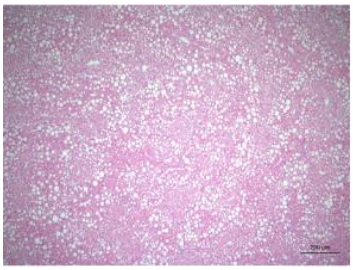

HFD/HFD

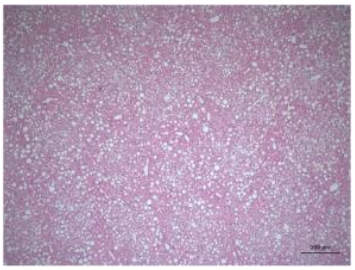

HFD/HFD+LB

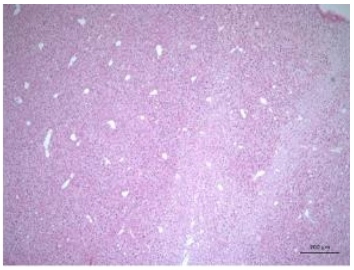

HFD/HFD+LB+TRF

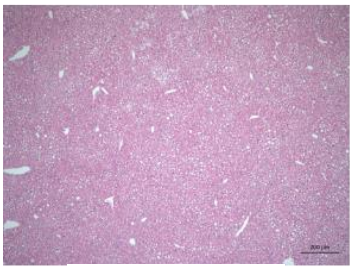

HFD/NFD

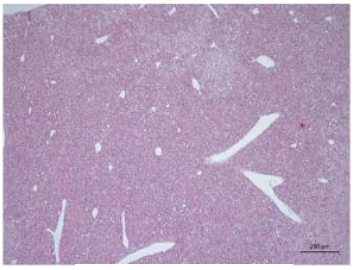

HFD/NFD+LB

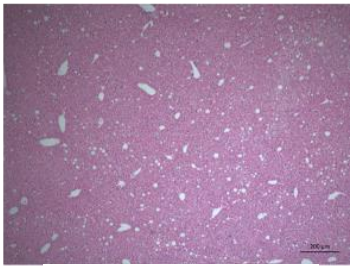

HFD/NFD+LB+TRF

Anhang 2

Studie I:

Power Guerra, N.; Müller, L.; Pilz, K.; Glatzel, A.; Jenderny, D.; Janowitz, D.; Vollmar, B.; Kuhla, A. Dietary-Induced Low-Grade Inflammation in the Liver. *Biomedicines* **2020**, 8(12). https://doi.org/10.3390/biomedicines8120587.

biomedicines

MDPI

Article

Dietary-Induced Low-Grade Inflammation in the Liver

Nicole Power Guerra [1], Luisa Müller [1,2], Kristin Pilz [3], Annika Glatzel [1], Daniel Jenderny [1], Deborah Janowitz [3], Brigitte Vollmar [1] and Angela Kuhla [1,*]

[1] Rudolf-Zenker-Institute for Experimental Surgery, Medical University Rostock, 18057 Rostock, Germany; nicole.guerra@uni-rostock.de (N.P.G.); luisa.mueller2@uni-rostock.de (L.M.); annika.glatzel@uni-rostock.de (A.G.); daniel.jenderny@uni-rostock.de (D.J.); brigitte.vollmar@med.uni-rostock.de (B.V.)

[2] Department of Psychosomatic Medicine and Psychotherapy, University of Rostock, 18147 Rostock, Germany

[3] Department of Psychiatry, University of Greifswald, 17489 Greifswald, Germany; kristin.pilz@med.uni-greifswald.de (K.P.); deborah.janowitz@med.uni-greifswald.de (D.J.)

* Correspondence: angela.kuhla@uni-rostock.de; Tel.: +49-381-494-2503

Received: 19 October 2020; Accepted: 7 December 2020; Published: 9 December 2020

Abstract: The literature describes a close correlation between metabolic disorders and abnormal immune responses, like low-grade inflammation (LGI), which may be one mechanistic link between obesity and various comorbidities, including non-alcoholic fatty liver disease (NAFLD). In our study, we investigated the influence of dietary composition on obesity-derived LGI in the liver. We used a dietary induced obesity mouse model of C57BL/6J mice fed with high fat diet (HFD, 60% fat, 20% protein, 20% carbohydrates) and two different controls. One was rich in carbohydrates (10% fat, 20% protein, 70% carbohydrates), further referred to as the control diet (CD), and the other one is referred to as the standard diet (SD), with a more balanced macronutrient content (9% fat, 33% protein, 58% carbohydrates). Our results showed a significant increased NAFLD activity score in HFD compared to both controls, but livers of the CD group also differed in their macroscopic appearance from healthy livers. Hepatic fat content showed significantly elevated cholesterol concentrations in the CD group. Histologic analysis of the cellular immune response in the liver showed no difference between HFD and CD and expression analysis of immunologic mediators like interleukin (IL)-1β, IL-6, IL-10 and tumor necrosis factor alpha also point towards a pro-inflammatory response to CD, comparable to LGI in HFD. Therefore, when studying diet-induced obesity with a focus on inflammatory processes, we encourage researchers to carefully select controls and not use a control diet disproportionally rich in carbohydrates.

Keywords: high fat diet; control diet; non-alcoholic fatty liver disease; liver inflammation; low-grade inflammation

1. Introduction

Abnormal and excessive accumulation of adipose tissue in the context of severe overweight and obesity is one of the most challenging diseases of the 21st century. This is primarily due to the steadily increasing number of obese patients who are getting younger and younger [1]. In addition to a wide variety of cultural and social influences and a lack of exercise, a permanent oversupply of food rich in calories, and mostly also in fat, leads to weight gain with serious health issues.

As a consequence, obesity is one of the leading causes of the metabolic syndrome, which was described in 1989 by Kaplan [2]. The metabolic syndrome is associated with many other diseases [3,4] including non-alcoholic fatty liver disease (NAFLD), which is seen as the hepatic manifestation of

it [5]. One assumed reason for the prevalence of NAFLD and many other concomitant and secondary diseases of obesity is the persistence of systemic low-grade inflammation (LGI), starting from adipose tissue. However, there is no strict definition of LGI. In general, dietary-induced LGI is a sterile inflammation, which has also been given the name "metaflammation" (an inflammation of metabolic tissue) [3], which is highly entwined with immunometabolism [6]. Since the LGI differs in its triggering mechanisms from an infectious inflammation, both also likely differ in their consequences. While infectious inflammation in its physiological function triggers an immune response of the organism, sterile inflammation has predominantly pathological consequences, e.g., via the alteration of homeostatic checkpoints and the development of autoinflammatory disorders [7].

Interestingly, a close correlation between metabolic diseases and abnormal immune responses such as LGI is observed [3,8]. White adipose tissue is capable of expressing both, metabolic and immunological mediators [9], whose effects are not only local but can affect other organs like the liver or have a systemic impact. This is also shown by a generalized moderate upregulation of pro-inflammatory signaling cascades in overweight and obesity. Important mediators in this context include interleukin (IL)-1β, IL-6 and tumor necrosis factor alpha (TNFα) [10–12]. Moreover, a downregulation of anti-inflammatory mediators such as IL-10 has been reported [12]. All of the above mentioned mediators take part in well-orchestrated and tightly regulated signaling cascades and derailments of them may be responsible for a LGI-mediated interaction between obesity and NAFLD [13,14]. However, which long-term influences in the diet are present, defined as at least 6 months of corresponding diet, on obesity-derived LGI in the liver has not yet been investigated in detail in mice.

A diet-induced obesity mouse model consisting of a 60% high fat diet (HFD) is used in this project to observe the effects of obesity-derived LGI on the liver. As an additional approach, we wanted to investigate the impact of dietary composition of two different low-fat controls on the liver, with a special focus on LGI. One control group received the HFD-manufacturers recommended control diet (CD), broadly used in research [15–18]. This CD matches the HFD regarding sucrose content (as a percent of calories) and fiber structure but has generally a high carbohydrate content and in particular a high starch content ([19]; Product Data—DIO Series Diets, Research Diets Inc., Lane, NJ, USA). As the literature hints towards the role of carbohydrate-rich diets as promotors of systemic LGI, e.g., by oxidative stress induction [20,21], it would be of high interest to have a closer look if this mechanism affects the liver as well. In contrast, the literature suggests that protein-rich diets have anti-inflammatory effects and also reduce liver fat [22], which is an important note when considering studying dietary-induced effects of LGI on the liver. Therefore, the other control group received the in-house standard diet (SD) with matched calorie content to CD but lower carbohydrate content and increased protein content compared to CD and HFD.

2. Experimental Section

2.1. Animal Models

For the experiments, female C57BL/6J mice at the age of 4 weeks were purchased from Charles River (Sulzfeld, Germany). In compliance with our own previous and ongoing investigations, female mice were used for comparability between different studies. Mice were kept in standard cages with 4 to 5 animals per cage, in a temperature controlled room (21 ± 3 °C) with a 12/12 h day-night cycle (lights on from 06:00 am to 06:00 pm CET) containing a twilight period of 30 minutes. The mice were blindly divided into three groups, which were fed different diets and water supply ad libitum over a period of 6 months. After one week of acclimatization, the food was adjusted to the corresponding diet, with designated compositions shown in Figure 1. One group received an HFD (D12492; Research Diets Inc., Lane, NJ, USA), hereinafter referred to as the HFD group (n = 31). The other group received the recommended CD (D12450J; Research Diets Inc., Lane, NJ, USA), hereinafter referred to as the

CD group (n = 16). The third group received SD (ssniff® R/M-H, ssniff Spezialdiäten GmbH, Soest, Germany) and is hereinafter referred to as the SD group (n = 15).

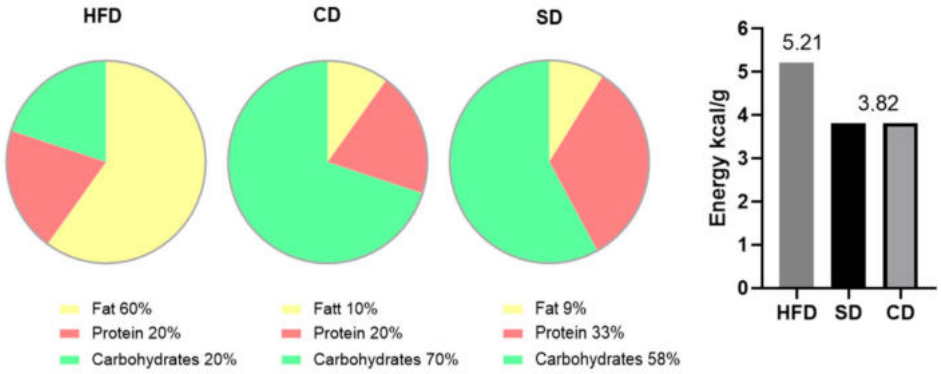

Figure 1. Composition of high fat diet (HFD), control diet (CD) and standard diet (SD) in % of total calories and energy density in kcal/g.

All animal experimental work was carried out with permission of the local Animal Research Committee (Landesamt für Landwirtschaft, Lebensmittelsicherheit und Fischerei (LALLF)) of the state Mecklenburg-Western Pomerania (LALLF M-V/TSD/7221.3-2-001/18, approved on 1 March 2018) and all animals received human care according to the EU Directive 2010/63/EU.

2.2. Blood Sampling and Tissue Preparation

Mice were anaesthetized with 5 vol.% isoflurane (Baxter, Unterschleißheim, Germany), 0.8 L/min O_2 (Air Liquide, Hamburg, Germany) and 1.25 L/min N_2O (Air Liquide, Hamburg, Germany) and blood was taken retrobulbary to exsanguinate the mice. Blood samples were kept at 4 °C until plasma preparation the same day. Therefore, samples were centrifuged at 1200 rpm and 6 °C for 10 min (Centrifuge 5424, Eppendorf, Leipzig, Germany) and supernatant was collected and stored at −80 °C. Then, mice were transcardially perfused with 20–25 mL 0.9% NaCl (Braun, Melsungen Germany) with an estimated flow rate of 2.28–2.83 mL/min. For histological and immunohistochemical analysis, the left lateral liver lobe was dissected and fixed in 4% paraformaldehyde (PFA, ChemCruz, Dallas, TX, USA) solution for five days, embedded in paraffin (Carl Roth, Karlsruhe, Germany) and sectioned in 4 µm thin tissue slices. For molecular analysis, the remaining liver was homogenized and snap frozen in liquid nitrogen and stored at −80 °C.

2.3. Biochemistry

Directly after blood collection, blood sugar concentration in the naive blood sample was assessed with the glucose meter Contour®XT (Bayer, Leverkusen, Germany) according to the manufacturer´s instructions. In the stored plasma samples, aspartate aminotransferase (AST) and alanine aminotransferase (ALT) activities were measured spectrophotometrically as indicators of hepatocellular disintegration and necrosis. The extinction at 340/378 nm was measured with the cobas®c111Analyzer (Roche Diagnostics GmbH, Penzberg, Germany). Measurement of plasma triglycerides was performed using Triglyceride Colorimetric Assay Kit (Nr.: 10010303, Cayman Chemical Company, Hamburg, Germany) according to the manufacturer's instructions. Results are provided in the Supplementary Materials (Table S1).

2.4. Histology, Immunohistochemistry and Image Analysis

Hematoxylin (Merck, Darmstadt, Germany) and eosin (Merck, Darmstadt, Germany) (H&E) staining was performed using standard protocols. Pictures were recorded on a microscope type BX51 with a Color View Soft Imaging System and the corresponding software cellSens Standard 1.14 (all from Olympus, Hamburg, Germany).

From the H&E stained specimens, analyses of tissue content of microvesicular fat was performed using the public domain image analysis software ImageJ (v.1.47) (protocol provided in the supplements as ImageJ Code S1). Furthermore, a NAFLD Activity Score (NAS) was generated to characterize diet-induced liver damage. Following the description by Kleiner et al. [23], the parameters steatosis (score 0–3), hepatocellular ballooning (score 0–2) and lobular inflammation (score 0–3) were used to calculate NAS (total score 0–8). Steatosis was assessed at 50× magnification and ballooning at 100× magnification. Inflammation was assessed by counting inflammatory foci from 20 representative low-power fields (LPF) (200× magnification) with an inflammatory focus characterized as a grouping of at least five inflammatory cells in the tissue, which are not arranged in a row [24]. Examples for the different assigned scores are provided as representative images in the supplements (Figure S1).

For assessment of tissue infiltration of granulocytes as another hallmark of manifestation of LGI in the liver, sectioned paraffin-embedded liver tissue was stained for chloracetate esterase (CAE) with Naphthol AS-D chloroacetate (Sigma-Aldrich, Darmstadt, Germany) and counterstained with hematoxylin (Merck, Darmstadt, Germany). For quantification, the total number of hepatocytes and CAE positive cells (CAE^+) was counted in 20 consecutive high-power fields (HPF) at 400× magnification.

As a second cellular indicator for LGI in the liver, macrophages were stained immunohistochemically. Therefore, overnight incubation (4 °C) with the first antibody (rat anti mouse-F4/80 [MCA497] from Bio-Rad, Hercules, CA, USA) was followed by 1 h incubation at room temperature with the secondary antibody (goat anti rat [MCA497] from Bio-Rad, Hercules, CA, USA) stained with the chromogen Permanent Red (Ref. K0640, DAKO GmbH, Jena, Germany) and counterstained with hematoxylin (Merck, Darmstadt, Germany). For quantification, the total number of hepatocytes was counted in 20 consecutive HPF at 400× magnification and semiautomatic quantification of F4/80 positive cells ($F4/80^+$) was performed via ImageJ (protocol provided in the supplements as ImageJ Code S2).

2.5. Cholesterol Assay

For assessment of hepatic cholesterol content, Cholesterol Quantitation Kit (Calbiochem®, Merck, Darmstadt, Germany) was performed according to manufacturer instructions from 30 µg snap frozen liver tissue.

2.6. Quantitative Real-Time PCR

RNA isolation from snap frozen liver tissue was performed with RNeasy Mini Kit (Qiagen, Venlo, The Netherlands) according to the manufacturer's instructions. RNA integrity was verified by agarose gel electrophoresis and RNA concentration was assessed by absorption measurement with NanoDrop (Thermo Fisher Scientific, Waltham MA, USA). Isolated RNA was transcribed into cDNA with SuperScript™ (Invitrogen, Thermo Fisher Scientific, Waltham MA, USA) and deoxyribonucleosidtriphosphates (Thermo Fisher Scientific, Waltham, MA, USA) were added. Cytokine analyses were performed via quantitative real-time PCR in a BioRad iQ5 Multicolor Real Time PCR Detection System (Conquer Scientific, San Diego, CA, USA) with iQ™ SYBR® Green Supermix (Bio-Rad, Hercules, CA, USA). Primer sequences are shown in Table 1. Measurement results are corrected against the housekeeping gene 40S ribosomal protein S18 (RPS18) and relative quantification was carried out by usage of the $2^{-\Delta\Delta CT}$ method.

2.7. Statistical Analysis

Statistical analysis was performed using GraphPad Prism 8.0.1 (GraphPad Software Inc., San Diego, CA, USA). Data were checked for normality with the Kolmogorov–Smirnov test (for scoring data) or Shapiro–Wilk test and variances of ANOVA were verified by Bartlett's test. If SDs were not significantly different with $p > 0.05$, an ordinary one-way ANOVA was performed followed by Turkey post hoc test, otherwise Brown–Forsythe and Welch ANOVA followed by Tamhane's T2 multiple comparisons test was performed. If data were not normally distributed, the Kruskal–Wallis test with Dunn's post

hoc test for multiple comparisons was conducted. Data are presented as mean ± standard deviation and statistical significance was set at $p < 0.05$. The ROUT method based on the false discovery rate (Q = 0.01) was used to identify and remove outliers if possible and necessary. For further details, see figure legends.

Table 1. Primers used for quantitative real-time PCR.

Primer	Orientation	Sequence
RPS18	Forward Reverse	5′-AGGATGTGAAGGATGGGAAG-3′ 5′-TTGGATACACCCACAGTTCG-3′
TNFα	Forward Reverse	5′-ACATTCGAGGCTCCAGTGAATTCGG-3′ 5′-GGCAGGTCTACTTTGGAGTCATTGC-3′
IL-1β	Forward Reverse	5′-CCCAAGCAATACCCAAAGAA-3′ 5′-TTGTGAGGTGCTGATGTACCA-3′
IL-6	Forward Reverse	5′-TCTGACCACAGTGAGGAATGTCCAC-3′ 5′-TGGAGTCACAGAAGGAGTGGCTAAG-3′
IL-10	Forward Reverse	5′-GCCTTGCAGAAAAGAGAGCT-3′ 5′-AAAGAAAGTCTTCACCTGGC-3′

3. Results

3.1. Dietary Impact on Body and Liver Weight

After feeding the mice their respective diet for 6 months, their body weight was measured and liver tissue was collected for further analysis. Animals are shown as representative images (Figure 2a). Analysis of body weight revealed significantly elevated values in the HFD group (Figure 2b, $p < 0.0001$ vs. CD and SD group). Body weight did not differ between the CD and SD group (Figure 2b).

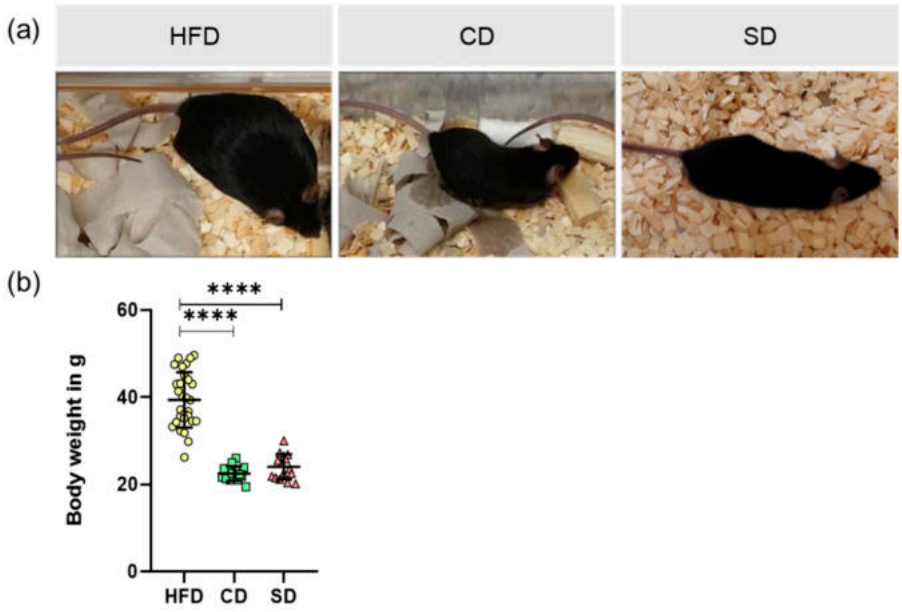

Figure 2. (**a**) Representative images of appearances from mice fed high fat diet (HFD), control diet (CD) or standard diet (SD); (**b**) Body weights of mice in the different groups (HFD: $n = 29$; CD: $n = 15$, SD: $n = 15$), presented as mean ± standard deviation. Significance of differences between the groups was tested by Brown–Forsythe and Welch ANOVA, **** $p < 0.0001$.

Macroscopic appearances of the livers in situ are shown as representative images (Figure 3a). While dissecting the liver, we noticed a visual deviation of both the HFD and CD group to a healthy looking liver as displayed by the SD group. Analysis of liver weight again revealed significantly elevated values in the HFD group (Figure 3b) ($p < 0.0001$ vs. CD group and $p = 0.013$ vs. SD group) and no significant difference between the CD and SD group.

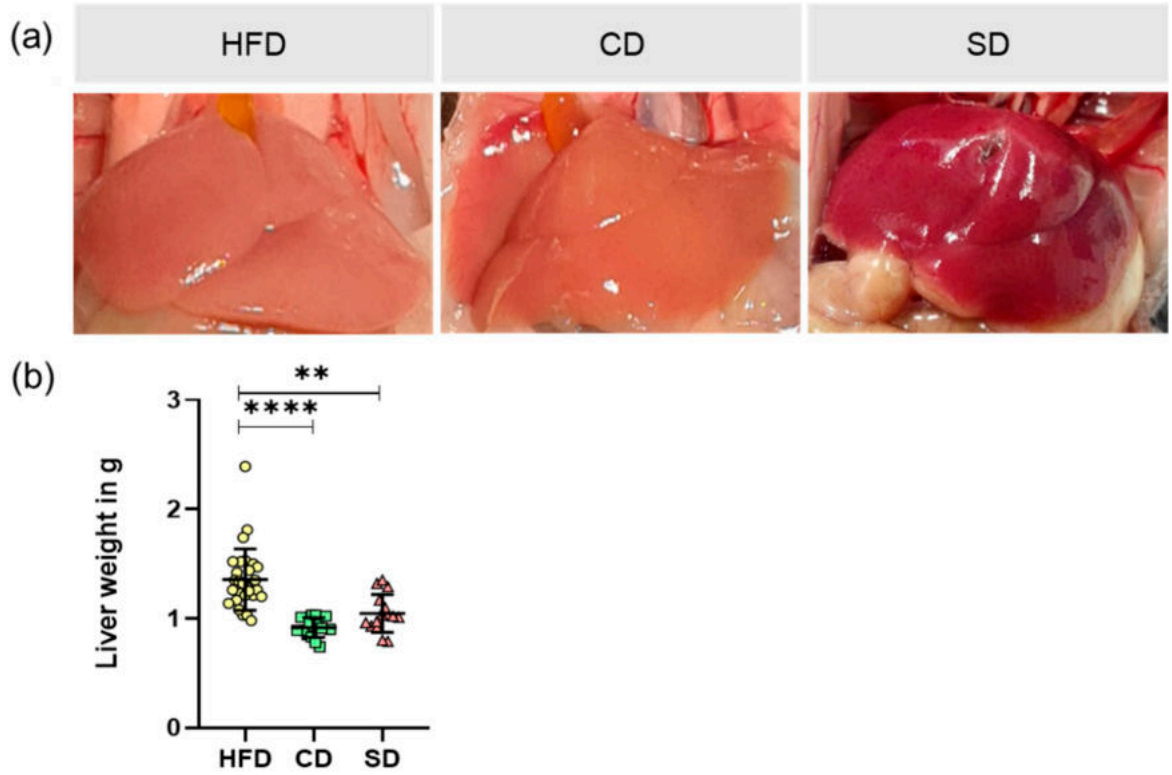

Figure 3. (**a**) Representative in situ images of mice livers from mice fed high fat diet (HFD), control diet (CD) or standard diet (SD); (**b**) Liver weight of the different groups (HFD: $n = 29$; CD: $n = 15$, SD: $n = 15$) presented as mean ± standard deviation. Significance of differences between the groups was tested by one-way ANOVA on Ranks (Kruskal–Wallis); **** $p < 0.0001$, ** $p < 0.01$.

3.2. Dietary Induced Liver Steatosis

The basis for the increased liver weight is probably diet-induced liver steatosis. To analyze this parameter, the microvesicular liver fat content was determined in H&E stained tissue, with representative images shown in Figure 4a. Liver tissue of the HFD group showed excessive macro- and microvesicular fat deposits. In addition, in liver tissue of the CD group, fat depots, mostly microvesicular, were found. Image analysis led to a significantly higher fat quantity in HFD compared to the CD and SD group (Figure 4b, $p = 0.0007$ vs. CD group and $p < 0.0001$ vs. SD group) but not between the SD and CD group. Tissue fat content alone therefore did not serve as an explanation for the macroscopically observed brightening of livers of the CD group. Subsequently we found that in the livers of the CD group, the amount of hepatic cholesterol was significantly higher than in the HFD group ($p = 0.024$) but not in the SD group (Figure 4c).

As an additional parameter to assess the impact of the different diets on the liver, we calculated the NAS for the different groups, according to exemplary scoring in Supplement Figure S1. Fat deposits (representative images shown in Figure 5a) in the HFD group indicated pathological changes in all liver samples. The HFD group, with mostly a score of 2, showed a significantly higher liver steatosis than the CD and SD group (Figure 5b), both $p < 0.0001$) with a score mostly between 0 and 1. The CD group did not differ significantly from the SD group, which is in line with the above shown quantification of liver fat. The SD group constantly showed a score of 0 in all samples, which corresponds to a healthy

liver. As a second parameter for the NAS, ballooning, a form of cell injury and death through fat accumulation, was assessed (Figure 5a). In all our samples, none of the hepatocytes showed ballooning injury to any extent, therefore score 2 was not assigned once. As some samples showed a few ballooned hepatocytes in the HFD group, represented by a score of 1, the scoring was significantly higher than in the CD and SD groups (Figure 5b), $p < 0.0001$) as there were no ballooned cells observed in the livers of the low-fat diets, assigned to score 0. The third parameter to calculate NAS is lobular inflammation (Figure 5a). In all samples, no massive inflammation of liver tissue, assigned to score 3, was found. With 2–4 inflammatory foci per LPF, a stout inflammation, defined as score 2, could be seen in a few livers of the HFD group. Interestingly, when it comes to inflammation, there was only a significant difference between the HFD and SD group (Figure 5b), $p = 0.003$) but not between the HFD and CD group. In the overall result, the examined parameters steatosis, ballooning and inflammation contributed to the NAS result with significantly higher values in the HFD group compared to the CD and SD group (Figure 5b), $p < 0.0001$ vs. CD and SD group). This hints toward a damaging effect of the HFD on the liver.

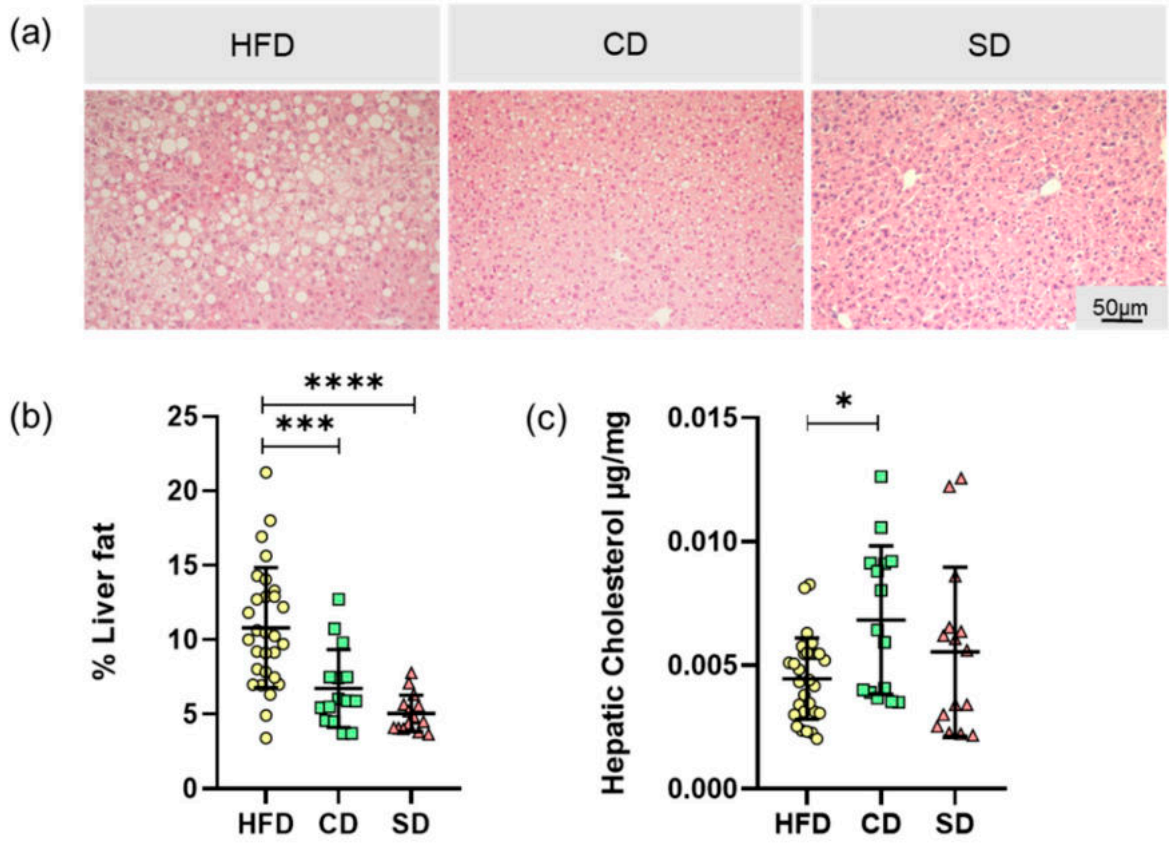

Figure 4. (**a**) Representative LPFs of the livers from mice fed high fat diet (HFD), control diet (CD) or standard diet (SD) (200× magnification, scale bar representing 50 µm valid for all three images); (**b**) Percentage of hepatic vesicular fat content; (**c**) Hepatic cholesterol concentration of the HFD, CD and SD group. Data (HFD: $n = 29$; CD: $n = 15$, SD: $n = 15$) presented as mean ± standard deviation. Significance of differences between the groups was tested by Brown–Forsythe and Welch ANOVA in (**b**) or one-way ANOVA on Ranks (Kruskal–Wallis) in (**c**); **** $p < 0.0001$, *** $p < 0.001$, * $p < 0.05$.

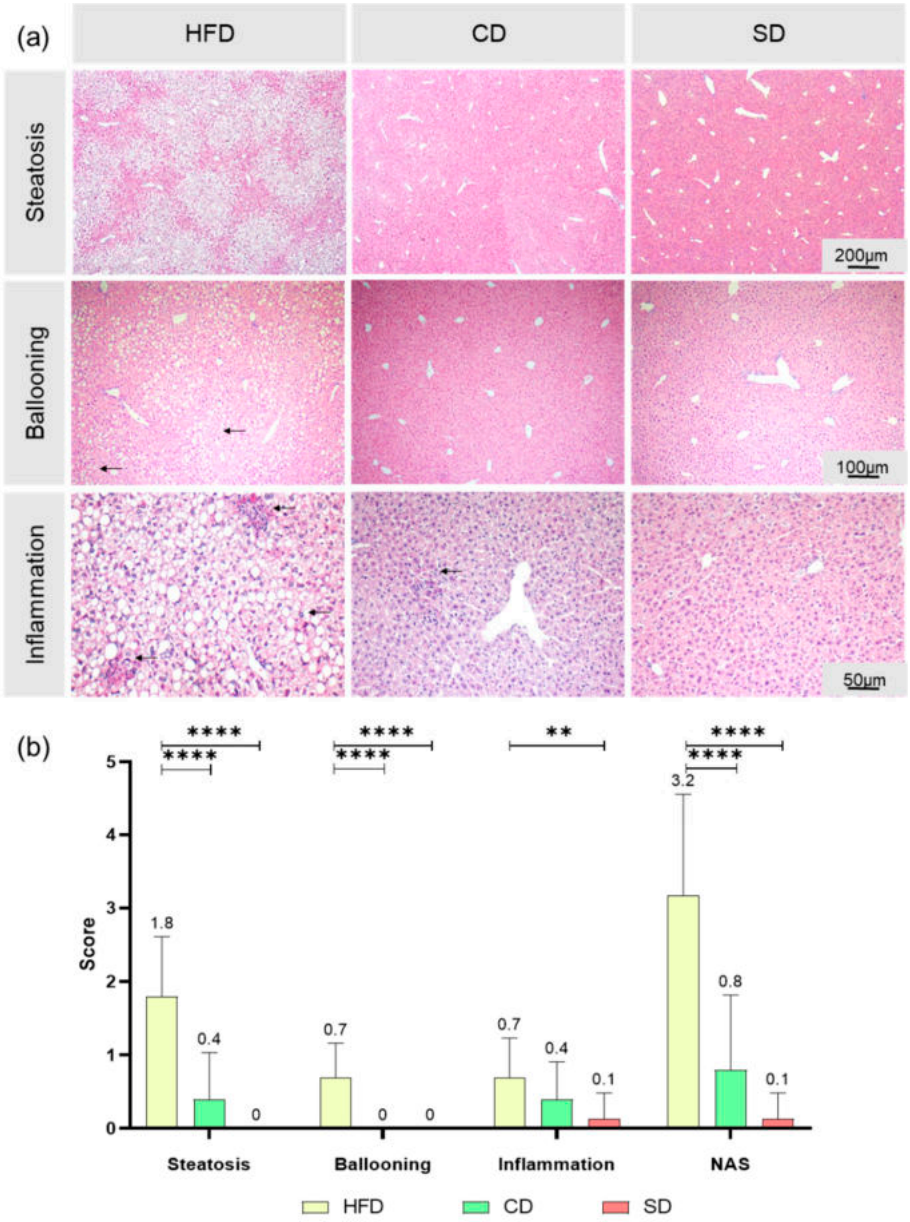

Figure 5. (**a**) Representative images of steatosis (50× magnification, scale bar represents 200 µm valid for all three images), ballooning (100× magnification, scale bar representing 100 µm valid for all three images) with black arrows indicating damaged cells, and inflammation (200× magnification, scale bar representing 50 µm valid for all three images) with black arrows indicating inflammatory foci in livers from mice fed high fat diet (HFD), control diet (CD) or standard diet (SD); (**b**) Assessments of scores for steatosis, ballooning and inflammation as well as calculation of NAS for the groups (HFD: $n = 29$; CD: $n = 15$, SD: $n = 15$). Data presented as mean ± standard deviation. Significance of differences between the groups was tested by one-way ANOVA on Ranks (Kruskal–Wallis); **** $p < 0.0001$, ** $p < 0.01$.

3.3. Dietary-Induced LGI in the Livers of the HFD Group and CD Group

As already indicated by macroscopy changes in the livers of the CD group, potential pathogenic effects of the carbohydrate rich diet emerged, and only a significant difference between the HFD and SD group was observed when scoring lobular inflammation in the NAS assessment. Thus, we chose to gain a more in-depth look into LGI processes in the liver. Therefore, we analyzed the cellular immune reaction by quantification of CAE^+ and $F4/80^+$ cells in the liver, relativized to the total number of

hepatocytes per HPF (Figure 6a). The data we obtained substantiate the results from inflammation scoring in NAS, again showing a significant difference between the HFD and SD group (Figure 6b), CAE$^+$: $p = 0.0003$, Figure 6c), F4/80$^+$: $p = 0.0002$,) but not between the HFD and CD group. Additionally, in both analyses, there was a significant difference between both controls (Figure 6b), CAE$^+$: $p < 0.0001$, Figure 6c), F4/80$^+$: $p = 0.006$). In conclusion, compared to the SD group, the CD group had significantly increased amounts of immune cells in the liver.

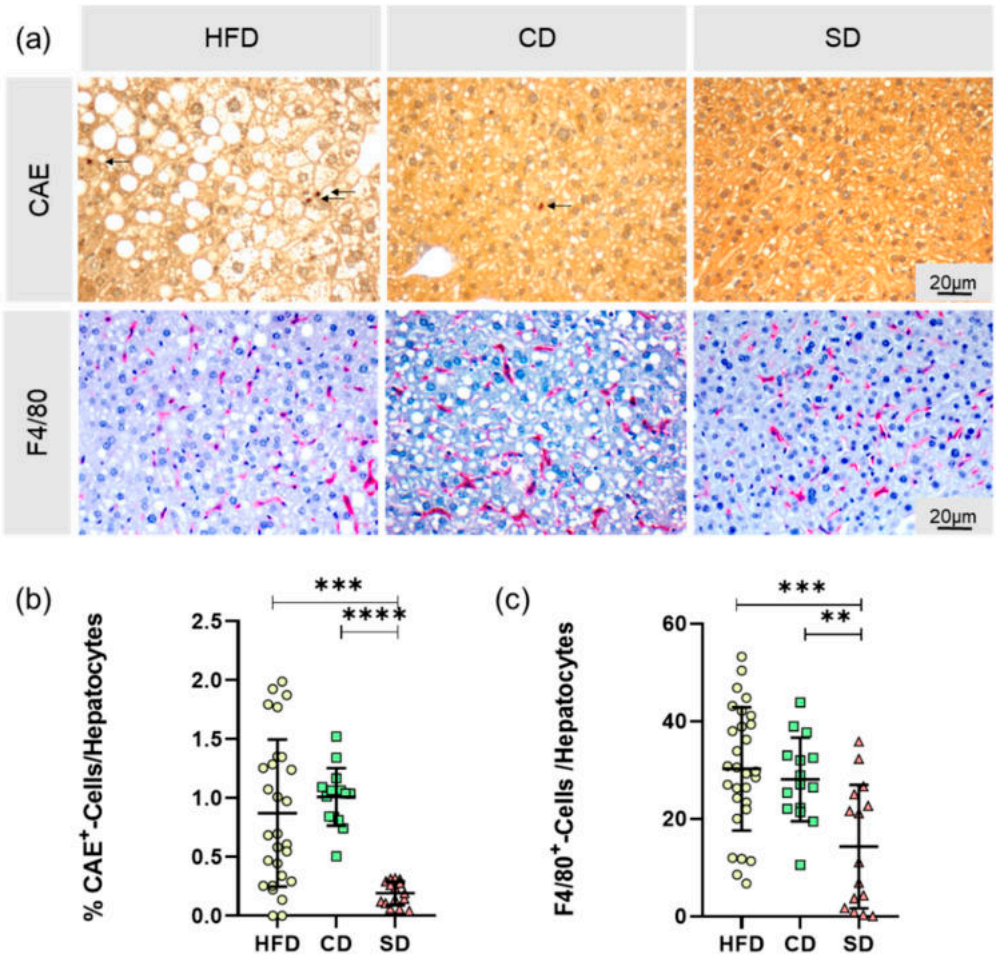

Figure 6. (**a**) Representative images of CAE-staining with CAE$^+$-cells indicated by arrows and F4/80-staining with F4/80$^+$-cells stained in red (both at 400× magnification, scale bar representing 20 µm valid for all images) of livers from mice fed high fat diet (HFD), control diet (CD) or standard diet (SD); (**b**) Relative amount of granulocytes (CAE$^+$) (HFD: $n = 28$; CD: $n = 15$, SD: $n = 15$); (**c**) Relative amount of macrophages (F4/80$^+$) (HFD: $n = 29$; CD: $n = 15$, SD: $n = 15$). Data presented as mean ± standard deviation. Significance of differences between the groups was tested by one-way ANOVA on Ranks (Kruskal–Wallis) in (**b**) or ordinary one-way ANOVA in (**c**); **** $p < 0.0001$, *** $p < 0.001$ ** $p < 0.01$.

In addition to the cellular immune response, we investigated the humoral immune response in liver LGI. As one of the most important synthesis organs, the liver is able to produce many immunogenic mediators. For quantification of the pro-inflammatory cytokines IL-1β, IL-6 and TNFα as well as the anti-inflammatory IL-10, hepatic RNA expression was evaluated by quantitative real-time PCR (Figure 7a–d)). The IL-1β levels in the CD group were significantly lower than in the HFD ($p < 0.0001$) and SD group (Figure 7a), $p < 0.0001$ vs. HFD group, $p = 0.0021$ vs. SD group). This was astonishingly reverted for IL-6 levels where we saw a significant increase in comparison to the HFD and SD group (Figure 7b), $p = 0.0106$ CD vs. HFD group, $p = 0.0124$ CD vs. SD group). Only TNFα values were as expected highest in the HFD group, which was significant compared to SD (Figure 7c), $p = 0.0052$)

but not to the CD group. In addition, a significant elevation of TNFα expression in the CD group compared to the SD group (Figure 7c), $p = 0.005$) was found. For IL-10, we found significantly increased expression when comparing the HFD and CD group with the SD group (Figure 7d), $p = 0.0136$ HFD vs. SD and $p = 0.0275$ CD vs. SD). The results depicting overall a heterogeneous effect of LGI on cytokine expression, but of note, the CD and SD group always differed significantly.

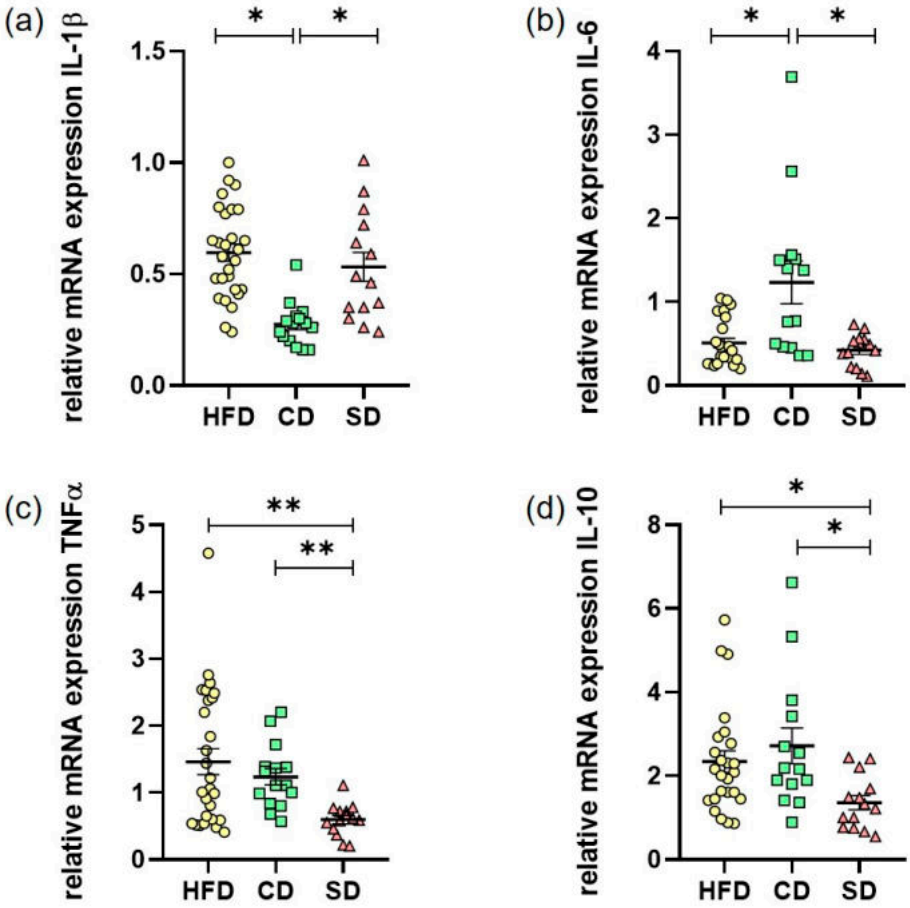

Figure 7. (**a**) Hepatic mRNA expression in the high fat diet (HFD), control diet (CD) or standard diet (SD) group of IL-1β (HFD: $n = 28$, CD: $n = 14$, SD: $n = 14$); (**b**) Hepatic mRNA expression of IL-6 (HFD: $n = 24$, CD: $n = 15$, SD: $n = 14$); (**c**) Hepatic mRNA expression of TNFα (HFD: $n = 28$, CD: $n = 15$, SD: $n = 14$); (**d**) Hepatic mRNA expression of IL-10 (HFD: $n = 25$, CD: $n = 15$, SD: $n = 14$). Data presented as $2^{-\Delta\Delta Ct}$ values determined by quantitative real-time PCR; Data presented as mean ± standard deviation. Significance of differences between the groups was tested by ordinary one-way ANOVA in (**a**) or one-way ANOVA on Ranks (Kruskal–Wallis) in (**b**–**d**) or; ** $p < 0.01$, * $p < 0.05$.

4. Discussion

Obesity is not merely a health risk itself, but often associated with other concomitant and secondary diseases [3,4,25]. It has become a serious disease of the 21st century due to its steadily increasing prevalence [1], and therefore is of great interest to study underlying disease mechanisms. One mechanism believed to contribute to disease progression is dietary-induced LGI starting from adipose tissue and later also becoming systemic and manifesting in other organs like the liver [26]. This is explainable by the close phylogenetic relationship between the liver and adipose tissue as well as the immune and hematopoietic system, which have evolved from formerly common structures [3]. In humans, as well as in many other mammals, hepatocytes and adipocytes are in close proximity to immune cells and have unhindered access to blood vessels [27–29]. Assuming that within the

framework of the common evolutionary lineage, common signaling molecules and pathways have also been conserved.

To draw more detailed conclusions of dietary effects on liver LGI, a diet-induced obesity mouse model was used in this study. We chose a HFD model to map the development of obesity and especially inflammation. Due to a diet rich in calories and fat, C57BL/6J mice on HFD show a diet-induced obesity phenotype mirroring the situation in obese humans in western industrial countries [30]. The induction of obesity by such a model is usually less artificial and therefore findings are better translatable to humans. This is especially the case because corresponding genotypes of genetically obese mice models like Lep^{ob} /Lep^{ob} mice or mice with tubby gene mutations [31,32] are rarely found in humans.

In our work, we aimed to investigate the dietary impact on effects of obesity-derived LGI in the liver. With our experimental approach, we were able to show an adverse effect of HFD on the liver, represented mainly through an elevated NAS. Surprisingly, when looking especially on LGI processes, the carbohydrate-rich control diet also exacerbated the pro-inflammatory response in the liver.

In terms of assessing dietary effects on mice, body and liver weights of the animals were determined. As expected, mice of the HFD group had significantly increased body and liver weights, whereas the values of the CD and SD group were at the lower limit of the age- and sex-specific normal range [33]. The reason for the increased body and liver weights is diet-induced fat accumulation, examined by analysis of liver fat content as well as determination of hepatic cholesterol. Mice of the HFD group showed significantly increased liver fat content of more than 10%, whereas both the controls were in the same range of liver fat content as healthy mice, which is about 5–8% [24,34].

Contrary to this finding, the hepatic cholesterol assay revealed a significantly increased cholesterol content in the CD group. Cholesterol has lipotoxic effects, mainly mediated by the induction of oxidative stress, which are able to activate pro-inflammatory signaling pathways and thus lead to NAFLD progression, even in lean individuals [35]. This provides a possible explanation for macroscopically observed pathological changes in the livers of the CD group. Therefore, in our experiments, the liver of the CD group with normal liver fat-content but high cholesterol showed a liver LGI equal to mice fed with HFD, which is comparable to previous results of HFD vs. carbohydrate-rich diet [36]. We suggest that starch is the main mediator of the elevated cholesterol content and the pro-inflammatory effects seen in the CD group, which is in line with results of Duwaerts et al. [37], describing a pathogenic effect of diets rich in starch on the liver, independent of calories and nutrient proportions [37]. From a nutritional point of view, CD as well as HFD are rich in lards, contributing to a pro-inflammatory profile [38] in both groups. Additionally, a high carbohydrate amount in the CD also contributes to that [20,21], whilst an elevated protein content, such as in the SD group, exerts more anti-inflammatory effects [22].

To explore the dietary effect on the mice livers in depth, they were histologically processed and analyzed according to aspects that are relevant in NAFLD diagnostics [23,24]. The NAS, created within the scope of evaluation, showed a more than fourfold increase in the HFD group compared to the CD and SD group, mainly due to steatosis. In the HFD group, this indicates the beginning and progression of NAFLD, described in the literature as an organic manifestation of the metabolic syndrome [5]. This damaging effect on the livers also became apparent by significantly increasing ALT and AST plasma values in the HFD group (Supplementary Materials Table S1). A persistent LGI may be a mechanistic link between obesity and the various comorbidities, such as NAFLD. There is strong evidence from the literature that obesity exerts an influence on the immune system and manifests itself as a condition of chronic LGI [11,39]. LGI is triggered or promoted by intrinsic stress factors, tissue dysfunction and changes in homeostatic checkpoints, which commonly occur in obesity [7]. The expression and characterization of a liver manifestation of LGI, triggered by HFD-induced obesity, were therefore another focus of the experiments.

Further characterization of obesity-associated LGI in the liver focused on the local cellular immune response. Cell damage induced in the context of NAFLD can lead to reduced liver function [40] with extensive consequences on the hepatic synthesis performance. In addition to inflammatory foci in the liver, assessed by NAFLD scoring, the number of granulocytes and the number of macrophages was

determined. Due to the heterogeneity of the macrophage population in the liver, we only counted F4/80+ cells, mainly consisting of tissue resident Kupffer cells and macrophages recruited from the bloodstream [41]. In the calculated ratios of both granulocytes and macrophages to the number of hepatocytes, significantly increased values were observed in the HFD group as well as in the CD group. Not only mature macrophages were attracted from the bloodstream, but also myeloid progenitor cells through a closely regulated interaction of genes for chemokines, chemokine receptors, adhesion molecules, myeloid markers and inflammatory cytokines [42]. Therefore, as a further step to characterize diet induced liver LGI, hepatic expression of different cytokines was determined.

In addition to hepatocytes themselves, it is commonly known that immune cells in the liver also play a major role in the expression inflammatory mediators [43]. In our work, determined hepatic expression levels of cytokines do not provide a homogeneous pattern. According to TNFα elevations in obesity shown by other working groups [10,39,44], we were able to show an elevation of hepatic TNFα expression in the HFD group too, but also in the CD group compared to the SD group. Whilst the expression of pro-inflammatory TNFα was in line with the shown cellular immune response, the results of the other three analyzed cytokines differed and were partially contradictory. In contrast to increased IL-6 levels in obesity described in the literature [45], the HFD group only showed a slight increase in hepatic expression compared to the SD group. The hepatic IL-6 expression in the CD group was even higher than in the HFD group, again underpinning the pro-inflammatory potential of the carbohydrate-rich CD. A significantly lower IL-1β and elevated IL-10 level in the CD group may be explainable by an overshooting anti-inflammatory counter-regulation, as IL-10 especially is able to alter the expression of other cytokines [46].

In conclusion, our results show obesity derived liver damage associated with an organic manifestation of a LGI in the livers of the HFD group. Even if not leading to a significant increase of NAS in the CD group over the experimental time, an increased inflammatory potential was shown in the group fed with a diet rich in carbohydrates. Therefore, when studying diet-induced obesity with a focus on inflammatory processes like LGI, we would not suggest using a control diet disproportionately rich in carbohydrates.

Supplementary Materials: The following are available online at http://www.mdpi.com/2227-9059/8/12/587/s1, Table S1: Blood Parameters blood glucose concentration, triglyceride concentration, AST and ALT concentration in the high fat diet (HFD), control diet (CD) and standard diet (SD) group presented as mean ± standard deviation, ImageJ code S1: Code for semiautomatic quantification of liver fat, ImageJ code S2: Code for quantification of F4/80+-cells, Figure S1: Representative images for scoring of steatosis (Score 0-3, 50 x magnification, scale bar represents 200 µm valid for all four), ballooning (Score 0-1, 100x magnification, scale bar represents 100 µm valid for both) with black arrows indicating damaged cells, and inflammation (Score 0-2, 200x magnification, scale bar represents 50 µm valid for all three) with black arrows indicating inflammatory foci

Author Contributions: Conceptualization, A.K. and D.J. (Deborah Janowitz); methodology, A.K. and N.P.G.; validation, N.P.G., A.K., B.V.; formal analysis, N.P.G., L.M., A.G., D.J. (Daniel Jenderny); investigation, N.P.G., L.M., K.P., A.G., D.J. (Daniel Jenderny); resources, A.K., D.J. (Deborah Janowitz), B.V.; data curation, N.P.G., A.K.; writing—original draft preparation, N.P.G. and L.M.; writing—review and editing, A.K. and B.V.; visualization, N.P.G. and L.M.; supervision, A.K., B.V., D.J. (Deborah Janowitz); project administration, A.K. and D.J. (Deborah Janowitz); funding acquisition, A.K. and D.J. (Deborah Janowitz); animal care, N.P.G. and D.J. (Daniel Jenderny). All authors have read and agreed to the published version of the manuscript.

Funding: This research was funded by grant from the Deutsche Forschungsgemeinschaft, Bonn, Germany (KU 3280/1-2 and JA 2872/1-2).

Acknowledgments: The authors cordially thank the technicians of the Rudolf-Zenker Institute for Experimental Surgery and of the Central Animal Care Facility, Rostock University Medical Center for their valuable assistance.

Conflicts of Interest: The authors declare no conflict of interest.

References

1. WHO. Obesity and Overweight. 2018. Available online: https://www.who.int/en/news-room/fact-sheets/detail/obesity-and-overweight (accessed on 19 May 2019).
2. Kaplan, N.M. The Deadly Quartet. *Arch. Intern. Med.* **1989**, *149*, 1514–1520. [CrossRef] [PubMed]

3. Hotamışlıgil, G.S. Inflammation and metabolic disorders. *Nat. Cell Biol.* **2006**, *444*, 860–867. [CrossRef]
4. Schattenberg, J.M.; Schuppan, D. Nonalcoholic steatohepatitis. *Curr. Opin. Lipidol.* **2011**, *22*, 479–488. [CrossRef] [PubMed]
5. Marchesini, G.; Brizi, M.; Bianchi, G.; Tomassetti, S.; Bugianesi, E.; Lenzi, M.; McCullough, A.J.; Natale, S.; Forlani, G.; Melchionda, N. Nonalcoholic Fatty Liver Disease: A Feature of the Metabolic Syndrome. *Diabetes* **2001**, *50*, 1844–1850. [CrossRef] [PubMed]
6. Hotamisligil, G.S. Inflammation, metaflammation and immunometabolic disorders. *Nat. Cell Biol.* **2017**, *542*, 177–185. [CrossRef]
7. Medzhitov, R. Origin and physiological roles of inflammation. *Nat. Cell Biol.* **2008**, *454*, 428–435. [CrossRef]
8. Lumeng, C.N.; Saltiel, A.R. Inflammatory links between obesity and metabolic disease. *J. Clin. Investig.* **2011**, *121*, 2111–2117. [CrossRef]
9. Juge-Aubry, C.E.; Henrichot, E.; Meier, C.A. Adipose tissue: A regulator of inflammation. *Best Pr. Res. Clin. Endocrinol. Metab.* **2005**, *19*, 547–566. [CrossRef]
10. Kim, K.-A.; Gu, W.; Lee, I.-A.; Joh, E.-H.; Kim, D.-H. High Fat Diet-Induced Gut Microbiota Exacerbates Inflammation and Obesity in Mice via the TLR4 Signaling Pathway. *PLoS ONE* **2012**, *7*, e47713. [CrossRef]
11. Wellen, K.E.; Hotamisligil, G.S. Obesity-induced inflammatory changes in adipose tissue. *J. Clin. Investig.* **2003**, *112*, 1785–1788. [CrossRef]
12. Wu, Z.; Xu, J.; Tan, J.; Song, Y.; Liu, L.; Zhang, F.; Zhang, Y.; Li, X.; Chi, Y.; Liu, Y. Mesenteric adipose tissue B lymphocytes promote local and hepatic inflammation in non-alcoholic fatty liver disease mice. *J. Cell. Mol. Med.* **2019**, *23*, 3375–3385. [CrossRef] [PubMed]
13. Koyama, Y.; Brenner, D.A. Liver inflammation and fibrosis. *J. Clin. Investig.* **2017**, *127*, 55–64. [CrossRef]
14. Saltiel, A.R.; Olefsky, J.M. Inflammatory mechanisms linking obesity and metabolic disease. *J. Clin. Investig.* **2017**, *127*, 1–4. [CrossRef] [PubMed]
15. DeGuise, M.; Chehade, L.; Tierney, A.; Beauvais, A.; Kothary, R. Low fat diets increase survival of a mouse model of spinal muscular atrophy. *Ann. Clin. Transl. Neurol.* **2019**, *6*, 2340–2346. [CrossRef]
16. Marei, W.F.A.; Smits, A.; Mohey-Elsaeed, O.; Pintelon, I.; Ginneberge, D.; Bols, P.E.J.; Moerloose, K.; Leroy, J.L.M.R. Differential effects of high fat diet-induced obesity on oocyte mitochondrial functions in inbred and outbred mice. *Sci. Rep.* **2020**, *10*, 1–14. [CrossRef]
17. Penke, M.; Larsen, P.S.; Schuster, S.; Dall, M.; Jensen, B.A.; Gorski, T.; Meusel, A.; Richter, S.; Vienberg, S.G.; Treebak, J.T.; et al. Hepatic NAD salvage pathway is enhanced in mice on a high-fat diet. *Mol. Cell. Endocrinol.* **2015**, *412*, 65–72. [CrossRef]
18. Wang, P.; Shao, X.; Bao, Y.; Zhu, J.; Chen, L.; Zhang, L.; Ma, X.; Zhong, X.-B. Impact of obese levels on the hepatic expression of nuclear receptors and drug-metabolizing enzymes in adult and offspring mice. *Acta Pharm. Sin. B* **2020**, *10*, 171–185. [CrossRef] [PubMed]
19. Ulman, E.A. The "Original" High-Fat Diets for Diet Induced Obesity. 2011. Available online: https://www.weizmann.ac.il/vet/sites/vet/files/uploads/diet_d12451_d12492.pdf (accessed on 9 October 2020).
20. Blaak, E.E.; Antoine, J.; Benton, D.; Björck, I.; Bozzetto, L.; Brouns, F.; Diamant, M.; Dye, L.; Hulshof, T.; Holst, J.J.; et al. Impact of postprandial glycaemia on health and prevention of disease. *Obes. Rev.* **2012**, *13*, 923–984. [CrossRef]
21. Minihane, A.M.; Vinoy, S.; Russell, W.R.; Baka, A.; Roche, H.M.; Tuohy, K.M.; Teeling, J.L.; Blaak, E.E.; Fenech, M.; Vauzour, D.; et al. Low-grade inflammation, diet composition and health: Current research evidence and its translation. *Br. J. Nutr.* **2015**, *114*, 999–1012. [CrossRef]
22. Markova, M.; Pivovarova, O.; Hornemann, S.; Sucher, S.; Frahnow, T.; Wegner, K.; Machann, J.; Petzke, K.J.; Hierholzer, J.; Lichtinghagen, R.; et al. Isocaloric Diets High in Animal or Plant Protein Reduce Liver Fat and Inflammation in Individuals With Type 2 Diabetes. *Gastroenterology* **2017**, *152*, 571–585. [CrossRef]
23. Kleiner, D.E.; Brunt, E.M.; Van Natta, M.; Behling, C.; Contos, M.J.; Cummings, O.W.; Ferrell, L.D.; Liu, Y.-C.; Torbenson, M.S.; Unalp-Arida, A.; et al. Design and validation of a histological scoring system for nonalcoholic fatty liver disease. *Hepatology* **2005**, *41*, 1313–1321. [CrossRef] [PubMed]
24. Liebig, M.; Hassanzada, A.; Kämmerling, M.; Genz, B.; Vollmar, B.; Abshagen, K. Microcirculatory disturbances and cellular changes during progression of hepatic steatosis to liver tumors. *Exp. Biol. Med.* **2017**, *243*, 1–12. [CrossRef]

25. Singh-Manoux, A.; Czernichow, S.; Elbaz, A.; Dugravot, A.; Sabia, S.; Hagger-Johnson, G.; Kaffashian, S.; Zins, M.; Brunner, E.J.; Nabi, H.; et al. Obesity phenotypes in midlife and cognition in early old age: The Whitehall II cohort study. *Neurology* **2012**, *79*, 755–762. [CrossRef] [PubMed]
26. Sikaris, K.A. The Clinical Biochemistry of Obesity. *Clin. Biochem. Rev.* **2004**, *25*, 165–181. [PubMed]
27. Lonardo, A.; Caldwell, S.H.; Loria, P. Clinical physiology of NAFLD: A critical overview of pathogenesis and treatment. *Expert Rev. Endocrinol. Metab.* **2010**, *5*, 403–423. [CrossRef]
28. Milic, S.; Lulić, D.; Štimac, D. Non-alcoholic fatty liver disease and obesity: Biochemical, metabolic and clinical presentations. *World J. Gastroenterol.* **2014**, *20*, 9330–9337.
29. Wree, A.; Kahraman, A.; Gerken, G.; Canbay, A. Obesity Affects the Liver—The Link between Adipocytes and Hepatocytes. *Digestion* **2010**, *83*, 124–133. [CrossRef]
30. Collins, S.; Martin, T.L.; Surwit, R.S.; Robidoux, J. Genetic vulnerability to diet-induced obesity in the C57BL/6J mouse: Physiological and molecular characteristics. *Physiol. Behav.* **2004**, *81*, 243–248. [CrossRef]
31. Kleinendorst, L.; Abawi, O.; Van Der Kamp, H.J.; Alders, M.; Meijers-Heijboer, H.E.; Van Rossum, E.F.; Akker, E.L.V.D.; Van Haelst, M.M. Leptin receptor deficiency: A systematic literature review and prevalence estimation based on population genetics. *Eur. J. Endocrinol.* **2020**, *182*, 47–56. [CrossRef]
32. Tschöp, M.H.; Heiman, M.L. Rodent obesity models: An overview. *Exp. Clin. Endocrinol. Diabetes* **2001**, *109*, 307–319. [CrossRef]
33. Jax.org b6j-data-summary.xlsx. Available online: https://www.jax.org/de/-/media/jaxweb/files/jax-mice-and-services/b6j-data-summary.xlsx (accessed on 14 September 2020).
34. Echeverría, F.; Valenzuela, R.; Bustamante, A.; Álvarez, D.; Ortiz, M.; Espinosa, A.; Illesca, P.; Gonzalez-Mañan, D.; Videla, L.A. High-fat diet induces mouse liver steatosis with a concomitant decline in energy metabolism: Attenuation by eicosapentaenoic acid (EPA) or hydroxytyrosol (HT) supplementation and the additive effects upon EPA and HT co-administration. *Food Funct.* **2019**, *10*, 6170–6183. [CrossRef] [PubMed]
35. Tirosh, O. Hypoxic Signaling and Cholesterol Lipotoxicity in Fatty Liver Disease Progression. *Oxidative Med. Cell. Longev.* **2018**, *2018*, 1–15. [CrossRef] [PubMed]
36. Da Silva-Santi, L.G.; Antunes, M.M.; Caparroz-Assef, S.M.; Carbonera, F.; Masi, L.N.; Curi, R.; Visentainer, J.V.; Bazotte, R.B. Liver Fatty Acid Composition and Inflammation in Mice Fed with High-Carbohydrate Diet or High-Fat Diet. *Nutrients* **2016**, *8*, 682. [CrossRef] [PubMed]
37. Duwaerts, C.C.; Amin, A.M.; Siao, K.; Her, C.; Fitch, M.; Beysen, C.; Turner, S.M.; Goodsell, A.; Baron, J.L.; Grenert, J.P.; et al. Specific Macronutrients Exert Unique Influences on the Adipose-Liver Axis to Promote Hepatic Steatosis in Mice. *Cell. Mol. Gastroenterol. Hepatol.* **2017**, *4*, 223–236. [CrossRef] [PubMed]
38. Wang, X.; Cheng, M.; Zhao, M.; Ge, A.; Guo, F.; Zhang, M.; Yang, Y.; Liu, L.; Yang, N. Differential effects of high-fat-diet rich in lard oil or soybean oil on osteopontin expression and inflammation of adipose tissue in diet-induced obese rats. *Eur. J. Nutr.* **2012**, *52*, 1181–1189. [CrossRef]
39. Van Der Heijden, R.A.; Sheedfar, F.; Morrison, M.C.; Hommelberg, P.P.H.; Kor, D.; Kloosterhuis, N.J.; Gruben, N.; Youssef, S.A.; De Bruin, A.; Hofker, M.H.; et al. High-fat diet induced obesity primes inflammation in adipose tissue prior to liver in C57BL/6j mice. *Aging* **2015**, *7*, 256–268. [CrossRef]
40. Targher, G. Non-alcoholic fatty liver disease, the metabolic syndrome and the risk of cardiovascular disease: The plot thickens. *Diabet. Med.* **2007**, *24*, 1–6. [CrossRef]
41. Morinaga, H.; Mayoral, R.; Heinrichsdorff, J.; Osborn, O.; Franck, N.; Hah, N.; Walenta, E.; Bandyopadhyay, G.; Pessentheiner, A.R.; Chi, T.J.; et al. Characterization of Distinct Subpopulations of Hepatic Macrophages in HFD/Obese Mice. *Diabetes* **2014**, *64*, 1120–1130. [CrossRef]
42. Obstfeld, A.E.; Sugaru, E.; Thearle, M.; Francisco, A.-M.; Gayet, C.; Ginsberg, H.N.; Ables, E.V.; Ferrante, A.W. C-C Chemokine Receptor 2 (CCR2) Regulates the Hepatic Recruitment of Myeloid Cells That Promote Obesity-Induced Hepatic Steatosis. *Diabetes* **2010**, *59*, 916–925. [CrossRef]
43. Robinson, M.W.; Harmon, C.; O'Farrelly, C. Liver immunology and its role in inflammation and homeostasis. *Cell. Mol. Immunol.* **2016**, *13*, 267–276. [CrossRef]
44. Marques, P.; Collado, A.; Martínez-Hervás, S.; Domingo, E.; Benito, E.; Piqueras, L.; Real, J.T.; Ascaso, J.F.; Sanz, M.-J. Systemic Inflammation in Metabolic Syndrome: Increased Platelet and Leukocyte Activation, and Key Role of CX3CL1/CX3CR1 and CCL2/CCR2 Axes in Arterial Platelet-Proinflammatory Monocyte Adhesion. *J. Clin. Med.* **2019**, *8*, 708. [CrossRef] [PubMed]

45. Wieckowska, A.; Papouchado, B.G.; Li, Z.; Lopez, R.; Zein, N.N.; Feldstein, A.E. Increased Hepatic and Circulating Interleukin-6 Levels in Human Nonalcoholic Steatohepatitis. *Am. J. Gastroenterol.* **2008**, *103*, 1372–1379. [CrossRef] [PubMed]
46. Moore, K.W.; Malefyt, R.D.W.; Coffman, R.L.; O'Garra, A. INTERLEUKIN-10AND THEINTERLEUKIN-10 RECEPTOR. *Annu. Rev. Immunol.* **2001**, *19*, 683–765. [CrossRef] [PubMed]

Anhang 3

Studie IV:

Müller, L., **Power Guerra, N.**, Stenzel, J., Rühlmann, C., Lindner, T., Krause, B. J., Vollmar, B., Teipel, S. y Kuhla, A. Long-Term Caloric Restriction Attenuates β-Amyloid Neuropathology and Is Accompanied by Autophagy in APPswe/PS1delta9 Mice. *Nutrients* **2021**, 13(3). https://doi.org/10.3390/nu13030985.

nutrients

MDPI

Article

Long-Term Caloric Restriction Attenuates β-Amyloid Neuropathology and Is Accompanied by Autophagy in APPswe/PS1delta9 Mice

Luisa Müller [1,2,3], Nicole Power Guerra [1], Jan Stenzel [4], Claire Rühlmann [1], Tobias Lindner [4], Bernd J. Krause [4,5], Brigitte Vollmar [1,4], Stefan Teipel [2,3,6] and Angela Kuhla [1,3,*]

1 Rudolf-Zenker-Institute for Experimental Surgery, Medical University Rostock, 18057 Rostock, Germany; luisa.mueller2@uni-rostock.de (L.M.); nicole.guerra@uni-rostock.de (N.P.G.); Claire_ruehlmann@web.de (C.R.); brigitte.vollmar@med.uni-rostock.de (B.V.)
2 Department of Psychosomatic Medicine and Psychotherapy, University of Rostock, 18147 Rostock, Germany; stefan.teipel@med.uni-rostock.de
3 Centre for Transdisciplinary Neurosciences Rostock (CTNR), University of Rostock, 18147 Rostock, Germany
4 Core Facility Multimodal Small Animal Imaging, Rostock University Medical Center, 18057 Rostock, Germany; jan2.stenzel@gmail.com (J.S.); tobias.lindner@med.uni-rostock.de (T.L.); bernd.krause@med.uni-rostock.de (B.J.K.)
5 Department of Nuclear Medicine, Rostock University Medical Center, 18057 Rostock, Germany
6 German Center for Neurodegenerative Diseases (DZNE)–Rostock/Greifswald, 18147 Rostock and 17489 Greifswald, Germany
* Correspondence: angela.kuhla@uni-rostock.de; Tel.: +49-381-494-2503

Citation: Müller, L.; Power Guerra, N.; Stenzel, J.; Rühlmann, C.; Lindner, T.; Krause, B.J.; Vollmar, B.; Teipel, S.; Kuhla, A. Long-Term Caloric Restriction Attenuates β-Amyloid Neuropathology and Is Accompanied by Autophagy in APPswe/PS1delta9 Mice. *Nutrients* **2021**, *13*, 985. https:// doi.org/10.3390/nu13030985

Academic Editors: Susanne Klaus and Takuya Chiba

Received: 4 February 2021
Accepted: 16 March 2021
Published: 18 March 2021

Abstract: Caloric restriction (CR) slows the aging process, extends lifespan, and exerts neuroprotective effects. It is widely accepted that CR attenuates β-amyloid (Aβ) neuropathology in models of Alzheimer's disease (AD) by so-far unknown mechanisms. One promising process induced by CR is autophagy, which is known to degrade aggregated proteins such as amyloids. In addition, autophagy positively regulates glucose uptake and may improve cerebral hypometabolism—a hallmark of AD—and, consequently, neural activity. To evaluate this hypothesis, APPswe/PS1delta9 (tg) mice and their littermates (wild-type, wt) underwent CR for either 16 or 68 weeks. Whereas short-term CR for 16 weeks revealed no noteworthy changes of AD phenotype in tg mice, long-term CR for 68 weeks showed beneficial effects. Thus, cerebral glucose metabolism and neuronal integrity were markedly increased upon 68 weeks CR in tg mice, indicated by an elevated hippocampal fluorodeoxyglucose [^{18}F] ([^{18}F]FDG) uptake and increased N-acetylaspartate-to-creatine ratio using positron emission tomography/computer tomography (PET/CT) imaging and magnet resonance spectroscopy (MRS). Improved neuronal activity and integrity resulted in a better cognitive performance within the Morris Water Maze. Moreover, CR for 68 weeks caused a significant increase of LC3BII and p62 protein expression, showing enhanced autophagy. Additionally, a significant decrease of Aβ plaques in tg mice in the hippocampus was observed, accompanied by reduced microgliosis as indicated by significantly decreased numbers of iba1-positive cells. In summary, long-term CR revealed an overall neuroprotective effect in tg mice. Further, this study shows, for the first time, that CR-induced autophagy in tg mice accompanies the observed attenuation of Aβ pathology.

Keywords: APPswe/PS1delta9; caloric restriction; [^{18}F]FDG-PET/CT; amyloid β; iba1; autophagy

1. Introduction

One hallmark of Alzheimer's disease (AD) is the accumulation of amyloid-β (Aβ), leading to formation of Aβ-plaques [1]. Transgenic animal models of Aβ pathology provide mechanistic insight into aspects of AD pathology related to Aβ accumulation and represent an important tool for translational AD research. Accordingly, APPswe/PS1delta9 mice, a well-established AD mouse model, display a variety of clinically relevant AD-like

symptoms, including increased parenchymal Aβ load, neuroinflammation, deficits in the cholinergic system, and cognitive impairment at an age of 4 months when developing first Aβ depositions [2]. Overall, neural activity in AD is linked with altered cerebral glucose metabolism. Accordingly, several clinical studies [3,4] have reported that hypometabolism is a well-described pathological hallmark of AD.

It is widely accepted that caloric intake may influence the relative risk for AD [5,6]. Most remarkably, while high caloric intake may promote AD neuropathology, experimental evidence strongly supports the hypothesis that caloric restriction (CR) prevents it. In this context, CR has attenuated Aβ deposition in several AD mouse models [7–10], whereby the duration of CR with 4 weeks [8] or 36 weeks [10] strongly differed. Moreover, Patel et al. and colleagues [8] showed reduced Aβ-associated astrocyte activation upon CR. Besides diminishing Aβ pathology, CR led to the reduction of neuronal loss in hippocampus [11] and to the improvement of cognitive deficits [12].

One process induced by CR is autophagy, a catabolic mechanism that degrades and recycles organelles and misfolded proteins such as Aβ. Therefore, autophagy is important in Aβ clearance from tissues [13]. Interestingly, AD-associated phenomena like neuroinflammation and glial activation can impair autophagy functionality, further amplifying neurodegeneration [14]. In this context, it has been reported that CR may induce glial autophagy, which is known to have a neuroprotective effect in AD [15]. In detail, autophagy is characterized by translocation of autophagy-gene-related (Atg) protein LC3BII together with sequestosom-1 (p62) to the autophagosome membrane, both commonly used as markers of autophagosome formation [16].

To date, no study has assessed whether CR-induced improvement in cognition is accompanied by autophagy. Moreover, the success of CR seems to be dependent on the duration of CR [17]. For example, our working group was able to show that only a lifelong CR for 74 weeks improved cognition performance in C57BL6 mice [18]. However, studies with AD mice have revealed an enhancement of cognition after 14 weeks CR [7,8]. To address this subject, we subjected APPswe/PS1delta9 mice to short-term (16 weeks) or long-term (68 weeks) CR and studied to what extent reduced amyloid pathology and improved cognition was accompanied with increased autophagy.

2. Materials and Methods

2.1. Animals

The study was performed in female APPswe/PS1delta9 (tg) mice co-expressing human amyloid-β precursor protein (APP) K594N and M595L mutation, as well as the human presenilin (PS) 1, L166P mutation under the control of the mouse prion protein promotor [19,20]. The APPswe/PS1delta9 mice were hemizygotes on B6xC3H and C57BL6 mouse backgrounds, and all mice were bred in-house. Female littermates of B6xC3H, as well as C57BL6 mice, were pooled and served as control group (wild-type; wt). Mice at the age of 4 weeks were fed either ad libitum (AL) or a caloric-restricted diet (CR, 60% of ad libitum chow) for 16 weeks (16 weeks or short-term, n = 5–10 for each group) or 68 weeks (68 weeks or long-term, n = 5–10 for each group). All mice were housed in standard cages in a temperature-controlled room (22 °C ± 2 °C) on a 12 h light/dark cycle (light on at 06:00 a.m.), with free access to water under specified pathogen-free conditions. At the beginning and end of the experiment, body weight was examined. Blood glucose was measured directly before sacrifice. The experimental protocol was approved by the local Animal Research Committee (Landesamt für Landwirtschaft, Lebensmittelsicherheit und Fischerei (LALLF) of the state Mecklenburg-Western Pomerania (LALLF M-V/TSD/7221.3-1.1-002/14)). All animals received care according to the German legislation on protection of animals and the Guide for the Care and Use of Laboratory Animals (European Directive 2010/63/EU).

2.2. Magnetic Resonance Imaging (MRI) and Spectroscopy (MRS)

In vivo imaging (representative Figure 1a), as well as single-voxel spectroscopy, was per-

formed according to the methodology described by Rühlmann et al. [21]. Spectra (exemplary in Figure 1b) were analyzed with jMRUI spectroscopy software (version 5.2) [22,23] and the jMRUI2XML package [24]. N-acetylaspartate/creatine ratios (NAA/Cr) were calculated. Therefore, the Hankel-Lanczos Singular Value Decomposition (HLSVD) method with 5 components was applied [25].

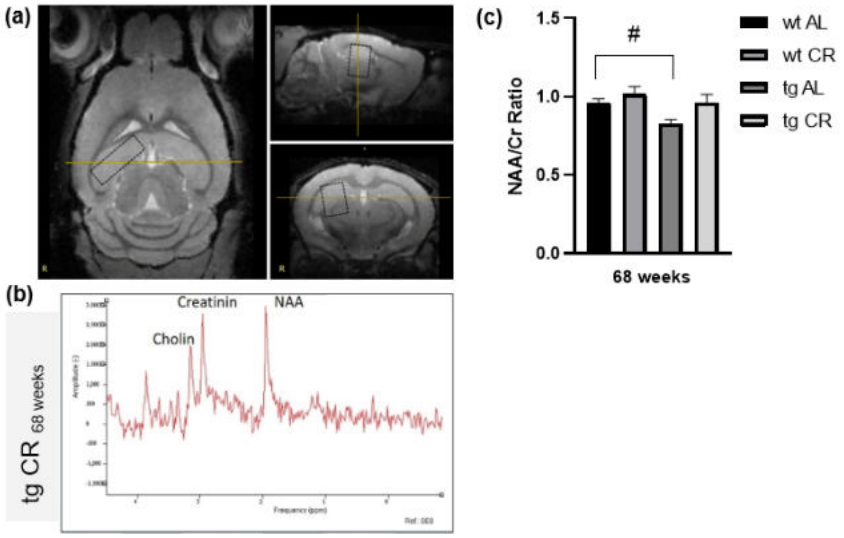

Figure 1. Representative magnetic resonance image including measured voxel (**a**). Example of magnetic resonance spectroscopy (MRS) with the prominent metabolites N-acetylaspartate (NAA resonates at 2.0 ppm) and creatine (Cr resonates at 3.0 ppm) from a transgenic APPswe/PS1delta9 (tg) mouse (**b**). Quantification of N-acetylaspartate/creatine (NAA/Cr) ratios in the brains of wild-type (wt) and tg mice fed either ad libitum (AL) or a caloric-restricted diet (CR, 60% of ad libitum) for 68 weeks (**c**). Values are given as mean ± SEM. Significance of differences between the groups was tested by one-way ANOVA on Ranks (Kruskal–Wallis) with Dunn's post hoc test for multiple comparisons: # $p < 0.05$ vs. wt.

2.3. Positron Emission Tomography/Computer Tomography (PET/CT) Imaging and PET/CT-Data Analysis

PET/CT imaging and data analysis were performed according to previous works of our group [21,26,27] using PMOD software (version 3.7; PMOD Technologies LLC, Zürich, Switzerland). The processed PET images were subsequently co-registered with the mouse brain volume-of-interest (VOI) template (Mouse Mirrione atlas), and the PMOD software and tracer uptake values were extracted for each delineated VOI. Due to the fact that mice differed in body weight, the injected dose percentage per gram (ID%/g) was chosen as unit of measurement and acquired for each VOI.

2.4. Morris Water Maze Test

The Morris Water Maze (MWM) was performed as measure for spatial reference memory according to previously published work [18]. The amount of platform crosses, latency to first platform crossing, time spent on platform, and north (N)-quadrant crosses were monitored in real time by a video camera (15E objective, Computar, CBC Europe, Düsseldorf, Germany with Camera CCA1300-60gm, Basler AG, Ahrensburg, Germany), with subsequent digital analysis (Ethovision XT II.5, Noldus Information Technology, Wageningen, The Netherlands).

2.5. Sampling

At the end of the experiment, all mice were anesthetized with a mixture of ketamine (98 mg/kg bodyweight, medistar, Ascheberg, Germany) and xylazine (6.5 mg/kg bodyweight, Bayer, Leverkusen, Germany), exsanguinated by puncture of the vena cava inferior for immediate separation of plasma, and harvested of brain tissue.

2.6. Immunohistochemistry

Brain tissue was fixed in 4% phosphate-buffered formalin, embedded in paraffin and sliced in 4 µm-thin sections. The sections were put on X-tra Adhesive Precleaned Micro Slides (Leica, Wetzlar, Germany) and exposed to mouse monoclonal anti-Aβ antibody (clone 6E10; 1:1000, BioLegend, San Diego, CA, USA, as described by the authors of [28]) and goat polyclonal anti-iba1 antibody (1:1000, Abcam, Berlin, Germany). DAB chromogen Universal LSAB® kits (System-HRP; DakoCytomation, Dako, Jena, Germany) were used for development according to the manufacturer's instructions. The sections were counterstained with hemalaun (Merck, Darmstadt, Germany), and images were acquired on microscope type BX51 with a Color View Soft Imaging System and the corresponding software cellSens Standard 1.14 (all from Olympus, Hamburg, Germany). Appropriate negative staining images are provided in Appendix A (Figure A1). Within the hippocampus (n = 5–10 of each mouse strain and feeding), the number and the area of anti-Aβ positive plaques, as well as the number of iba1-positive cells, were assessed and measured semiautomatically with ImageJ 1.47 v. in a high-power field (HPF) and are given in n/HPF and μm^2 for the area.

2.7. Western Blot Analysis of Brain Tissue

Harvested brain tissue was further processed for protein isolation. For this purpose, brain tissue was homogenized in lysis buffer (10 mM Tris pH 7.5, 10 mM NaCl, 0.1 mM EDTA, 0.5% Triton-X 100, 0.02% NaN_3 and 0.2 mM PMSF, protease inhibitor cocktail), incubated for 30 min on ice, and centrifuged for 10 min at 4 °C and 10,000× g. Protein contents were assayed by bicinchoninic acid method (Pierce Biotechnology, Rockford, IL, USA) with 2.5% BSA (Pierce Biotechnology, Rockford, IL, USA) as standard, as already described by the authors of [29]. On 14% (for LC3B) or 10% (for p62) SDS gels, 15 µg protein from brain tissue was separated and transferred to a polyvinyldifluoride membrane (Immobilon-P; Millipore, Burlington, MA, USA). After blockade with 2.5% BSA (Pierce Biotechnology, Rockford, IL, USA), membranes were incubated overnight at 4 °C with a rabbit polyclonal anti-p62 antibody (1:8000, Abcam, Berlin, Germany) and a rabbit polyclonal anti-LC3B antibody (1:1000, Sigma L7543, Sigma-Aldrich, Darmstadt, Germany). Exemplary raw images of western blot analysis of LC3B and p62 are shown in Appendix A (Figures A2 and A3). The anti-LC3B antibody is able to detect both isoforms, LC3BI (~18 kDa) and LC3BII (~16 kDa), which can be distinguished by their corresponding molecular weight, as seen in the original blots (Appendix A, Figure A2). Afterward, a secondary HRP-linked anti-rabbit antibody (1:10,000, cell signaling 7074, Cell Signaling Technology, Frankfurt am Main, Germany) was applied. Visualization of protein expression was performed by means of luminol-enhanced chemiluminescence (ECL plus; Amersham Pharmacia Biotech, Amersham, UK). After digitalization with the ChemiDoc™ XRS System (Bio-Rad Laboratories, Hercules, CA, USA), signals were densitometrically assessed (Quantity One; Bio-Rad Laboratories, Hercules, CA, USA) and normalized to the density of β-actin signal in the respective specimen (acquired with mouse monoclonal anti-β-actin antibody; 1:20,000; Sigma, A5441 and secondary HRP-linked anti-mouse antibody; 1:60,000; Sigma, A9044, Sigma-Aldrich, Darmstadt, Germany).

2.8. Statistical Analysis

Data were checked for normal distribution with the Shapiro–Wilk test and variances of standard deviations were verified by Bartlett's test. If standard deviations were not significantly different with $p > 0.05$, an ordinary one-way ANOVA was performed, followed by Sidak's multiple comparisons test or unpaired student t-test followed by Bonferroni correction with p threshold of 0.0166 was performed. Otherwise, Brown–Forsythe and Welch ANOVA were performed followed by Tamhane's T2 multiple comparisons test. If data were not normally distributed, the Kruskal–Wallis test with Dunn's post hoc test for multiple comparisons or Mann–Whitney test, followed by Bonferroni correction with p threshold of 0.0166, was conducted. All data are expressed as mean ± standard error of

mean (SEM). Statistical analysis was performed using the GraphPadPrism version 8.0.1 (GraphPad software, San Diego, CA, USA).

3. Results

3.1. Short-Term CR (16 Weeks) Showed No Effect in Glucose Uptake and Cognition Performance

CR vs. AL feeding for 16 weeks resulted in a significant decrease of bodyweight in wt and tg mice ($p \leq 0.0001$, student t-test followed by Bonferroni correction, Table 1). Of utmost interest, blood sugar concentrations were almost unaffected by CR in both mouse strains (Table 1). In our study, short-term CR did not change [^{18}F]FDG uptake (Table 2) nor cognitive performance (Table 3). Therefore, in the following evaluations, we only refer to the long-term CR.

Table 1. Blood glucose concentrations and body weight of short- (16 weeks) and long-term (68 weeks) ad libitum (AL) or caloric-restricted (CR, 60% of ad libitum) diet-fed wild-type (wt) and transgenic (tg) mice (all mice revealed starting weight of approximately 19 g). Values are given as mean ± SEM. Significance of differences between the groups was tested by unpaired student t-test or Mann–Whitney test, both followed by Bonferroni correction with p threshold of 0.0166: ** $p < 0.005$; *** $p \leq 0.0001$ vs. AL.

Genotype	**wt**		**tg**	
Feeding for 16 Weeks	**AL**	**CR**	**AL**	**CR**
Blood glucose (mmol/L)	7.94 ± 0.54	** 5.62 ± 0.27	7.15 ± 0.25	5.70 ± 0.27
Body weight (g)	28.90 ± 3.42	*** 20.26 ± 0.47	31.35 ± 0.95	*** 20.62 ± 0.44
Feeding for 68 Weeks	**AL**	**CR**	**AL**	**CR**
Blood glucose (mmol/L)	6.80 ± 0.27	6.78 ± 0.34	7.55 ± 0.05	6.15 ± 0.34
Body weight (g)	33.72 ± 2.29	*** 23.15 ± 0.55	28.88 ± 2.65	** 21.95 ± 0.71

Table 2. [^{18}F]FDG uptake (ID%/g) measurements of short-term (16 weeks) ad libitum (AL) or caloric restricted (CR, 60% of ad libitum) diet-fed wild-type (wt) and transgenic (tg) mice. Values are given as mean ± SEM. Significance of differences between the groups was tested by Brown–Forsythe and Welch ANOVA, followed by Tamhane's T2 multiple comparisons test (cortex) or ordinary one-way ANOVA and Sidak's multiple comparisons test (hippocampus).

Genotype	**wt**		**tg**	
Feeding for 16 Weeks	**AL**	**CR**	**AL**	**CR**
[^{18}F]FDG uptake (ID%/g)				
cortex	4.65 ± 0.25	4.90 ± 0.20	5.35 ± 0.25	5.18 ± 0.33
hippocampus	5.42 ± 0.28	5.46 ± 0.22	6.19 ± 0.31	5.94 ± 0.38

Table 3. Morris Water Maze parameters of short-term (16 weeks) ad libitum (AL) or caloric restricted (CR, 60% of ad libitum) diet-fed wild-type (wt) and transgenic (tg) mice. Values are given as mean ± SEM. Significance of differences between the groups was tested by unpaired student t-test, followed by Bonferroni correction with p threshold of 0.0166.

Genotype	**wt**		**tg**	
Feeding for 16 Weeks	**AL**	**CR**	**AL**	**CR**
Platform crosses (n)	6.0 ± 1.0	7.4 ± 1.5	5.0 ± 1.0	3.8 ± 0.9
Latency to first platform crossing (s)	10.1 ± 5.5	12.6 ± 4.2	37.7 ± 12.4	27.0 ± 7.1
Time spent on platform (s)	1.6 ± 0.5	2.9 ± 0.6	1.6 ± 0.6	1.5 ± 0.2
N-quadrant crosses (n)	18.3 ± 2.7	20.0 ± 2.3	19.5 ± 1.5	14.4 ± 1.2

3.2. Long-Term (68 Weeks) CR Significantly Increased [^{18}F]FDG Uptake

^{1}H-MRS demonstrated a significant reduction of the NAA/Cr ratio (p = 0.0272; Figure 1c) in tg vs. wt mice upon AL feeding. During CR feeding, the NAA/Cr ratio

of tg mice tended to be elevated in contrast to AL-fed tg mice ($p = 0.0523$) and reached similar values as wt mice (Figure 1c). Whereas CR for 68 weeks caused significant reductions of approximately 30% of bodyweight in wt ($p \leq 0.0001$, student t-test followed by Bonferroni correction) and tg mice ($p = 0.0027$, Mann–Whitney test followed by Bonferroni correction) vs. AL feeding, the blood sugar concentrations were almost unchanged (Table 1). Long-term CR vs. AL feeding in tg mice resulted in a significant increase of [^{18}F]FDG uptake in the cortex ($p = 0.0161$, student t-test followed by Bonferroni correction, Figure 2a) and hippocampus ($p = 0.0035$, student t-test followed by Bonferroni correction, Figure 2b) with representative PET-CT images (Figure 2c).

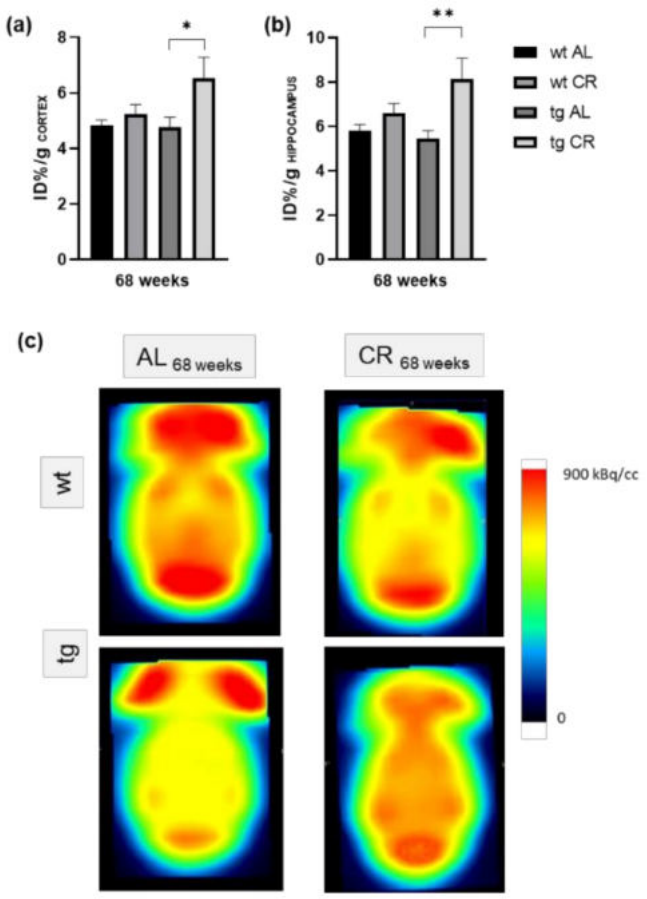

Figure 2. Quantification of [^{18}F]FDG uptake in the cortex (**a**) and hippocampus (**b**) given as ID%/g of wild-type (wt) and transgenic APPswe/PS1delta9 (tg) mice. Mice were fed either ad libitum (AL) or a caloric-restricted (CR, 60% of ad libitum) diet for 68 weeks. Values are given as mean ± SEM. Significance of differences between the groups was tested by unpaired student t-test followed by Bonferroni correction with p threshold of 0.0166: * $p < 0.05$ or ** $p < 0.005$ vs. AL. Visual comparison of representative Images of [^{18}F]FDG uptake in the brain of wt and tg mice (**c**).

3.3. Long-Term CR Increased Working Memory

Mice were tested in the spatial reference memory version of the MWM upon long-term CR. All mice were trained to find the platform (escape latencies were monitored, data not shown). In the trial, the platform was removed, and the number of platform crossings during 60 s was measured. The number of platform crosses measured in tg mice was almost half of those in wt mice upon AL feeding (Figure 3a). Long-term CR improved working memory performance as indicated by an almost two-fold increase of platform crosses in both mouse strains, whereas the increase was significant in tg mice ($p = 0.0161$, student t-test followed by Bonferroni correction Figure 3a). Moreover, latency to first platform crosses was found tendentially (up to three-fold) increased in tg mice when compared

to wt mice. CR shortened latency in wt and significantly shortened latency in tg mice ($p = 0.0069$, student t-test followed by Bonferroni correction, Figure 3b). Correspondingly, time spent on platform was reduced up to eight-fold in tg vs. wt mice and was increased up to 4-fold upon long-term CR vs. AL in tg mice (Figure 3c). Additionally, the number of N-quadrant crosses was found tendentially decreased in tg vs. wt mice ($p = 0.0200$, student t-test followed by Bonferroni correction), and again significantly increased upon CR when compared to AL feeding ($p = 0.0018$, student t-test followed by Bonferroni correction; Figure 3d).

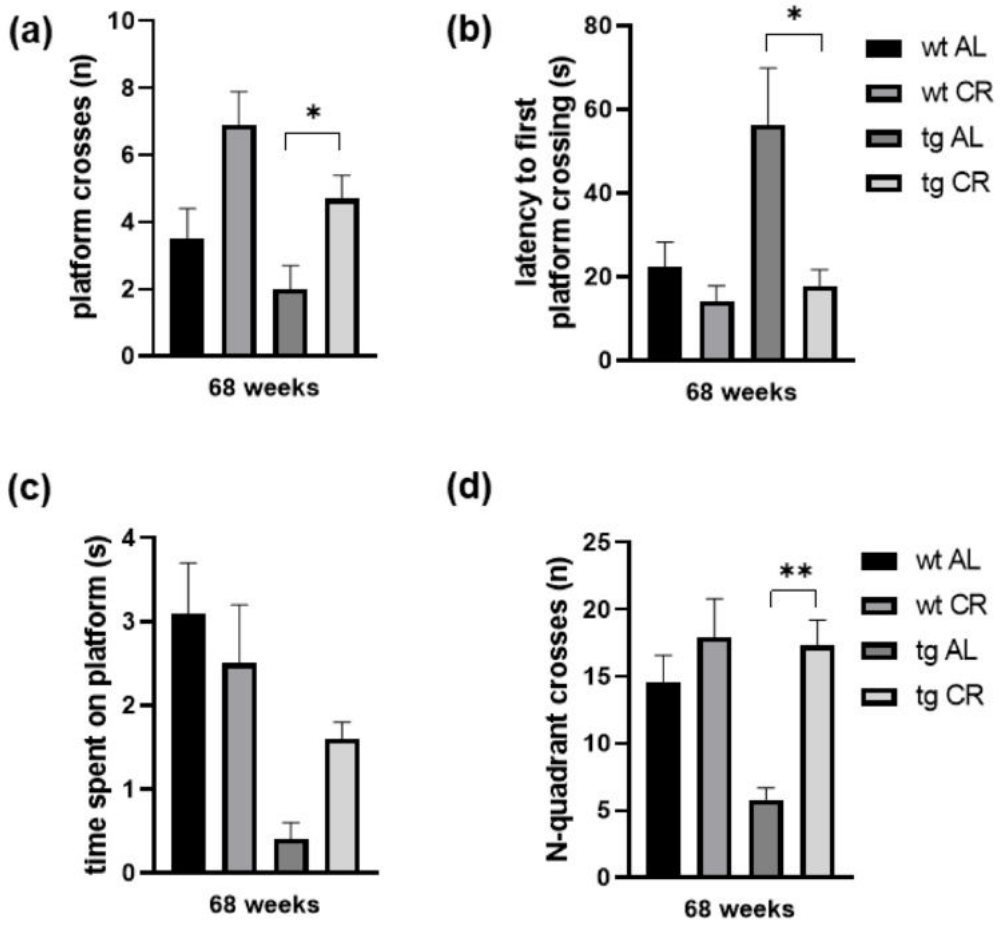

Figure 3. Number (*n*) of platform crosses during 60 s (**a**), latency (in s) to first platform crossing (**b**), time (in s) spent on platform (**c**), and n of north (N)-quadrant crosses (**d**) were measured for wild-type (wt) and transgenic APPswe/PS1delta9 (tg) mice. Mice were fed either ad libitum (AL) or a caloric-restricted diet (CR, 60% of ad libitum) for 68 weeks. Values are given as mean ± SEM. Significance of differences between the groups was tested by unpaired student *t*-test, followed by Bonferroni correction with *p* threshold of 0.0166: * $p < 0.05$ or ** $p < 0.005$ vs. AL.

3.4. Long-Term CR Increased Autophagy

The analysis of LC3BII protein expression revealed no difference between AL-fed wt and tg mice, while CR caused a marked increase of LC3BII expression which was significant in tg mice (Figure 4a; $p = 0.0392$). The analysis of p62 protein expression revealed a slight decrease in AL-fed tg vs. wt mice (Figure 4b). Protein expression of p62 was markedly increased upon CR in both mouse strains but was increased more significantly in tg mice ($p = 0.0176$) (Figure 4b).

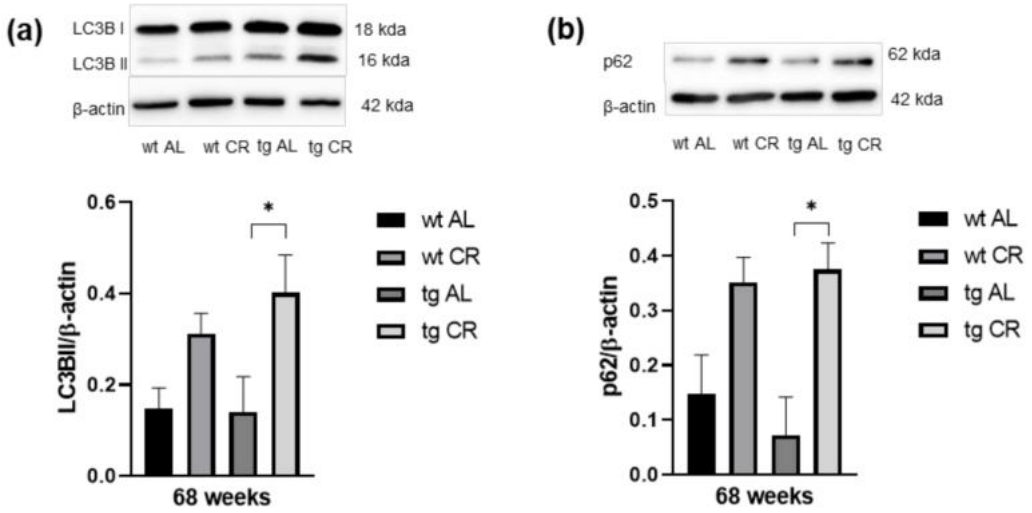

Figure 4. Representative Western blots, as well as densitometric analysis of (**a**) LC3BII and (**b**) p62 expression in brain of wild-type (wt) and transgenic APPswe/PS1delta9 (tg) mice. Mice were fed either ad libitum (AL) or a caloric-restricted diet (CR, 60% of ad libitum) for 68 weeks. Signals were corrected to that of β-actin. Values are given as mean ± SEM. Significance of differences between the groups was tested by one-way ANOVA on Ranks (Kruskal–Wallis) with Dunn's post hoc test for multiple comparisons: * $p < 0.05$ vs. AL.

3.5. Long-Term CR Reduced Aβ-Plaque Load and Size as Well as Accompanying Neuroinflammation

Analysis of Aβ-stained brain sections of tg mice (Figure 5a–f) revealed a mean plaque number of 39.5 ± 7.0 per HPF in the cortex (Figure 5a) and 59.1 ± 7.0 per HPF in the hippocampus (Figure 5d), and an average plaque size of 2.6 ± 0.2 µm2 in the cortex (Figure 5b) and 2.4 ± 0.2 μm^2 in the hippocampus (Figure 5e). In the wt samples, no Aβ plaque could be detected (not detected, n.d.). Nevertheless, the respective images are provided in Appendix A (Figure A4). Long-term CR significantly reduced the Aβ plaque number (21.3 ± 3.4; $p < 0.0001$; student t-test followed by Bonferroni correction; Figure 5d) and plaque area (1.3 ± 0.1 μm^2; $p < 0.0001$; student t-test followed by Bonferroni correction; Figure 5e) in the hippocampus.

The presence of plaque was accompanied by neuroinflammatory processes, displayed by a 40% increase of cortical (Figure 6a,b) and a significant increase of hippocampal ($p = 0.0009$; Figure 6c,d) iba1-positive cells in tg mice compared to wt mice. The reduction of plaque load and size in the hippocampus upon long-term CR in tg mice was accompanied by a significantly decreased number of iba1-positive hippocampal cells ($p = 0.0329$; Figure 6c).

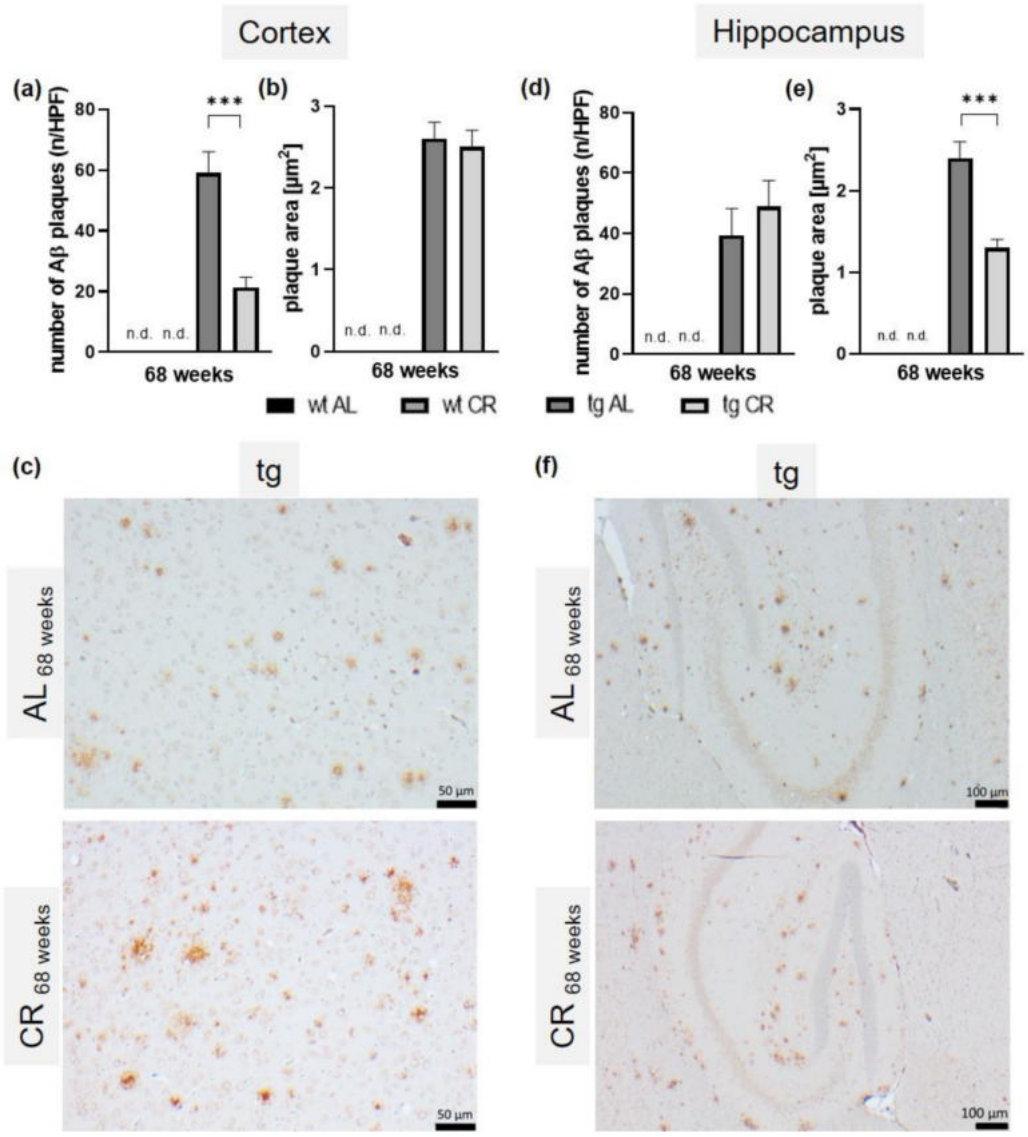

Figure 5. Quantitative analysis of the number of cortical (**a**) and hippocampal (**d**) amyloid-β (Aβ) plaques (*n*) per high-power field (HPF) and the cortical (**b**) and hippocampal (**e**) Aβ-plaque area (µm^2) of wild-type (wt; not detectable n.d.) and transgenic APPswe/PS1delta9 (tg) mice and representative immunohistochemical images of cortical (scale bar representing 50 µm (**c**)) and hippocampal (scale bar representing 100 µm (**f**)) Aβ-stained (6E10) brain sections of tg mice. Mice were fed either ad libitum (AL) or a caloric-restricted diet (CR, 60% of ad libitum) for 68 weeks. Significance of differences between the groups was tested by unpaired student t-test, followed by Bonferroni correction with p threshold of 0.0166: *** $p \leq 0.001$ vs. AL.

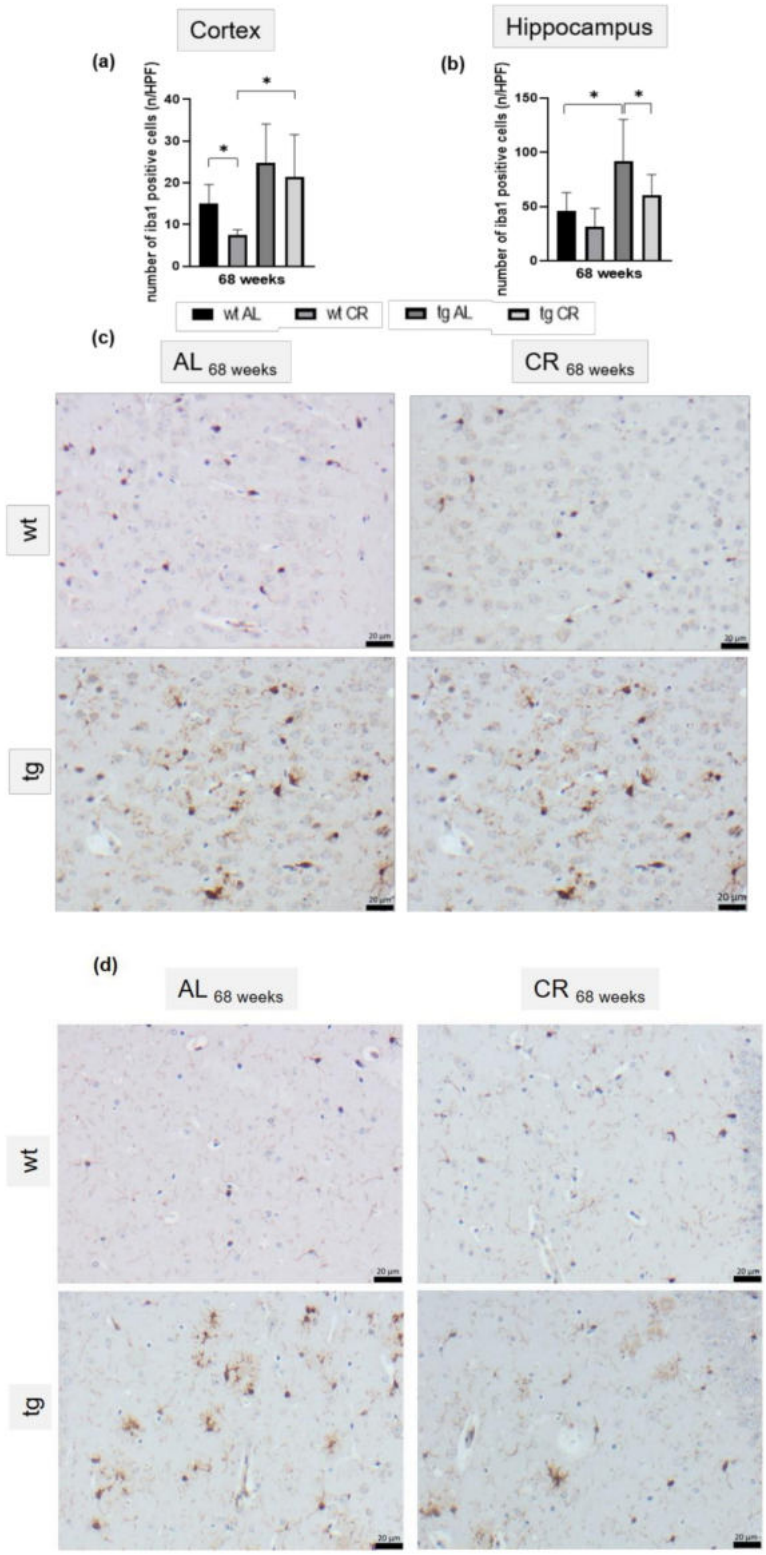

Figure 6. Quantitative analysis of the number of iba1-positive cortical (**a**) and hippocampal cells (**b**) per high-power field (*n*/HPF) of wild-type (wt) and transgenic APPswe/PS1delta9 (tg) mice and representative immunohistochemical images of cortical (**c**) and hippocampal (**d**) iba1-stained brain sections (scale bar representing 20 µm) of wt and tg mice. Mice were fed either ad libitum (AL) or a caloric-restricted diet (CR, 60% of ad libitum) for 68 weeks. Values are given as mean ± SEM; Significance of differences between the groups was tested by Brown–Forsythe and Welch ANOVA, followed by Tamhane's T2 multiple comparisons test (**a**) or ordinary one-way ANOVA and Sidak's multiple comparisons test (**b**): * $p < 0.05$.

4. Discussion

The main finding of the study was that CR ameliorates cognitive function by a measurable increase of glucose uptake, indicating a CR-induced increase in neuronal activity. This was accompanied by attenuated Aβ deposition and related microglia activation in the hippocampus. Overall, we speculate that this might be a result of CR-activated autophagy, but further investigation is needed to support this hypothesis.

CR-mediated attenuation of Aβ neuropathology in AD mouse studies has already been well described in literature. Mouton et al. [7] reported that CR reduced the total Aβ volume by about one-third in APP/PS1 mice. Moreover, Patel et al. [8] showed that, besides decreased plaque load and size, the immune-reactive area around Aβ plaques was markedly reduced upon CR in APP/PS1 mice as indicated by decreased numbers of astrocytes (GFAP-positive cells). Similarly, the current study demonstrates that the plaque load and size, as well as the number of activated microglia (iba1-positive cells), were significantly reduced in tg mice in the hippocampus. However, this could only be observed upon 68 weeks of CR. In contrast, 16-week ongoing CR showed no influence on Aβ pathology, although the study of Patel et al. [8] stated otherwise and was able to show an anti-amyloidogenic effect after 14 weeks of CR in double-transgenic APP/PS1 mice starting at 2 months of age. In contrast, longer CRs of 7 and 14 months were used by Halagappa et al. [12], showing that only CR of 14 months reduced Aβ levels and improved cognitive performance, as analyzed by MWM, in another transgenic mouse strain (3xTgAD) starting at 3 months of age. In this context, we are also able to show that only long-term CR attenuated the working memory of tg mice. Current literature has discussed whether better cognitive performance is mediated by CR-induced reduction of neuronal loss. Dong et al. [11] reported that CR significantly increased cell density in the CA3 region in the hippocampus. Moreover, CR has been described to prevent age-related disease or normal signs of age [30]. In this sense, the senescent (72-week-old) wt mice used in the current study benefited from low caloric intake, as indicated by better cognitive performance upon 68 weeks of CR. This anti-aging effect has been reported by several other groups [31–33]. In case of the AD mice, not only anti-aging processes are relevant for the neuroprotection, but anti-amyloidogenic mechanisms are also important [10]. Herein, it is shown that the mature form of ADAM10—an enzyme with α-secretase activity for the proteolytic processing of APP—was significantly upregulated in CR-fed Tg2576 mice [10], resulting in reduced Aβ plaque load. Since APPswe/PS1delta9 mice do not show any changes of ADAM10 expression in the hippocampus compared with their control littermates [34], we refrained from further investigating this pathway. Beside the anti-amyloidogenic process, CR is also able to induce autophagy, a well-documented catabolic mechanism which is known to degrade aggregated proteins [35], including Aβ. This processing pathway is characterized by translocation of Atg protein LC3BII, together with sequestosom-1 (p62) to the autophagosome membrane, which is commonly used as marker of autophagosome formation [16]. However, in AD animal models, autophagic activities have not yet been studied extensively as an underlying cause for the beneficial effects of CR [36]. Thus, it is still unclear if elevated autophagy has predominantly neuroprotective or neurodegenerative effects, as reported findings are partially contradictive. For example, CR-induced upregulation of SIRT-1 [37] may induce neuroprotective effects by upregulating autophagy through downstream signaling [36,38], whereas the neuroprotective effects of CR-upregulated BDNF [39] are due to autophagy suppression [40]. To complement the ambivalent data, the current study found that CR-fed tg mice exhibited a significant increase in autophagy. This was shown by elevated LC3BII and p62 levels, suggesting a neuroprotective mechanism of CR by restoration of cognitive function to wt levels through autophagy-induced Aβ degradation. Further experiments should be carried out in the future to clarify to what extend autophagy is the main driver of Aβ degradation.

Moreover, autophagy is also essential for accurate cellular and energy homeostasis. In this context, autophagy positively regulates glucose uptake via upregulation of GLUT-1 protein expression [41]. Therefore, it may be concluded that increased FDG uptake upon

CR in tg mice is a consequence of increased autophagic activity. However, it can also be assumed that CR-induced autophagy and the associated Aβ degradation lead to improved neuronal activity per se, indicated by increased FDG uptake. Restrictively, it is known that reduced blood glucose concentration may enhance FDG uptake [42]. However, due to the barely changed blood glucose concentration upon CR, this does not seem to be the reason for the increased FDG uptake in CR-fed tg mice. In general, measurement of the effect of CR by [^{18}F]FDG PET-CT opens the possibility to monitor CR-induced neuroprotection using a noninvasive method and, in particular, in a longitudinal manner. In addition to [^{18}F]FDG-PET/CT, 1H-MRS represents another in vivo technique which allows for the characterization of metabolic changes in AD brains [43,44]. NAA, as a representative metabolite of neuronal integrity, is found to be reduced in AD, indicating neuronal malfunction either due to diminished neuronal density, neuronal cell loss, or partially reversible neuronal dysfunction [45], and correlates with disease progression [46]. Further, APP/PS1 mice also show significantly decreased NAA to Cr ratio [28,45,47], which was also observed in the present study. Upon long-term CR, NAA/Cr ratios were increased, reaching the same values as those found in wt mice, indicating improved neuronal integrity. However, the transfer of findings from transgenic animal models to humans is limited [48]. Nevertheless, the use of quantitative neuroimaging methods possibly aids the improvement of translational potential of preclinical AD research regarding brain metabolism or morphology [49].

5. Conclusions

In summary, the present study showed, for the first time, that the known CR-induced Aβ degradation [7,8] is accompanied by increased autophagy and improved neuronal activity as well as integrity, resulting in a better cognitive performance. Further studies need to clarify to what extent the observed increased autophagy in CR tg mice (upon 68 weeks CR) is responsible for the attenuation of the Aβ pathology.

Author Contributions: Conceptualization: A.K.; Methodology: L.M., N.P.G., J.S., C.R., T.L., A.K.; Validation: L.M., B.V., A.K.; Formal Analysis: L.M., J.S., C.R., T.L., A.K.; Investigation: J.S., C.R., T.L.; Resources: B.J.K., B.V., S.T., A.K.; Data Curation: L.M., A.K.; Writing—Original Draft Preparation: L.M., A.K.; Writing—Review and Editing: B.V., S.T., A.K.; Visualization: L.M., T.L., A.K.; Supervision: B.J.K., B.V., S.T., A.K.; Project administration: A.K.; Funding acquisition: A.K.; Animal Care: N.P.G., C.R. All authors have read and agreed to the published version of the manuscript.

Funding: This study was supported by a grant from the Deutsche Forschungsgemeinschaft, Bonn, Germany (KU 3280/1-2).

Institutional Review Board Statement: The experimental protocol was approved by the local Animal Research Committee (Landesamt für Landwirtschaft, Lebensmittelsicherheit und Fischerei (LALLF) of the state Mecklenburg-Western Pomerania (LALLF M-V/TSD/7221.3-1.1-002/14)). All animals received care according to the German legislation on protection of animals and the Guide for the Care and Use of Laboratory Animals (European Directive 2010/63/EU).

Informed Consent Statement: Not applicable.

Data Availability Statement: The data presented in this study are available on request from the corresponding author.

Acknowledgments: The authors cordially thank the technicians of the Institute for Experimental Surgery, Central Animal Care Facility, Core Facility Multimodal Small Animal Imaging for their valuable assistance and the staff of the Department of Nuclear Medicine for the production of the radiotracer [^{18}F]FDG.

Conflicts of Interest: The other authors declare that they have no conflict of interest.

Appendix A

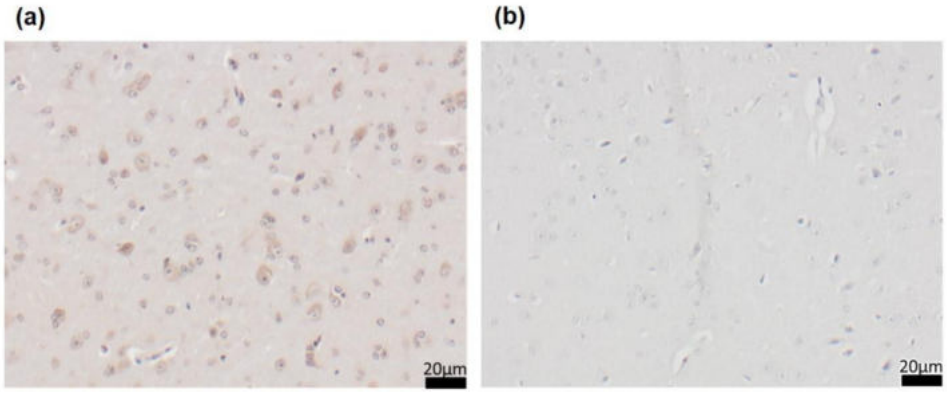

Figure A1. Negative controls of (**a**) 6E10 anti-Aβ staining and (**b**) iba1 staining.

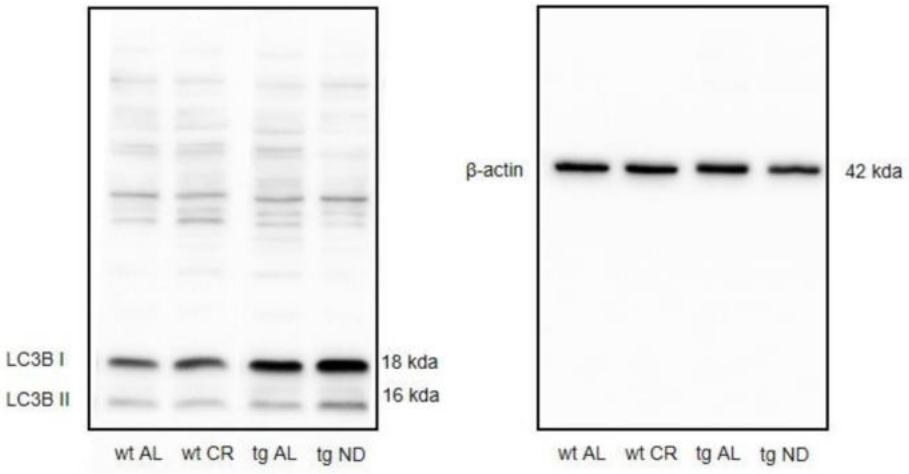

Figure A2. Raw Western blot:of LC3B and β-actin on 14% SDS gel.

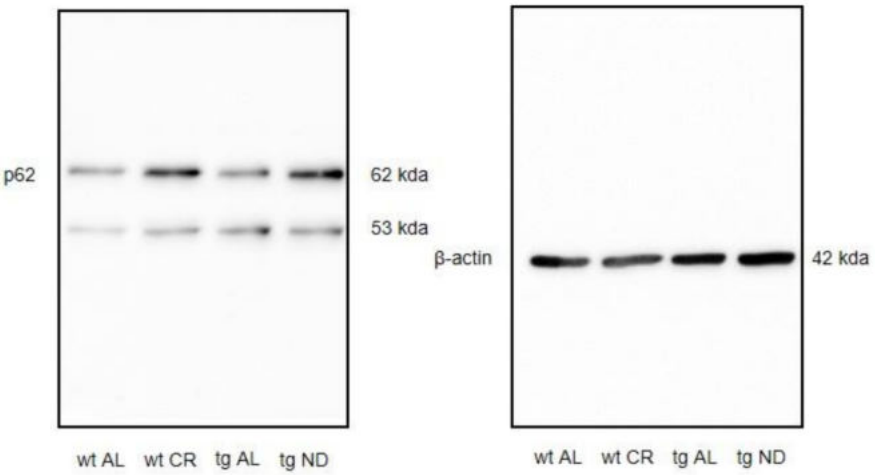

Figure A3. Raw Western blot of p62 and β-actin on 10% SDS gel.

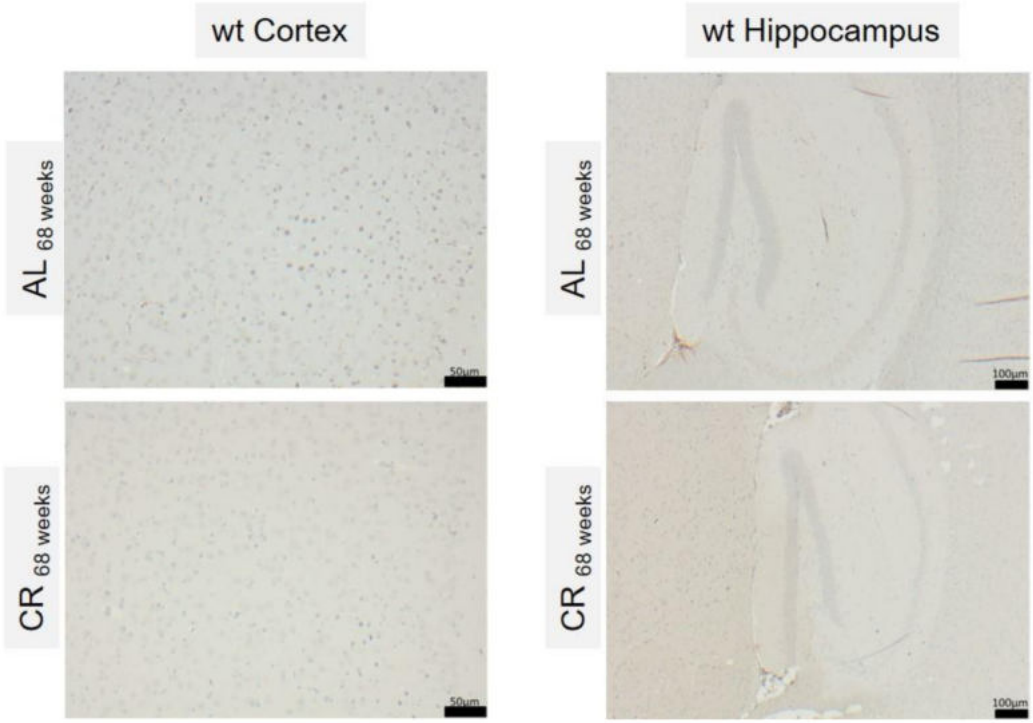

Figure A4. Representative immunohistochemical images of cortical (scale bar representing 50 µm) and hippocampal (scale bar representing 100 µm) Aβ-stained (6E10) brain sections of wt mice.

References

1. Hyman, B.T. The neuropathological diagnosis of Alzheimer's disease: Clinical-pathological studies. *Neurobiol. Aging* **1997**, *18* (Suppl. 4). [CrossRef]
2. Malm, T.; Koistinaho, J.; Kanninen, K. Utilization of APPswe/PS1dE9 Transgenic Mice in Research of Alzheimer's Disease: Focus on Gene Therapy and Cell-Based Therapy Applications. *Int. J. Alzheimer's Dis.* **2011**, *2011*, 517160. [CrossRef] [PubMed]
3. Del Sole, A.; Clerici, F.; Chiti, A.; Lecchi, M.; Mariani, C.; Maggiore, L.; Mosconi, L.; Lucignani, G. Individual cerebral metabolic deficits in Alzheimer's disease and amnestic mild cognitive impairment: An FDG PET study. *Eur. J. Nucl. Med. Mol. Imaging* **2008**, *35*, 1357–1366. [CrossRef]
4. Herholz, K.; Carter, S.F.; Jones, M. Positron emission tomography imaging in dementia. *Br. J. Radiol.* **2007**, *80*, S160–S167. [CrossRef]
5. Singh-Manoux, A.; Czernichow, S.; Elbaz, A.; Dugravot, A.; Sabia, S.; Hagger-Johnson, G.; Kaffashian, S.; Zins, M.; Brunner, E.J.; Nabi, H.; et al. Obesity phenotypes in midlife and cognition in early old age: The Whitehall II cohort study. *Neurology* **2012**, *79*, 755–762. [CrossRef] [PubMed]
6. Xu, W.L.; Atti, A.R.; Gatz, M.; Pedersen, N.L.; Johansson, B.; Fratiglioni, L. Midlife overweight and obesity increase late-life dementia risk: A population-based twin study. *Neurology* **2011**, *76*, 1568–1574. [CrossRef]
7. Mouton, P.R.; Chachich, M.E.; Quigley, C.; Spangler, E.; Ingram, D.K. Caloric restriction attenuates amyloid deposition in middle-aged dtg APP/PS1 mice. *Neurosci. Lett.* **2009**, *464*, 184–187. [CrossRef] [PubMed]
8. Patel, N.V.; Gordon, M.N.; Connor, K.E.; Good, R.A.; Engelman, R.W.; Mason, J.; Morgan, D.G.; Morgan, T.E.; Finch, C.E. Caloric restriction attenuates Abeta-deposition in Alzheimer transgenic models. *Neurobiol. Aging* **2005**, *26*, 995–1000. [CrossRef]
9. Schafer, M.J.; Alldred, M.J.; Lee, S.H.; Calhoun, M.E.; Petkova, E.; Mathews, P.M.; Ginsberg, S.D. Reduction of β-amyloid and γ-secretase by calorie restriction in female Tg2576 mice. *Neurobiol. Aging* **2015**, *36*, 1293–1302. [CrossRef]
10. Wang, J.; Ho, L.; Qin, W.; Rocher, A.B.; Seror, I.; Humala, N.; Maniar, K.; Dolios, G.; Wang, R.; Hof, P.R.; et al. Caloric restriction attenuates beta-amyloid neuropathology in a mouse model of Alzheimer's disease. *FASEB J.* **2005**, *19*, 659–661. [CrossRef]
11. Dong, W.; Wang, R.; Ma, L.-N.; Xu, B.-L.; Zhang, J.-S.; Zhao, Z.-W.; Wang, Y.-L.; Zhang, X. Influence of age-related learning and memory capacity of mice: Different effects of a high and low caloric diet. *Aging Clin. Exp. Res.* **2016**, *28*, 303–311. [CrossRef] [PubMed]
12. Halagappa, V.K.M.; Guo, Z.; Pearson, M.; Matsuoka, Y.; Cutler, R.G.; LaFerla, F.M.; Mattson, M.P. Intermittent fasting and caloric restriction ameliorate age-related behavioral deficits in the triple-transgenic mouse model of Alzheimer's disease. *Neurobiol. Dis.* **2007**, *26*, 212–220. [CrossRef] [PubMed]
13. Nilsson, P.; Loganathan, K.; Sekiguchi, M.; Matsuba, Y.; Hui, K.; Tsubuki, S.; Tanaka, M.; Iwata, N.; Saito, T.; Saido, T.C. Aβ secretion and plaque formation depend on autophagy. *Cell Rep.* **2013**, *5*, 61–69. [CrossRef] [PubMed]

14. Alirezaei, M.; Kemball, C.C.; Whitton, J.L. Autophagy, inflammation and neurodegenerative disease. *Eur. J. Neurosci.* **2011**, *33*, 197–204. [CrossRef]
15. Gregosa, A.; Vinuesa, Á.; Todero, M.F.; Pomilio, C.; Rossi, S.P.; Bentivegna, M.; Presa, J.; Wenker, S.; Saravia, F.; Beauquis, J. Periodic dietary restriction ameliorates amyloid pathology and cognitive impairment in PDAPP-J20 mice: Potential implication of glial autophagy. *Neurobiol. Dis.* **2019**, *132*, 104542. [CrossRef]
16. Moreira, P.I.; Santos, R.X.; Zhu, X.; Lee, H.-G.; A Smith, M.; Casadesus, G.; Perry, G. Autophagy in Alzheimer's disease. *Expert Rev. Neurother.* **2010**, *10*, 1209–1218. [CrossRef]
17. Hashimoto, T.; Watanabe, S. Chronic food restriction enhances memory in mice–analysis with matched drive levels. *Neuroreport* **2005**, *16*, 1129–1133. [CrossRef]
18. Kuhla, A.; Lange, S.; Holzmann, C.; Maass, F.; Petersen, J.; Vollmar, B.; Wree, A. Lifelong caloric restriction increases working memory in mice. *PLoS ONE* **2013**, *8*, e68778. [CrossRef]
19. Jankowsky, J.L.; Younkin, L.H.; Gonzales, V.; Fadale, D.J.; Slunt, H.H.; Lester, H.A.; Younkin, S.G.; Borchelt, D.R. Rodent A beta modulates the solubility and distribution of amyloid deposits in transgenic mice. *J. Biol. Chem.* **2007**, *282*, 22707–22720. [CrossRef]
20. Xiong, H.; Callaghan, D.; Wodzinska, J.; Xu, J.; Premyslova, M.; Liu, Q.-Y.; Connelly, J.; Zhang, W. Biochemical and behavioral characterization of the double transgenic mouse model (APPswe/PS1dE9) of Alzheimer's disease. *Neurosci. Bull.* **2011**, *27*, 221–232. [CrossRef]
21. Rühlmann, C.; Dannehl, D.; Brodtrück, M.; Adams, A.C.; Stenzel, J.; Lindner, T.; Krause, B.J.; Vollmar, B.; Kuhla, A. Neuroprotective Effects of the FGF21 Analogue LY2405319. *J. Alzheimer's Dis.* **2021**. [CrossRef]
22. Naressi, A.; Couturier, C.; Castang, I.; de Beer, R.; Graveron-Demilly, D. Java-based graphical user interface for MRUI, a software package for quantitation of in vivo/medical magnetic resonance spectroscopy signals. *Comput. Biol. Med.* **2001**. [CrossRef]
23. Stefan, D.; Di Cesare, F.; Andrasescu, A.; Popa, E.; Lazariev, A.; Vescovo, E.; Strbak, O.; Williams, S.; Starcuk, Z.; Cabanas, M.; et al. Quantitation of magnetic resonance spectroscopy signals: The jMRUI software package. *Meas. Sci. Technol.* **2009**. [CrossRef]
24. Mocioiu, V.; Ortega-Martorell, S.; Olier, I.; Jablonski, M.; Starčuková, J.; Lisboa, P.; Arús, C.; Julià-Sapé, M. From raw data to data-analysis for magnetic resonance spectroscopy—The missing link: jMRUI2XML. *BMC Bioinform.* **2015**, *16*, 378. [CrossRef] [PubMed]
25. Pijnappel, W.; Boogaart, A.V.D.; De Beer, R.; Van Ormondt, D. SVD-based quantification of magnetic resonance signals. *J. Magn. Reson.* **1992**. [CrossRef]
26. Kuhla, A.; Meuth, L.; Stenzel, J.; Lindner, T.; Lappe, C.; Kurth, J.; Krause, B.J.; Teipel, S.; Glass, Ä.; Kundt, G.; et al. Longitudinal 18FFDG-PET/CT analysis of the glucose metabolism in ApoE-deficient mice. *EJNMMI Res.* **2020**, *10*, 119. [CrossRef]
27. Stenzel, J.; Rühlmann, C.; Lindner, T.; Polei, S.; Teipel, S.; Kurth, J.; Rominger, A.; Krause, B.; Vollmar, B.; Kuhla, A. 18F-florbetaben PET/CT Imaging in the Alzheimer's Disease Mouse Model APPswe/PS1dE9. *Curr. Alzheimer Res.* **2019**, *16*, 49–55. [CrossRef] [PubMed]
28. Kuhla, A.; Rühlmann, C.; Lindner, T.; Polei, S.; Hadlich, S.; Krause, B.J.; Vollmar, B.; Teipel, S.J. APPswe/PS1dE9 mice with cortical amyloid pathology show a reduced NAA/Cr ratio without apparent brain atrophy: A MRS and MRI study. *Neuroimage Clin.* **2017**, *15*, 581–586. [CrossRef]
29. Kuhla, A.; Ludwig, S.C.; Kuhla, B.; Münch, G.; Vollmar, B. Advanced glycation end products are mitogenic signals and trigger cell cycle reentry of neurons in Alzheimer's disease brain. *Neurobiol. Aging* **2015**, *36*, 753–761. [CrossRef] [PubMed]
30. Liang, Y.; Liu, C.; Lu, M.; Dong, Q.; Wang, Z.; Wang, Z.; Xiong, W.; Zhang, N.; Zhou, J.; Liu, Q.; et al. Calorie restriction is the most reasonable anti-ageing intervention: A meta-analysis of survival curves. *Sci. Rep.* **2018**, *8*, 5779. [CrossRef] [PubMed]
31. Al-Regaiey, K.A. The effects of calorie restriction on aging: A brief review. *Eur. Rev. Med. Pharmacol. Sci.* **2016**, *20*, 2468–2473. [PubMed]
32. Speakman, J.R.; Mitchell, S.E. Caloric restriction. *Mol. Asp. Med.* **2011**, *32*, 159–221. [CrossRef] [PubMed]
33. Valdez, G.; Tapia, J.C.; Kang, H.; Clemenson, G.D.; Gage, F.H.; Lichtman, J.W.; Sanes, J.R. Attenuation of age-related changes in mouse neuromuscular synapses by caloric restriction and exercise. *Proc. Natl. Acad. Sci. USA* **2010**, *107*, 14863–14868. [CrossRef] [PubMed]
34. Huang, H.; Nie, S.; Cao, M.; Marshall, C.; Gao, J.; Xiao, N.; Hu, G.; Xiao, M. Characterization of AD-like phenotype in aged APPSwe/PS1dE9 mice. *AGE* **2016**, *38*, 303–322. [CrossRef]
35. Lilienbaum, A. Relationship between the proteasomal system and autophagy. *Int. J. Biochem. Mol. Biol.* **2013**, *4*, 1–26. [PubMed]
36. Yang, Y.; Zhang, L. The effects of caloric restriction and its mimetics in Alzheimer's disease through autophagy pathways. *Food Funct.* **2020**, *11*, 1211–1224. [CrossRef]
37. Quintas, A.; de Solís, A.J.; Díez-Guerra, F.J.; Carrascosa, J.M.; Bogónez, E. Age-associated decrease of SIRT1 expression in rat hippocampus: Prevention by late onset caloric restriction. *Exp. Gerontol.* **2012**, *47*, 198–201. [CrossRef] [PubMed]
38. Braidy, N.; Jayasena, T.; Poljak, A.; Sachdev, P.S. Sirtuins in cognitive ageing and Alzheimer's disease. *Curr. Opin. Psychiatry* **2012**, *25*, 226–230. [CrossRef]
39. Duan, W.; Lee, J.; Guo, Z.; Mattson, M.P. Dietary restriction stimulates BDNF production in the brain and thereby protects neurons against excitotoxic injury. *J. Mol. Neurosci.* **2001**, *16*, 1–12. [CrossRef]
40. Nikoletopoulou, V.; Sidiropoulou, K.; Kallergi, E.; Dalezios, Y.; Tavernarakis, N. Modulation of Autophagy by BDNF Underlies Synaptic Plasticity. *Cell Metab.* **2017**, *26*, 230–242.e5. [CrossRef]

41. Lee, Y.-R.; Wu, S.-Y.; Chen, R.-Y.; Lin, Y.-S.; Yeh, T.-M.; Liu, H.-S. Regulation of autophagy, glucose uptake, and glycolysis under dengue virus infection. *Kaohsiung J. Med. Sci.* **2020**. [CrossRef] [PubMed]
42. Coleman, R.A.; Liang, C.; Patel, R.; Ali, S.; Mukherjee, J. Brain and Brown Adipose Tissue Metabolism in Transgenic Tg2576 Mice Models of Alzheimer Disease Assessed Using 18F-FDG PET Imaging. *Mol. Imaging* **2017**, *16*, 1536012117704557. [CrossRef]
43. Arora, A.; Bhagat, N. Insight into the Molecular Imaging of Alzheimer's Disease. *Int. J. Biomed. Imaging* **2016**, *2016*, 7462014. [CrossRef]
44. Mlynárik, V.; Cacquevel, M.; Sun-Reimer, L.; Janssens, S.; Cudalbu, C.; Lei, H.; Schneider, B.L.; Aebischer, P.; Gruetter, R. Proton and phosphorus magnetic resonance spectroscopy of a mouse model of Alzheimer's disease. *J. Alzheimer's Dis.* **2012**, *31* (Suppl. 3), S87–S99. [CrossRef] [PubMed]
45. Clark, J.B. N-acetyl aspartate: A marker for neuronal loss or mitochondrial dysfunction. *Dev. Neurosci.* **1998**, *20*, 271–276. [CrossRef] [PubMed]
46. Ross, B.D.; Bluml, S.; Cowan, R.; Danielsen, E.; Farrow, N.; Tan, J. In vivo MR spectroscopy of human dementia. *Neuroimaging Clin. N. Am.* **1998**, *8*, 809–822.
47. Chen, S.-Q.; Cai, Q.; Shen, Y.-Y.; Wang, P.-J.; Teng, G.-J.; Zhang, W.; Zang, F.-C. Age-related changes in brain metabolites and cognitive function in APP/PS1 transgenic mice. *Behav. Brain Res.* **2012**, *235*, 1–6. [CrossRef] [PubMed]
48. Foley, A.M.; Ammar, Z.M.; Lee, R.H.; Mitchell, C.S. Systematic review of the relationship between amyloid-β levels and measures of transgenic mouse cognitive deficit in Alzheimer's disease. *J. Alzheimer's Dis.* **2015**, *44*, 787–795. [CrossRef]
49. Teipel, S.J.; Buchert, R.; Thome, J.; Hampel, H.; Pahnke, J. Development of Alzheimer-disease neuroimaging-biomarkers using mouse models with amyloid-precursor protein-transgene expression. *Prog. Neurobiol.* **2011**, *95*, 547–556. [CrossRef]

Anhang 4

Studie V:

Power Guerra, N.; Parveen, A.; Bühler, D.; Brauer, D.L.; Müller, L.; Pilz, K.; Witt, M.; Glass, Ä.; Bajorat, R.; Janowitz, D.; Wolkenhauer, O.; Vollmar, B.; Kuhla, A. Fibroblast Growth Factor 21 as a Potential Biomarker for Improved Locomotion and Olfaction Detection Ability after Weight Reduction in Obese Mice. *Nutrients* **2021**, 13(9), 2916. https://doi.org/10.3390/nu13092916.

nutrients

MDPI

Article

Fibroblast Growth Factor 21 as a Potential Biomarker for Improved Locomotion and Olfaction Detection Ability after Weight Reduction in Obese Mice

Nicole Power Guerra [1,2], Alisha Parveen [1], Daniel Bühler [1], David Leon Brauer [3], Luisa Müller [1,4,5], Kristin Pilz [6], Martin Witt [2], Änne Glass [7], Rika Bajorat [8], Deborah Janowitz [6], Olaf Wolkenhauer [3,9], Brigitte Vollmar [1,5] and Angela Kuhla [1,5,*]

1 Rudolf-Zenker-Institute for Experimental Surgery, Rostock University Medical Centre, Schillingallee 69a, 18057 Rostock, Germany; nicole.guerra@uni-rostock.de (N.P.G.); alisha.parveen@med.uni-rostock.de (A.P.); daniel.jenderny@uni-rostock.de (D.B.); luisa.mueller2@uni-rostock.de (L.M.); brigitte.vollmar@med.uni-rostock.de (B.V.)
2 Department of Anatomy, Rostock University Medical Centre, Gertrudenstraße 9, 18057 Rostock, Germany; martin.witt@med.uni-rostock.de
3 Department of Systems Biology and Bioinformatics, University of Rostock, Ulmenstraße 69, 18057 Rostock, Germany; david.brauer@uni-rostock.de (D.L.B.); olaf.wolkenhauer@uni-rostock.de (O.W.)
4 Department of Psychosomatic Medicine and Psychotherapy, Rostock University Medical Centre, Gehlsheimerstraße 20, 18147 Rostock, Germany
5 Centre for Transdisciplinary Neurosciences Rostock (CTNR), Rostock University Medical Centre, Gehlsheimerstraße 20, 18147 Rostock, Germany
6 Department of Psychiatry, University of Greifswald, Ellernholzstraße 1-2, 17489 Greifswald, Germany; kristin.pilz@med.uni-greifswald.de (K.P.); deborah.janowitz@helios-gesundheit.de (D.J.)
7 Institute for Biostatistics and Informatics, Rostock University Medical Centre, Ernst-Heydemann-Straße 8, 18057 Rostock, Germany; aenne.glass@med.uni-rostock.de
8 Department of Anesthesiology and Intensive Care Medicine, Rostock University Medical Centre, Schillingallee 35, 18057 Rostock, Germany; rika.bajorat@med.uni-rostock.de
9 Leibniz-Institute for Food Systems Biology, Technical University of Munich, Lise-Meitner-Straße 34, 85354 Freising, Germany
* Correspondence: angela.kuhla@uni-rostock.de; Tel.: +49-381-494-2503

Abstract: Obesity is one of the most challenging diseases of the 21st century and is accompanied by behavioural disorders. Exercise, dietary adjustments, or time-restricted feeding are the only successful long-term treatments to date. Fibroblast growth factor 21 (FGF21) plays a key role in dietary regulation, but FGF21 resistance is prevalent in obesity. The aim of this study was to investigate in obese mice whether weight reduction leads to improved behaviour and whether these behavioural changes are associated with decreased plasma FGF21 levels. After establishing a model for diet-induced obesity, mice were subjected to three different interventions for weight reduction, namely dietary change, treadmill exercise, or time-restricted feeding. In this study, we demonstrated that only the combination of dietary change and treadmill exercise affected all parameters leading to a reduction in weight, fat, and FGF21, as well as less anxious behaviour, higher overall activity, and improved olfactory detection abilities. To investigate the interrelationship between FGF21 and behavioural parameters, feature selection algorithms were applied designating FGF21 and body weight as one of five highly weighted features. In conclusion, we concluded from the complementary methods that FGF21 can be considered as a potential biomarker for improved behaviour in obese mice after weight reduction.

Keywords: FGF21; treadmill; time restricted feeding; machine learning; behaviour; diet-induced obesity; feature selection; high-fat diet

Citation: Power Guerra, N.; Parveen, A.; Bühler, D.; Brauer, D.L.; Müller, L.; Pilz, K.; Witt, M.; Glass, Ä.; Bajorat, R.; Janowitz, D.; et al. Fibroblast Growth Factor 21 as a Potential Biomarker for Improved Locomotion and Olfaction Detection Ability after Weight Reduction in Obese Mice. *Nutrients* **2021**, *13*, 2916. https://doi.org/10.3390/nu13092916

Academic Editor: George Dedoussis

Received: 6 July 2021
Accepted: 20 August 2021
Published: 24 August 2021

1. Introduction

Obesity is reaching a global epidemic scale and is defined as abnormal or excessive body fat accumulation [1]. Already in 1989, Kaplan described the "Deadly Quartet" of abdominal obesity, hypertension, hyperglycemia, and hypertriglyceridemia with accompanying low concentrations high-density lipoprotein cholesterol [2]. A promising candidate for reducing plasma concentrations of cholesterol and triglycerides is Fibroblast Growth Factor (FGF) 21 [3,4]. The hormone FGF21 is associated with fatty acid oxidation, lipolysis, increased energy dissipation, and hence weight reduction [5–7]. Astonishingly, obese humans and mice exhibit exceedingly high levels of circulating FGF21 plasma concentrations when compared to lean patients or wild type mice [8]. This evidence sparks the idea of whether FGF21 can be considered as a biomarker in obesity [9,10].

In obesity, food regulation and energy expenditure are heavily disturbed [1] (Figure 1). Obesity-related low-grade inflammation in adipose tissue is assumed at the origin of the disease, later leading to a neuroinflammation as described in Figure 1 [11,12]. The resulting gliosis is hypothesised to dysregulate endocrine balance in the hypothalamus, and thereby the in hypothalamus–pituitary axis (HPA), leading to altered nutrition intake [12,13]. Since FGF21 is intricately connected to nutritional regulation [14], the inflammation is thought to reduce FGF21 sensitivity [15]. As one consequence, body weight and fat increases, which in turn boosts low-grade inflammation. The inflammatory presence effectively leads to higher FGF21 production and a further imbalance of nutritional regulation, thus closing the vicious circle of obesity. Therefore, the increase in weight and in FGF21 concentration is described as an FGF21-resistance state [15,16].

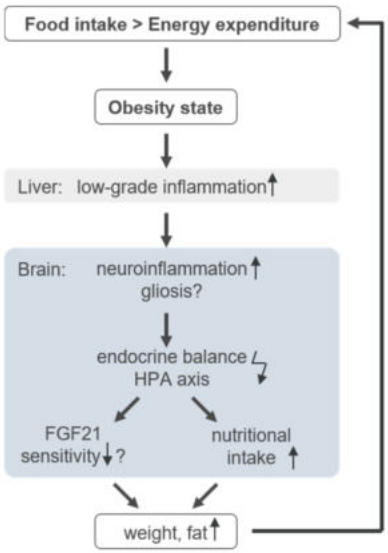

Figure 1. Infographic of the circulus vitiosus of obesity. Detailed information is provided in the text.

In addition, the presence of obesity reveals further impact on cognitional animal behaviour depending on the diet and nutrition model [17]. For example, in an animal model of diet-induced obesity (DIO) and in mice receiving a high-fat diet (HFD), olfactory dysfunctions and anxiety-like behaviour are shown to be favoured, which may lead to reduced activity per se [18,19]. In this context, it is described that obesity in adolescents aggravates physical inactivity and vice versa, which consequently increases the risk of overall and abdominal obesity in adulthood [20]. Thus, to overcome the vicious circle of obesity, intervention approaches such as treadmill exercise, a change in diet or fasting are suitable and common methods to lower FGF21 concentration while increasing FGF21 sensitivity [21–23]. The purpose of the study was to investigate in obese mice whether weight reduction leads to improved behaviour and whether these behavioural changes are associated with altered plasma FGF21 concentrations. We aimed to investigate if FGF21 may be considered in this context as a biomarker for behavioural improvement

after weight reduction. To investigate and evaluate this hypothesis, different analysis tools are on hand. Besides statistical analysis, machine learning (ML) models are able to improve prediction accuracy by discovering relevant features of high complexity [24]. In this study, we determine the weighted features by using three different feature selection (FS) algorithms which eliminate irrelevant or redundant features from the original data set [25]. Accordingly, informative features remain which in turn might indicate their biological significance. However, regarding smaller data sets with mouse studies, the repetition of experiments is low and group size is limited. Therefore, applied models are often prone to biasing issues due to the small sample size [26]. To target the problem at hand, we applied multiple classification models to ensure validation by quantity. The novelty of this study is the combination of the ML method with FS, considered as an additional tool, and statistical methods on a small data set of behavioural parameters to determine whether FGF21 may be a biomarker for weight loss in obese mice.

2. Materials and Methods

2.1. Experimental Design

For the experiments, 90 female C57BL/6J mice aged 4 weeks were purchased from Charles River (Sulzfeld, Germany). Mice were kept in standard cages with 5 animals per cage, in a temperature-controlled room (21 ± 3 °C) with a 12/12 h day-night cycle (lights on from 06:00 a.m. to 06:00 p.m.). Randomisation was not performed at this step as mice were purchased and equally handled. To establish the model of DIO, all 90 mice initially received a high-fat diet (HFD; D12492; Research Diets, Lane, USA) for 6 months. For the intervention in the following 6 months, cages were arbitrarily divided into six groups. The first group (n = 15) remained on HFD, hereinafter referred to as "HFD/HFD". The second group additionally participated in TM exercise (TSE System, Treadmill 303401; n = 15), referred to as "HFD/HFD + TM". The third group was also trained on treadmills and additionally received a time restriction on food (TRF) intake after the first three months of the intervention (n = 15), designated as the group "HFD/HFD + TM + TRF". In the fourth group, HFD was changed to a low-fat diet (LFD; D12450J; Research Diets, Lane, USA) (n = 15) and is hereafter referred to as "HFD/LFD". The fifth group also switched to LFD accompanied by TM exercise (n = 15) and named "HFD/LFD + TM". The last group (n = 15) underwent all three interventions and is designated as the group "HFD/LFD + TM + TRF". Graphical illustration of the experimental design is shown in Figure 2A. During the experiments, each mouse had ad libitum access to fresh water.

2.2. Intervention Parameters

After the establishment of a DIO model in mice, different intervention strategies were performed in order to evaluate their effectiveness.

2.2.1. Diet Change to LFD

Mirroring a healthier food intake, 45 mice changed as a first intervention parameter to an LFD containing 10% fat, 20% protein, and 70% carbohydrates and matching the HFD in structure of lards and protein composition. In contrast, HFD is composed of 60% fat, 20% protein, and 20% carbohydrates [27].

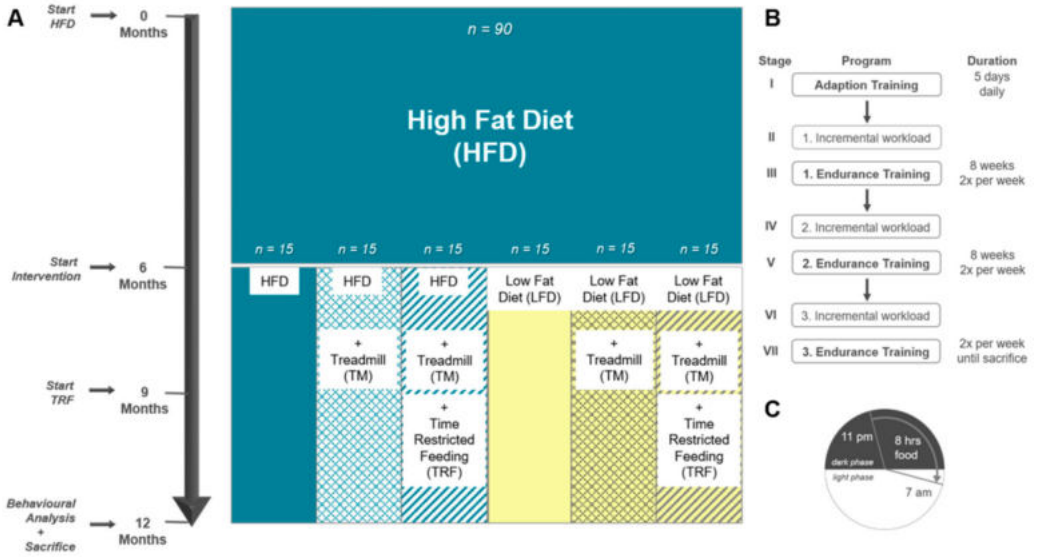

Figure 2. (**A**) Experimental design. A: Female C57BL/6J mice (n = 90) were fed 6 months on high-fat diet (HFD) to establish the model of DIO. Thereafter, mice were divided into 6 groups. The first group remained on HFD (n = 90). Groups two to six underwent an intervention. Second group: HFD plus treadmill exercise (TM; HFD/HFD + TM, n = 15); third group: HFD plus treadmill exercise, and time-restricted feeding (TRF; HFD/HFD + TM + TRF, n = 15); fourth group: diet change to a low-fat diet (LFD; HFD/LFD, n = 15); fifth group: diet change plus treadmill exercise (HFD/LFD + TM, n = 15), and sixth group: diet change, treadmill training and time-restricted feeding (HFD/LFD + TM + TRF, n = 15). When diet change was completed, treadmill training was applied. After 3 months of endurance exercise, time-restricted feeding was introduced. In the end, behaviour experiments were performed, and the mice were sacrificed. (**B**) Treadmill protocol consists of seven stages with three endurance sections. Prior to endurance training, an incremental workload test was performed in order to adjust the maximum velocity of the run. (**C**) Mice in the TRF group were restricted to food from 7 a.m. to 11 p.m. (16 h). Food supply was provided in the nocturnal active phase for 8 h.

2.2.2. TM Exercise

After the dietary change was accomplished, the second intervention parameter, TM exercise, was implemented for n = 60 mice. The protocol was adapted after Marinho et al. (2018) with modifications to mimic human patterns [28]. TM was performed twice a week in groups of five (Figure 2B). The velocity of the treadmill was set according to the speed of the mouse that performed as the slowest.

The treadmill program was composed of seven stages beginning with a five-day training of 10 min/d with a speed of 0.1 m/s and 0° incline in order to adapt to the treadmill. Favouring optimal lipid oxidation rather than carbohydrate combustion, the maximal lactate steady state for each mouse had to be determined [29]. Hereby, mice were subjected in the second stage to an interval training starting with 0.1 m/s and 0° incline. Increments of 0.05 m/s were adjusted every 300 s until voluntary exhaustion of mice. The maximum achieved velocity is defined as the workload, whereas 60% of the workload specified the speed for the endurance training. The incremental load test was performed once prior to endurance training [30]. The third stage provided an eight-week endurance training with two exercise days per week. At the beginning, mice started with 15 min/d and 0° incline endurance training at the previously obtained velocity. The duration increased by 15 min every 2 weeks up to a maximum of 60 min endurance training twice a week. Then, a second incremental load test (fourth stage) was performed to adjust the maximum workload and as a result the endurance speed. With the adjusted velocity a second eight-week endurance training was accomplished (fifth stage) with 60 min exercise twice a week. As the sixth stage, a third incremental load test was conducted followed by an adapted third endurance training. Treadmill exercise was maintained until the sacrifice of mice.

On days with behavioural experiments, no endurance training was performed to avoid any interference for upcoming analyses. Animals were excluded from TM exercise if they either did not accept the acclimatisation phase in the first stage or were no longer willing to perform certain exercises.

2.2.3. TRF

Temporary restriction of food is described as beneficial against obesity and metabolic disorders [21,31]. Therefore, a third intervention parameter, TRF, was applied for $n = 30$ mice after the implementation of the third phase of TM exercise (Figure 2C). The protocol was adapted after Hatori et al. (2012) [21] and maintained for 3 months until the sacrifice of mice. Food access was regulated by using an autofeeder (EHEIM, Deizisau, Germany) whose opening was enlarged. Food drop was set at 11 p.m. and controlled via a webcam with infrared light. At 7 a.m., mice were transferred to fresh cages with water supply, filled autofeeder, and no enrichments. To equalise animal handling to all groups, *ad libitum* fed mice were also transferred daily.

2.3. Behaviour Experiments

2.3.1. Buried Pellet Test (BPT) and Surface Pellet Test (SPT)

As cellular dynamics are modified in the olfactory bulb due to obesity, scent abilities might also be influenced [32]. Therefore, buried and surface pellet tests were conducted after Dragotto et al. (2019) [33] and Lehmkuhl et al. (2014) [34]. Briefly, mice were acclimated to a piece of sweetened pellet (Honey Llama Loops, Kellogg Company, EU) two days prior to testing. After overnight fasting of 9 h to a maximum of 16 h in their home cages, a single mouse was transferred to an ethanol wiped cage with 1 cm embedding. Each mouse was habituated for 1 h alone in a separated room. For the test, a new ethanol wiped cage was filled with 3 cm embedding and the cereal was buried 0.5 cm below the bedding surface next to one corner of the cage. Then, the subject was placed in the cage and latency time to uncover and lick or eat the pellet was measured. If the mouse did not find the pellet within 300 s, a score of 300 s was recorded. The test procedure was repeated on the subsequent day except that the cereal was placed on the surface (SPT). Thereby, motor deterioration and visual clues for finding the pellet were excluded [35].

2.3.2. Elevated plus Maze (EPM)

The EPM is a widely used maze providing information about anxiety-related behaviour in rodents as mice have a natural aversion to open areas [36,37]. After recovery of at least 24 h from the SPT, the EPM protocol was performed after Komada et al. (2008) [38]. The 60-cm-high grey EPM consists of two open arms (6 cm in width, 40 cm in length), and perpendicular to the open arms are two closed arms of the same dimensions with walls of 14.5 cm high. The cross at the centre of the four arms consists of a 6 cm × 6 cm square, where a camera system is positioned 1 m above the maze (Camera CCA1300–60 mg, Basler, and lens 15E, Computar, Japan). Prior to testing, animals were kept at least 1 h in the behaviour room. Then, the subject was placed in the ethanol wiped maze and was recorded for 300 s. Hereafter, the mouse was placed back in the home cage and the maze was cleaned with ethanol for the subsequent animal. All sessions were measured by using EthoVision XT 11.5 software (Nodulus Information Technology). The following parameters were evaluated: cumulative duration in open and closed arms (%), cumulative duration in centre (%), arm entries (%), centre entries (%), total distance in maze (cm), mean velocity (cm/s), and vertical activity by counting and adding manually all leanings, rearing, and jumps. Graphical visualisation was displayed over 300 s by using the EthoVision XT 11.5 software. Red colour reveals highest residence time and blue colour indicates lowest duration. Subsequently, movement patterns of obtained images were manually compared. Visited arm entries were counted and were assigned as follows: centre only, centre + one closed arm entry, centre + two closed arm entries, centre + two closed and one open arm entries, all areas.

2.3.3. Open Field (OF)

In the OF, not only can anxiety-like behaviour be observed, but also locomotor and exploration activity [39,40]. The protocol was performed after Seibenhener et al. (2015) [41]. The OF consists of a 50 cm x 50 cm square with 40 cm high walls whereby the square was divided virtually in the software into 16 small fields. The inner four squares represented the open area and were defined as centre. The remaining fields were specified as outer areas. In accordance with the EPM protocol, equal procedures were performed. The following parameters were evaluated: cumulative duration in centre and outer area (%), field entries (%), total distance in maze (cm), mean velocity (cm/s), and vertical activity by counting manually all rearing and jumps. Between both experiments, mice had a rest of a minimum of 3 h. Heatmap was created in accordance with EPM protocol. Visited area was examined and classified according to the following: only corners, outer area with less crossings, outer area with more crossings, outer area with half of centre visited, all areas visited.

2.4. Weight Control and Euthanasia

Body weight was measured weekly (Kern PCB, Lübeck, Germany) and final body weight was monitored prior to euthanasia. Under anaesthesia (5 vol.% isoflurane; Baxter, Unterschleißheim, Germany) the mice were exsanguinated retrobulbarly and thereby, blood was collected. Thereafter, a laparotomy was performed. The heart was punctured and perfused with 0.9% NaCl (Serag-Wiessner, Naila, Germany) with a flow rate of 2.59 mL/min for 12 min. The visceral and subcutaneous flanked fat deposits were harvested and weighed, and blood plasma was collected.

2.5. FGF21 ELISA of Blood Samples

FGF21 ELISA was performed following manufacturer's description (ab212160, abcam, Berlin, Germany). All plasma samples were diluted 1:5.

2.6. Statistics: Multiple Comparisons of Means

Statistical analysis was performed with GraphPad Prism 8.0.1 (GraphPad Software Inc., San Diego, CA, USA). The data were first checked for normality and lognormality with a Shapiro–Wilk test. In the case of 'vertical activity' in EPM and OF, the data was tested with Kolmogorov–Smirnov test, as observations were manually counted. For lognormal distributed data, the data set was transformed according to the formula $Y = log(Y)$. The ROUT method based on false discovery rate ($Q = 0.01$) was used to identify and remove outliers if possible and necessary.

If the data were normally distributed, One-Way ANOVA was performed. Homogeneity of group variances was checked with Bartlett's test. For homogenous data, an ordinary one-way ANOVA was performed followed by Tukey's post hoc test for multiple comparisons of means. Otherwise, Brown–Forsythe and Welch ANOVA were performed followed by Tamhane's T2 post hoc test for multiple comparisons of means. If the data was not normally distributed, Kruskal-Wallis test with Dunn's post hoc test for multiple comparisons was performed. For the ML models classification report, significance of differences was tested by Wilcoxon Signed Rank Test. Data are presented as mean ± standard deviation (SD) and statistical significance was set at $p < 0.05$. For further details, please see figure legends.

2.7. Data Analysis

2.7.1. Dimensionality Reduction

Analysis of FGF21 concentration, body composition, BPT, EPM, and OF yielded 32 observations with $n = 83$ mice divided into six groups (Figure 3, reduction of $n = 83$ was due to the exclusion criteria and death dropout of mice). Missing values in the data set were filled by calculating a stratified average value depending on y, where y represents the six intervention groups. For each task, data was correspondingly preprocessed and afterwards split into y (intervention groups) as a dependent variable and x (all other data;

Table S1). To correlate all 32 observations, Pearson's correlation was performed where linear relationship between two variables is measured. In the heatmap, plotted red colour (1.00–0.70) indicates a strong positive correlation, blue colour (−0.70–−1.00) reveals a strong negative correlation, whereas light colour above 0.40 or under −0.40 indicates moderate correlation [42]. To reveal the relation between the six intervention groups, Principal Component Analysis (PCA) was conducted. To perform PCA on a dataset where observed entities n were smaller than the observations on variables p ($n < p$), we used a modified PCA implementation in Python with svd_solver = 'arpack' [43].

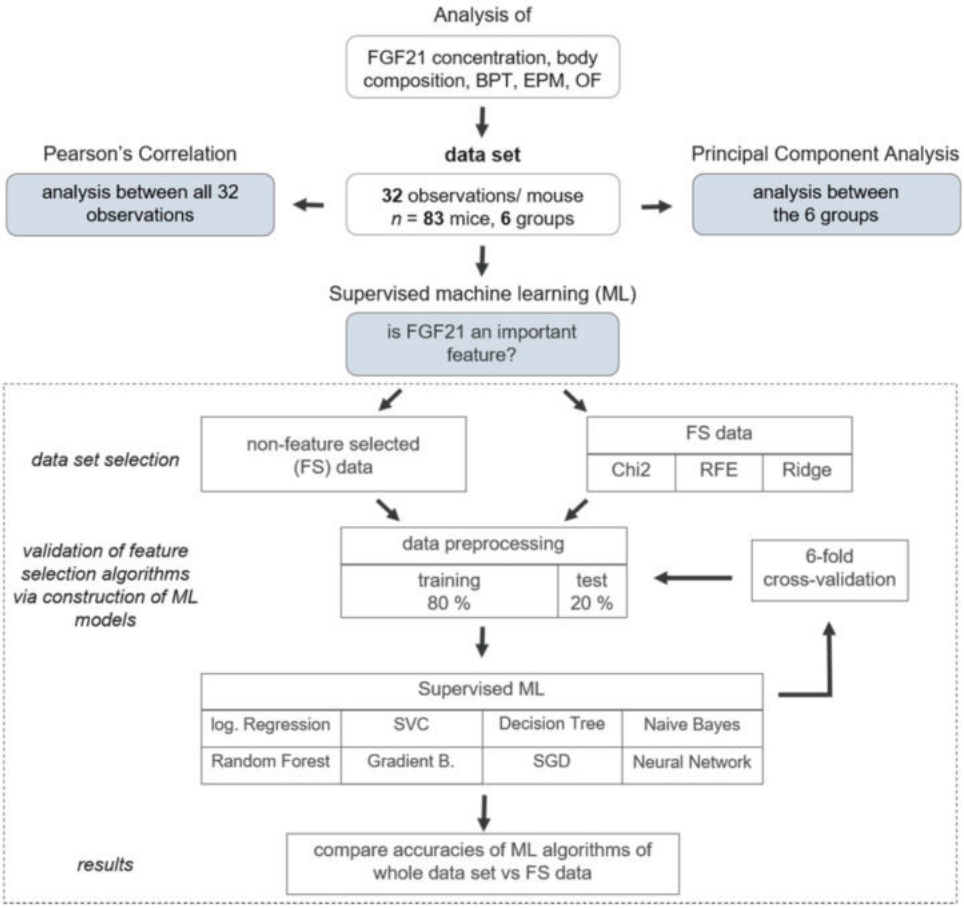

Figure 3. Analysis pipeline for dimensionality reduction and machine learning (ML) approaches. Analysis of Fibroblast Growth Factor (FGF) 21 concentration, body composition, buried pellet test (BPT), elevated plus maze (EPM), and open field (OF) yielded 32 observations with n = 83 mice divided into six groups. To determine pairwise correlations considering all 32 variables, Pearson's Correlation was performed. To reveal new insights and relation between the six intervention groups, Principal Component Analysis (PCA) was conducted. Ultimately, to predict whether FGF21 is an important feature in the data set, three different FS algorithms were applied, namely Chi-Square (Chi2), Ridge Regularisation (RIDGE), and Recursive Feature Elimination (RFE). To assess the viability of the FS algorithms, eight different ML models were constructed-based either on FS common data or non-feature selected data. Therefore, the data set was split into a training (80%) and test (20%) data set. The following supervised ML algorithms were used: Logistic Regression (log. Regression), Support Vector Classifier (SVC), Decision Tree, Naive Bayes, Random Forest, Gradient Boosting (Gradient B.), Stochastic Gradient Descent (SGD), and Neural Network. Each model was additionally verified by 6-fold cross-validation and as a result, accuracies were compared between non-feature selected data set and FS data.

2.7.2. Machine Learning Approach

To predict whether FGF21 is a putative biomarker for improved behaviour after weight reduction, the following procedure was implemented: To address the low sample size, three different FS algorithms were applied for the selection of the putative features, namely Chi-Square (Chi2), Ridge Regularisation (RIDGE), and Recursive Feature Elimination (RFE) for the selection of the putative features [44]. The selected features were visualised in a Venn diagram with InteractiVenn provided by Heberle et al. (2015) [45]. To assess the viability of the FS algorithms, eight different supervised ML models were constructed on both the FS data set (only the selected features) and the original, non-FS data set. To train the models, both data sets were split into training (80%) and test (20%) data sets. Then, eight different supervised ML algorithms were used (Logistic Regression, Support Vector Classifier (SVC), Decision Tree, Naive Bayes, Random Forest, Gradient Boosting (Gradient B.), Stochastic Gradient Descent (SGD), and Neural Network). For further evaluation, each model was verified using 6-fold cross-validation (CV). We opted against 10-fold CV since, on the one hand, we are working with a small data set and, on the other hand, we are considering six different experimental groups as the study design. Ultimately, accuracies (=recall), precision, and F1-scores were compared between the non-FS data set and the FS data set. A high F1-score indicates that a model exhibits low false positives and low false negatives. The full classification report with weighted averages for each model is displayed in Table S2.

2.7.3. Implementation in Python

For the analysis, Python (version 3.8) was used. The full data table and all coding sections were upload on 21 April 2021 and can be accessed under https://github.com/IEC-2020/Intervention, (accessed on 21 April 2021). All methods, libraries and classes used to accomplish this work are summarized in Table 1. Descriptions of all observations are listed in Table S1.

Table 1. List of applied algorithms with their respective implementations in Python.

Task		Library	Class
handling missing values	stratified mean	pandas, numpy	
correlations between all 32 observations	data preprocessing	sklearn.preprocessing	Normalizer
	Pearson's Correlation	scipy.stats.pearsonr	
	visualization	matplotlib.pyplot	
relations between the 6 intervention groups	data preprocessing	sklearn.preprocessing	Normalizer
	PCA	sklearn.decomposition	PCA
	visualization	matplotlib.pyplot	
feature selection	Chi2, data preprocessing	sklearn.preprocessing	MinMaxScaler
	Chi2	sklearn.feature_selection	chi2, SelectKBest
	RFE, data preprocessing	sklearn.data sets	make_friedman1
	RFE	sklearn.feature_selection	RFE
		sklearn.svm	SVR
	RIDGE, data preprocessing	sklearn.linear_model	Ridge
	RIDGE	sklearn.feature_selection	SelectFromModel
machine learning algorithms	data preprocessing	sklearn.preprocessing	Normalizer, StandardScaler
	logistic Regression	sklearn.linear_model	LogisticRegression
	SVC Classifier	sklearn.svm	SVC
	Decision Tree	sklearn.tree	DecisionTreeClassifier
	Naive Bayes	sklearn.naive_bayes	GaussianNB
	Random Forest	sklearn.ensemble	RandomForestClassifier
	Gradient Boosting	sklearn.ensemble	GradientBoostingClassifier
	SGD Classifier	sklearn.linear_model	SGDClassifier
	Neural Network	sklearn.neural_network	MLPClassifier
	cross validation	sklearn.model_selection	StratifiedKFold
	hyperparameter tuning	sklearn.model_selection	GridSearchCV

3. Results

3.1. Effect of LFD and TM Exercise on Body Composition and FGF21

A continuous administration of HFD led to a high increase in body weight within the first 6 months (Figure 4A). After the introduction of intervention parameters such as a diet change to LFD, TM exercise, and TRF, only the dietary adjustment led to weight loss within a few weeks (Figure 3A). Ultimately, body weight and fat weight are about 50% lower when comparing HFD/HFD groups to HFD/LFD groups Figure 4B–D; B: $p \leq 0.0012$ for HFD/HFD groups vs. HFD/LFD groups; C, D: $p < 0.0001$ for HFD/HFD groups vs. HFD/LFD groups, respectively). The same groups are also prominent regarding FGF21 concentration, exhibiting a significant reduction in the HFD/LFD groups (Figure 4E). HFD/LFD + TM revealed the lowest FGF21 plasma concentration with 366.8 ± 281.7 [pg/mL] (Figure 3E; $p < 0.0001$ for HFD/LFD + TM vs. HFD/HFD). Noteworthy, the HFD/HFD + TM + TRF group also displayed a significant reduction in FGF21 concentration compared to the HFD/HFD + TM group (Figure 4E; $p = 0.0053$). This phenomenon, where the combination of HFD with TM and TRF led to a significant change, was not observed in the other surveyed parameters. In conclusion, the transition to LFD exhibited the most significant effects, and the HFD/LFD + TM group was emphasised through the lowest FGF21 plasma levels.

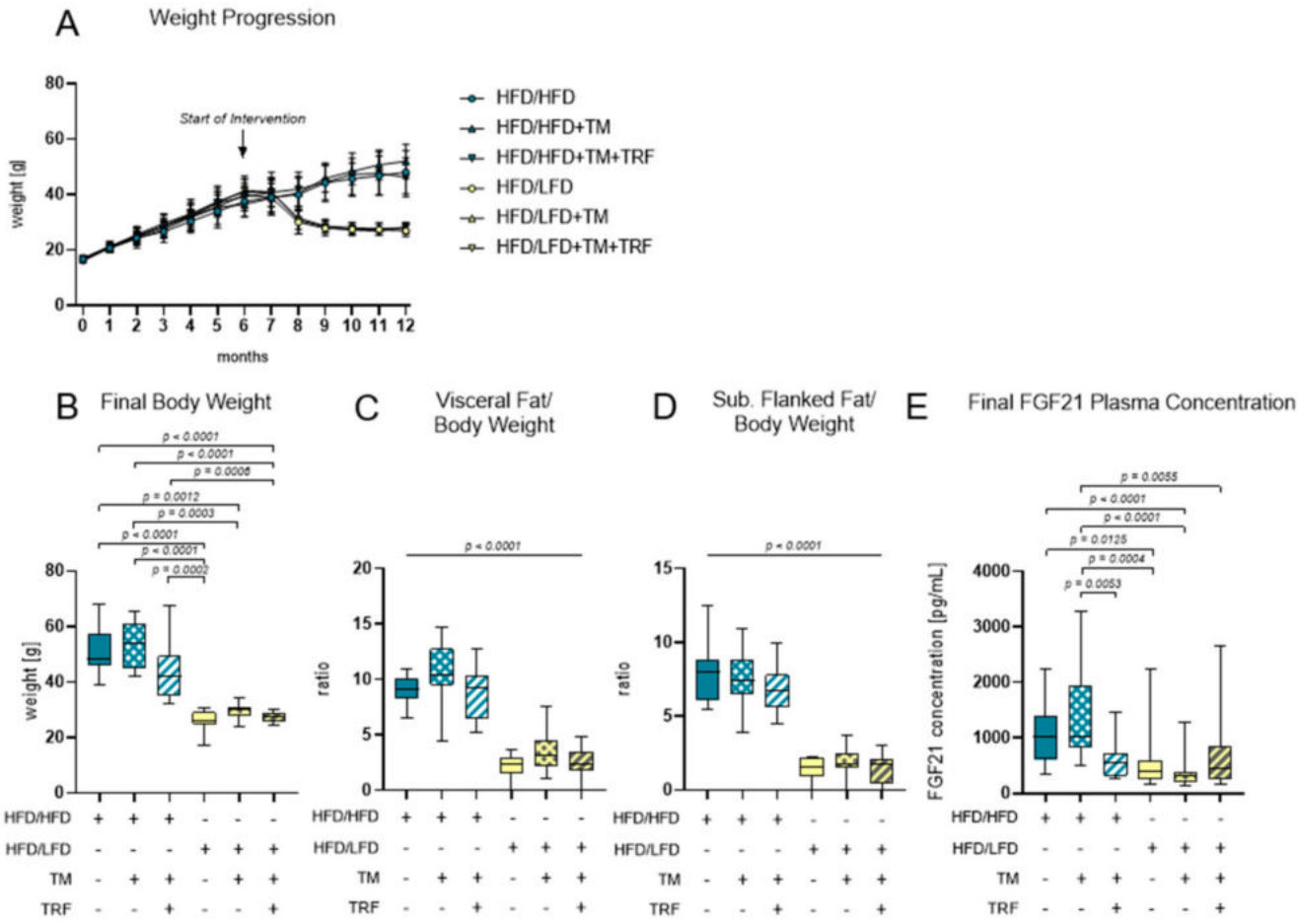

Figure 4. Body composition and FGF21 plasma concentrations. (**A**) Monthly weight progression with $n = 90$ mice at the beginning and $n = 84$ mice at final time point. (**B**) Final body weights [g] before euthanasia (HFD/HFD: $n = 13$, HFD/HFD + TM: $n = 13$, HFD/HFD + TM + TRF: $n = 15$, HFD/LFD: $n = 13$, HFD/LFD + TM: $n = 15$, HFD/LFD + TM + TRF: $n = 13$; total $n = 82$). (**C**) Ratio of visceral body fat deposits to body weight. (**D**) Ratio of subcutaneous flanked fat deposits to body weight. (**C**,**D**) All HFD/LFD groups showed a significant fat loss with $p < 0.0001$ when compared to all 3 HFD/HFD groups,

respectively. (**E**) FGF21 plasma concentration [pg/mL] of final blood sample (HFD/HFD: $n = 13$, HFD/HFD + TM: $n = 13$, HFD/HFD + TM + TRF: $n = 15$, HFD/LFD: $n = 13$, HFD/LFD + TM: $n = 15$, HFD/LFD + TM + TRF: $n = 14$; total $n = 83$). Blue dots and box plots indicate HFD groups, yellow dots and box plots indicate diet change to LFD. The table below the figure displays the individual groups, respectively. Table is read from top to bottom, where '+' denotes a diet or intervention, whereas '-' does not refer to this parameter. Significance of differences between groups was tested with either Kruskal–Wallis test followed by Dunn's post hoc test for multiple comparisons (B), Brown–Forsythe and Welch's ANOVA with Tamhane T2 post hoc test for multiple comparisons (C: F value (F) = 51.52, Degree of Freedom (DF) = 5; D: $F = 66.19$; $DF = 5$) or by ordinary One-Way ANOVA with Tukey's post hoc test for multiple comparisons (E: $F = 9.765$, $DF = 5$). Data are presented as mean ± SD and statistical significance was set at $p < 0.05$. Abbreviations: HFD: high-fat diet, LFD: low-fat diet, TM: treadmill, TRF: time-restricted feeding, FGF21: Fibroblast Growth Factor 21.

3.2. The Combination of LFD and TM Exercise Improves Behavioural Parameters

The combination of diet change to LFD and TM exercise also exhibited the highest effect in all three behavioural experiments, namely, EPM, OF, and BPT. In the EPM, activity was measured by recording the total distance travelled in the maze, the vertical activity of mice, the mean velocity while exploring the maze, the immobility of mice, the presence of mice in the maze and entries of every arm (Figure 5A–G). The HFD/HFD group showed reduced overall activity with the lowest mobility pattern and most time spent in closed arms (Figure 5A,E,F). Contrarily, HFD/LFD + TM reveals the highest activity with less immobility time and more presence in open arms (Figure 5A,E,F; immobility (E): $p = 0.0010$ vs. HFD/HFD, cumulative duration (F): $p \leq 0.0039$ vs. HFD/HFD). These findings suggest less anxiety-related behaviour in the HFD/LFD + TM group with overall increased activity. In the OF, the same behavioural parameters were exhibited as in EPM, whereas the closed arm is represented as the outer area and the open arm as the centre (Figure 6A–G). HFD/LFD + TM revealed the highest mean velocity and the lowest immobility pattern when compared to all other groups underpinning an increased activity pattern (Figure 6D,E; mean velocity (D): $p \leq 0.0022$ vs. all groups; immobility (E): $p \leq 0.0045$ vs. all groups). Correspondingly, in the BPT the same group became prominent (Figure 7A). In three groups, namely HFD/LFD, HFD/LFD + TM and HFD/HFD + TM + TRF, 75% of the mice finished the experiment within 67 s. Interestingly, the parameter "food restriction" led to a significant improvement of smell abilities in the HFD/HFD + TM + TRF group ($p = 0.0039$ vs. HFD/HFD + TM) but not in combination with LFD. Notably, every group had mice that did not find the pellet in the required time. In addition, the HFD/HFD + TM group showed difficulties in finding the pellet resulting in the highest latency times (Figure 6B).

3.3. HFD/LFD and HFD/LFD + TM Are the Most Prominent Intervention Groups

To further assess the relation between the obtained data, two different statistical methods were applied. As a first approach, Pearson's correlation was applied pairwise between all 32 observations from all experiments and is represented as a heatmap (Figure 8). Several strong positive (0.7–1) and negative correlations (−1–−0.7) are observed among certain parameters, such as body weight (1) to fat weight (rows 2,3), and finding the pellet in the BPT (row 5) to latency to lick or eat the pellet in the BPT (row 6), and vice versa. In a biological context, these correlations are causal; since body weight is manipulated by an HFD, fat deposits will also be affected. There is also causality between finding the pellet in the BPT and decreased time to eat or lick the pellet. Interestingly, strong negative correlations are revealed between FGF21 concentration (0) vs. mean velocity (row 28, OF) or distance moved in the OF (row 29). The observation implies if FGF21 concentration is increased, the velocity and distance travelled are minimised and vice versa. This plot demonstrates a variety of strong positive and negative correlations in a reasonably clear diagram highlighting parameters such as FGF21 concentration, body weight, mean velocity, and distance moved in mazes.

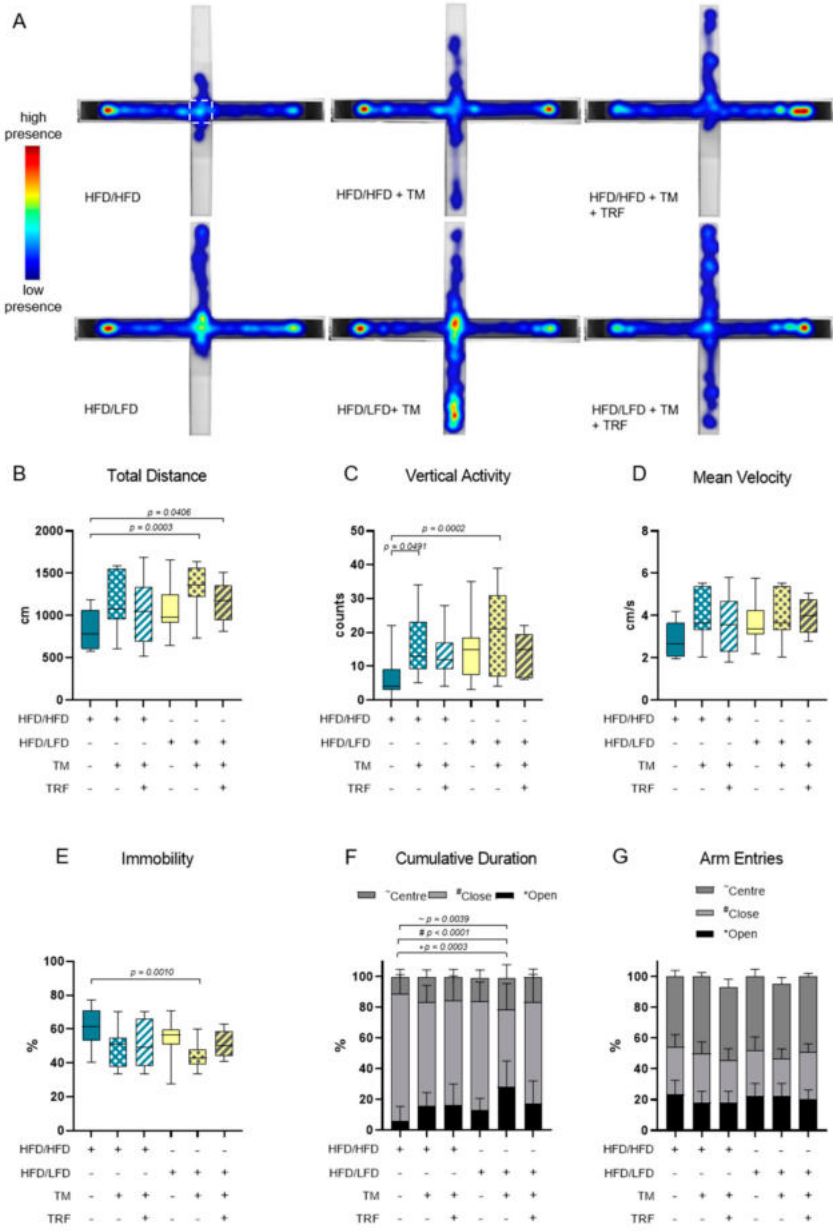

Figure 5. Elevated Plus Maze (EPM) analysis. The combination of a diet change and treadmill exercise leads to less anxiety-related behaviour. (**A**) Heatmap presentation of animal presence in the maze over 300 s whereas red colour reveals the highest residence and blue colour the lowest duration. The number of mice which exhibited the shown pattern amounted to: HFD/HFD: $n = 7/13$, HFD/HFD + TM: $n = 5/13$, HFD/HFD + TM + TRF: $n = 7/15$, HFD/LFD: $n = 7/13$, HFD/LFD + TM: $n = 12/15$, HFD/LFD + TM + TRF: $n = 8/13$, total $n = 82$. White dashed line indicates the centre. Boxplots indicate (**B**) total distance [cm] moved over 300 s, (**C**) vertical activity [counts] by manual counting of rearing, leanings and jumps, (**D**) mean velocity [cm/s] calculated from distance moved in maze over 300 s and (**E**) immobility pattern represented in [%]. (**F**,**G**) Column bars show cumulative duration [%] and arm entries [%] in centre (dark grey ~), in closed arm (light grey #) or in open arm (black *), respectively. Significance of differences were tested by Kruskal–Wallis with Dunn's post hoc test for multiple comparisons (F, G~) or by ordinary one-way ANOVA with Tukey's post hoc test for multiple comparisons (B: F = 2.043, DF = 5; C: F = 4.504, DF = 5; D: F = 2.149, DF = 5, E: F = 3931, DF = 5; G*: F = 2.043, DF = 5; G#: F = 2.006, DF = 5). Data are presented as mean ± SD and statistical significance was set at $p < 0.05$. Abbreviations: HFD: high-fat diet, LFD: low-fat diet, TM: treadmill, TRF: time-restricted feeding.

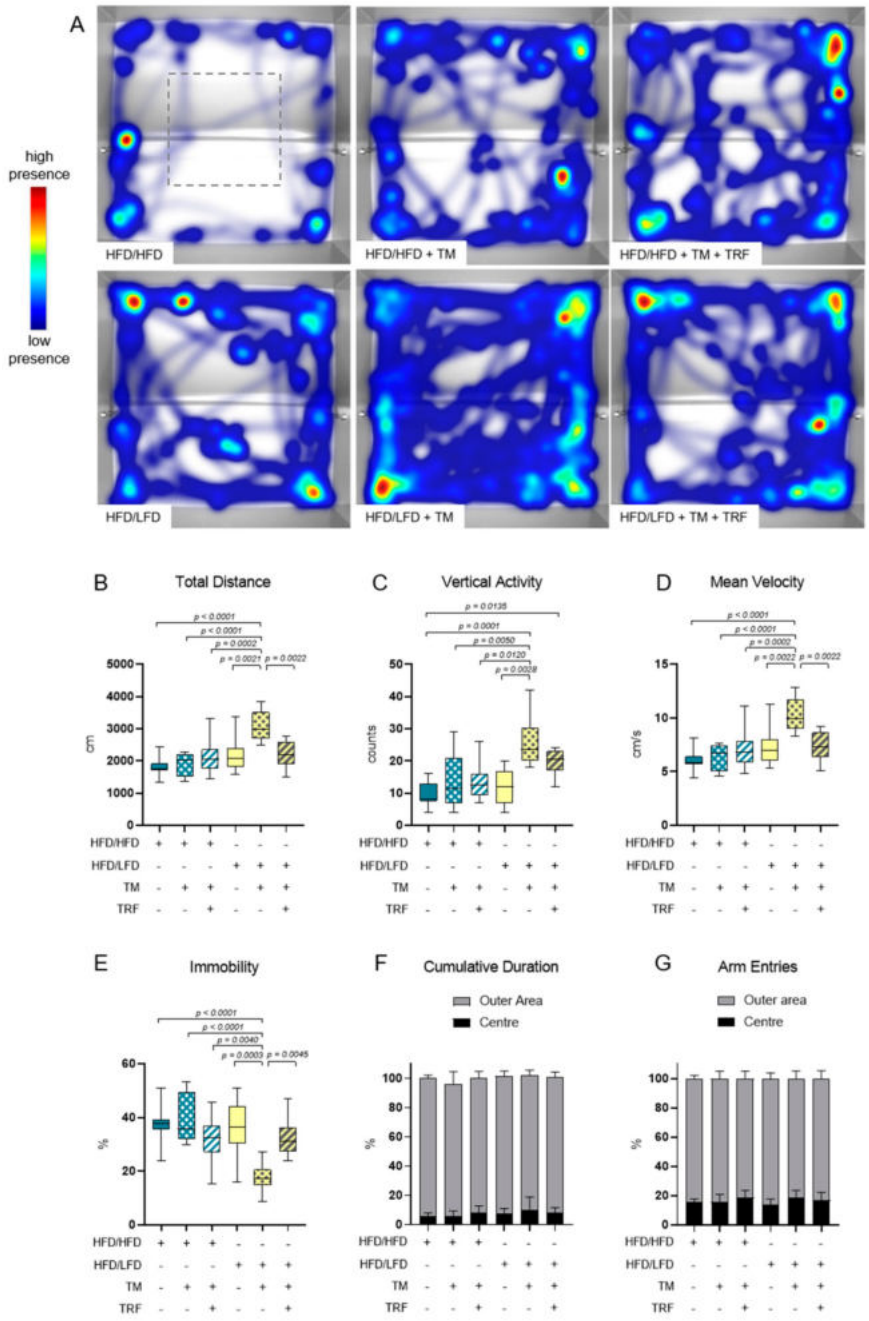

Figure 6. Open Field (OF) analysis. The combination of a diet change and treadmill exercise leads to more locomotor activity. (**A**) Heatmap presentation of animal presence in maze over 300 s whereas red colour reveals highest residence and blue colour lowest duration. The number of mice that exhibited the shown pattern amounted to: HFD/HFD: $n = 5/9$, HFD/HFD + TM: $n = 3/8$, HFD/HFD + TM + TRF: $n = 5/10$, HFD/LFD: $n = 3/8$, HFD/LFD + TM: $n = 5/10$, HFD/LFD + TM + TRF: $n = 4/9$; total $n = 54$. Grey dashed line indicates the centre. Boxplots indicate (**B**) total distance [cm] moved over 300 s, (**C**) vertical activity [counts] by manual counting of rearing, leanings and jumps, (**D**) mean velocity [cm/s] calculated from distance moved in maze over 300 s and (**E**) immobility pattern represented in [%]. (**F**,**G**) Column bars show cumulative duration [%] and arm entries [%] in the outer area (light grey) and the centre (black), respectively. Significance of differences were tested by Kruskal–Wallis with Dunn's post hoc test for multiple comparisons (F) or by ordinary one-way ANOVA with Tukey post hoc test for multiple comparisons (B: F = 9.756, DF = 5; C: F = 7056, DF = 5; D: F = 9.710, DF = 5; E: F = 8.886, DF = 5; G: F = 1.420, DF = 5). Data are presented as mean ± SD and statistical significance was set at $p < 0.05$. Abbreviations: HFD: high-fat diet, LFD: low-fat diet, TM: treadmill, TRF: time-restricted feeding.

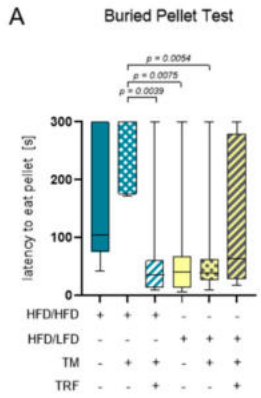

B

	Buried Pellet Test						Surface Pellet Test					
N° found	9	4	13	12	14	10	9	7	12	13	15	13
N° not found	4	9	2	1	1	3	1	6	3	0	0	0
HFD/HFD	+	+	+	-	-	-	+	+	+	-	-	-
HFD/LFD	-	-	-	+	+	+	-	-	-	+	+	+
TM	-	+	+	-	+	+	-	+	+	-	+	+
TRF	-	-	+	-	-	+	-	-	+	-	-	+

Figure 7. Results of the buried pellet test and surface pellet test. (**A**) Impaired sense of smell altered depending on intervention parameters. Boxplots indicate performance of HFD/HFD (n = 13), HFD/HFD + TM (n = 13), HFD/HFD + TM + TRF (n = 15), HFD/LFD (n = 13), HFD/LFD + TM (n = 15) and HFD/LFD + TM + TRF (n = 13). Significance of differences was tested by Kruskal–Wallis with Dunn's post hoc test for multiple comparisons. Data are presented as mean ± SD and statistical significance was set at $p < 0.05$. (**B**) Results of finding and not finding pellets in the buried pellet test and surface pellet test. Abbreviations: HFD: high-fat diet, LFD: low-fat diet, TM: treadmill, TRF: time-restricted feeding.

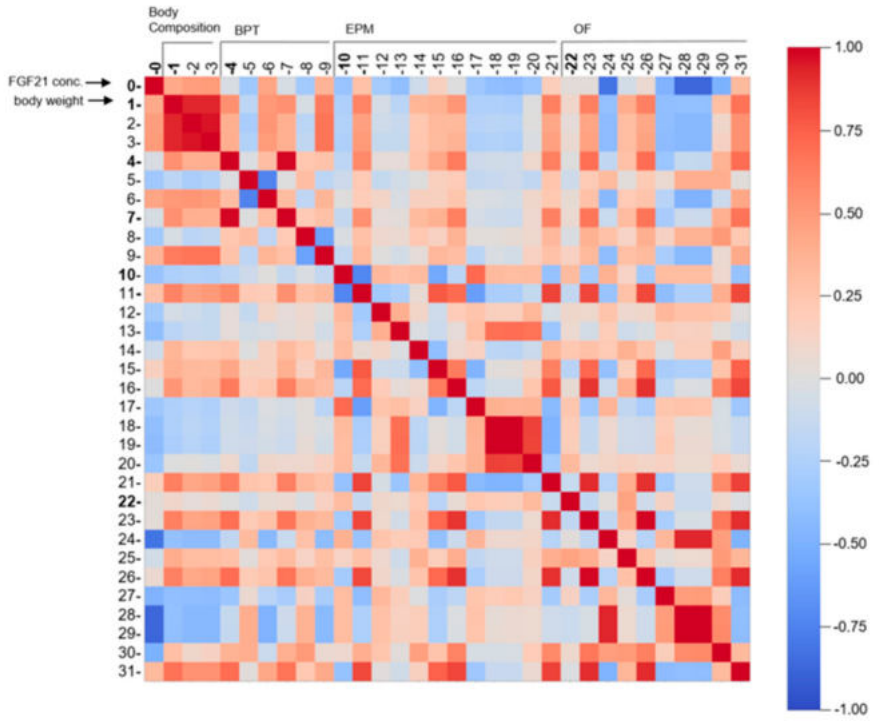

Figure 8. Pearson's correlation represented as a multidimensional heatmap. Pearson's correlation plot visualises the correlation values between all 32 acquired parameters. Scale bar represents the range of the correlation coefficients displayed. Red colour (1.00–0.70) indicates a strong positive correlation, blue colour (−0.70–−1.00) reveals a strong negative correlation, whereas light colour above 0.40 or under −0.40 indicates moderate correlation. Grey colour with coefficient approximately 0 displays no correlation. Numbers correspond to experiments as followed: 0 = FGF21 concentration (n = 82); 1–3 = Values of body composition (n = 80–81); 4–9 = Observations of BPT (n = 81); 10–21 = Observations of EPM (n = 76); 22–31 = Observations of OF (n = 53; see Table S1 for more information). All exact correlation values are displayed in Table S3. Abbreviations: FGF21: Fibroblast Growth factor 21, BPT: buried pellet test, EPM: elevated plus maze, OF: open field.

As a second approach, PCA was performed to find potential clustering between the intervention groups and to reveal new information about similarity (Figure 9). The intervention groups were used to colour the dot plot. Since Principal Component 1 (PC1) accounts for 74.68% of variances, the distance between data points on the *x*-axis represents a larger difference than on the PC2 axis, which accounts for 10.40% of variances. PC scores showing vertical "clusters" exhibit less variance and thus more similarities. The most striking PC scores are from the groups of HFD/LFD + TM (yellow), and partially of HFD/LFD (green) which are located around −0.2 of PC1. The dispersion of the HFD/LFD + TM group is the densest and exhibits a vertical "cluster" indicated by a dotted circle. These findings suggest that the parameters of dietary change to LFD in combination with TM display the greatest similarity to all intervention groups. The importance of the HFD/LFD + TM group is underpinned by behavioural analysis revealing improved performance. Additionally, HFD/LFD and HFD/LFD + TM are assumed to be closer related to each other when compared to the other groups, resulting in a greater impact of these interventions on the data set.

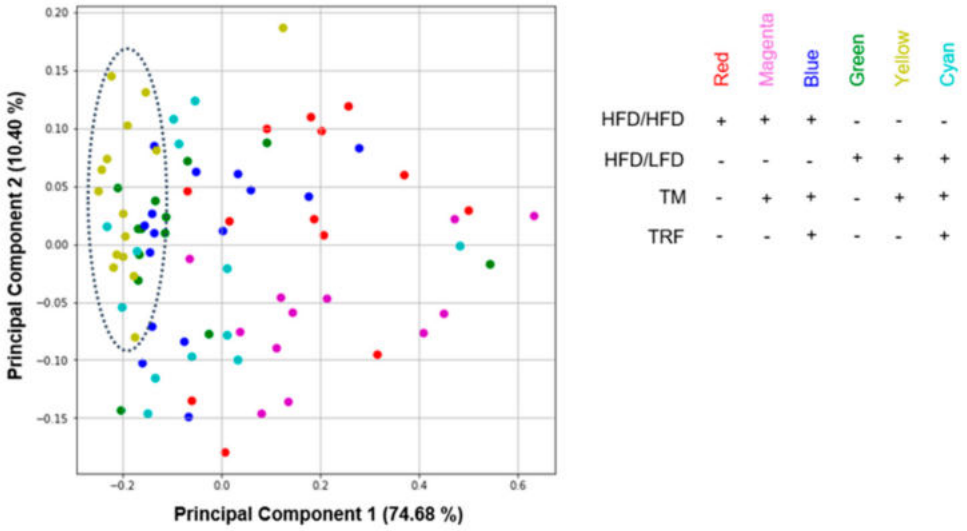

Figure 9. Dot plot of principal component analysis (PCA). All parameters from previously acquired experiments were further used for PCA construction (n = 83 mice with 32 observations, see Table S1 for more information). Components from HFD/LFD + TM (yellow) and in parts from HFD/LFD (green) concentrate more on the left part of the diagram revealing less variance and more similarity (dotted circle). All PCA variables are listed in Table S4. Abbreviations: HFD: high-fat diet, LFD: low-fat diet, TM: treadmill, TRF: time-restricted feeding.

3.4. FGF21, Body Weight, Olfactory Detection, and Mobility Pattern Are Highly Weighted Features

To corroborate the role of FGF21 as a putative biomarker for improved behaviour after weight reduction, a supervised ML approach was used. Three differently operating FS algorithms were applied (Chi2, RFE, and RIDGE) to select key features and to avoid overestimation [44], see Table S5 for all selected features. Afterwards, the selected candidate features were visualised in a Venn diagram yielding eight common features, namely FGF21 concentration, body weight, subcutaneous flanked fat, visceral fat, latency to eat or lick the pellet in the BPT and SPT, vertical activity, and mobility time in the OF (Figure 10A). Since fat deposits correlate strongly with body weight, as shown in the Pearson's correlation, these three features can be reduced to the feature 'body weight', providing a non-invasive parameter to measure. To further restrict the size of the common features, the crucial parameter of the olfactory analysis is the latency time in the BPT, since the SPT does not give any information about olfactory performance, but only about possible motor impairments. Therefore, the final five common features are FGF21 concentration, body weight, latency to eat or lick the pellet in the BPT, vertical activity, and mobility time in the OF.

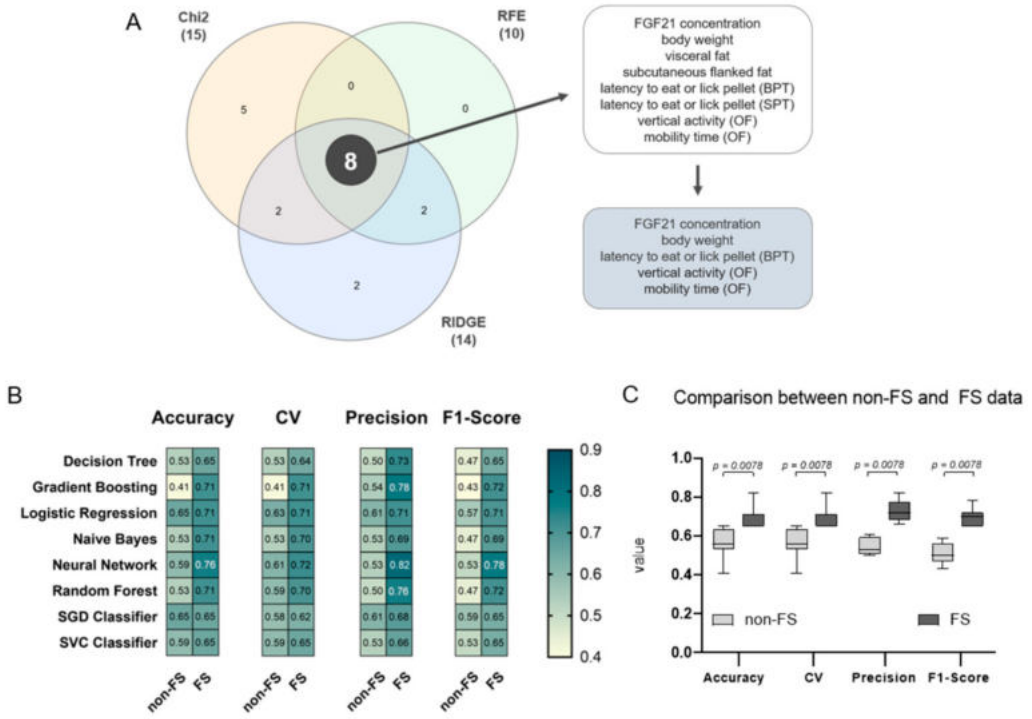

Figure 10. Feature extraction and validation of feature selected (FS) data. (**A**) To extract weighted features of the data set, three different FS algorithms were applied (Chi-Square (Chi2), Recursive feature elimination (RFE), and Ridge regularisation (RIDGE)). Generated features are represented in a Venn diagram revealing eight common features, namely Fibroblast Growth Factor (FGF) 21 concentration, body weight, subcutaneous flanked fat, visceral fat, latency to eat or lick the pellet in the BPT and SPT, vertical activity, and mobility time in the OF. These features can be further restricted in a biological context yielding five features, which are FGF21 concentration, body weight, and latency to eat or lick the pellet in the BPT, vertical activity, and mobility time in the OF. (**B**) Heatmap representation of the classification report for each ML model, namely Decision Tree, Gradient Boosting, Logistic Regression, Naive Bayes, Neural Network, Random Forest, SGD Classifier, and SVC Classifier. Dark petrol blue colour indicates a higher accuracy, mean accuracy in 6-fold cross-validation (CV), precision or F1-score; yellow colour indicates the contrary. For a complete classification report with the best parameters see Table S2. (**C**) Models based on the FS data set (dark grey) scored significantly higher compared to models based on the non-FS data set (light grey) with $p = 0.0078$, respectively. Significance of differences was tested by Wilcoxon Signed Rank Test where theoretical medians (*tm*) were set to the mean of the corresponding non-FS data: *tm* of accuracy = 0.56; *tm* of CV = 0.56; *tm* of precision = 0.54; and *tm* of F1-score = 0.51. Data are presented as mean ± SD and statistical significance was set at $p < 0.05$.

To validate the performance of the FS algorithms, a classification report with accuracy, mean accuracy in 6-fold CV, precision, and F1-scores was calculated for each ML model on both data sets (Figure 10B). ML models based on the eight selected features revealed significantly higher accuracies, CV, precision and F1-scores with $p = 0.0078$ compared to the non-FS, highlighting Neural Network above all (Figure 10C). On the one hand, a lower accuracy implies that most of the ML algorithms are not resulting in a reasonable model. On the other hand, a higher model accuracy indicates that either the feature selected data set is more suitable for the models, or that an overfitting phenomenon emerges. However, it is more likely that the eight common features are the main parameters in the data set and therefore highly weighted. Collectively, these observations support that FGF21, among the other selected features, is a putative biomarker for improved behaviour after weight reduction in the dataset.

4. Discussion

Exercise, dietary adjustments, or time-restricted eating are, to date, the only successful long-term treatments against obesity in humans and mice. The aim is to restore the balance between disturbed energy dissipation and energy intake [20,46]. In this process of energy homeostasis, FGF21 is involved by modulating the metabolism in healthy individuals as well as in obesity and could function as a putative biomarker for improved behaviour after weight reduction in obese mice [10,47]. Additionally, obese individuals displayed altered behaviour regarding physical activity, olfaction, and anxiety [19,20]. The purpose of the study was to assess whether FGF21 is still valid as a biomarker after weight reduction in HFD-mice using behavioural parameters.

We revealed that dietary change to LFD was able to counteract obesity in terms of body weight and fat reduction which is in line with previous studies [48]. Although endurance TM training in multiple studies has been shown to lead to weight reduction [23,49], other studies found no weight reduction [50]. The varying findings may probably result from different treadmill intensities and durations protocols [51]. Thus, in our study, a dietary change to LFD showed a significant impact on weight reduction compared to a moderate TM approach.

The intervention parameter TRF is also reported to reduce body weight and fat mass by coupling food intake to circadian rhythm. Therefore, food consumption is restricted to the active nocturnal phase of the mice and reveals a lasting effect on the metabolic status of the liver [21,52]. However, the study design of our intervention did not incorporate a group which only combined TRF with an HFD or LFD. As a result, we were unable to observe positive effects of TRF in terms of weight reduction. Potentially, the weight reduction in the HFD group with TM and TRF might have been counterbalanced by the muscle gain, as aerobic training led to up to 6% hypertrophy of the quadriceps in humans [53]. Consequently, the weight reduction effects of the additional intervention of TRF were absent.

Nevertheless, TRF exhibited positive effects in combination with HFD and TM regarding FGF21 concentration and weight reduction [54]. One consequence of obesity is FGF21 resistance, which is described by high circulating FGF21 concentrations and greatly increased body weight [16]. We assume, since FGF21 has a circadian rhythm which is disrupted by an HFD, TRF rebalances the oscillation of FGF21 by coupling the food intake in a daytime-dependent manner [21,55]. This potential restoration of rebalance by the TRF regimen was shown by the recovery of an HFD-induced dysregulation of the oestrous cyclicity and FGF21 signalling has been proposed as a key player [56]. Therefore, we speculate that the decrease of FGF21 in the HFD group including TM and TRF might be a hint for the beneficial effect of TRF, as employment of TM alone did not lead to a decrease of circulating FGF21 concentrations. However, physical exercise was shown to reduce FGF21 concentration and was proposed to recover FGF21 sensitivity in obese mice and to rebalance the metabolic interaction between adipose tissue, liver and skeletal muscle [23]. This favourable impact on reducing FGF21 concentration by TM is not observed in our data with TM alone but in combination with a dietary change to LFD.

Furthermore, dietary change to LFD with TM resulted in less anxiety-related behaviour, overall higher activity, and better olfactory abilities when compared to HFD mice. Exercise training was reported to reduce anxiety sensitivity by modulating stressors to the HPA axis [57,58]. Among the stressors is the HFD, which leads to increased FGF21 concentrations as a nutritional response. FGF21 is in turn involved in metabolic stress processes and has been also described as a stressor [14]. It has been proposed that FGF21 could directly influence the hypothalamus and thus stimulate the HPA axis [59]. We suspect that, triggered by an HFD, a stress-induced increase in FGF21 concentration negatively modulates the HPA axis. This modulation is rescued by TM, which is manifested by a reduction in anxiety-related behaviour. Apparently, the positive effect on behaviour is not solely attributable to TM, otherwise, we would have observed this beneficial effect in combination with HFD and TM. Rather, the combination of LFD with TM is decisive; in

other words, the combination of a reduction in nutritional stress—which is accompanied by a reduction in inflammation—and the positive effect resulting from physical activity are the pivotal factors for a promising intervention against behavioural dysfunction in obesity.

Concerning behavioural analysis, we assumed that TRF alone was beneficial [60], but we showed that the combination of dietary change to LFD and TM was also conducive. We also expected at least a similar effect when combining all three intervention strategies, if not even a magnified result. Surprisingly, the positive effect in behavioural analysis achieved by LFD and TM was diminished in combination with TRF, especially in the OF. Our group showed in a previous study that lifelong caloric restriction—a model for combatting obesity in terms of calorie reduction—led to more anxiety-related behaviour in EPM but a significant increase of working memory in female mice [61,62]. Gathering the information, we suspect that TRF is likely to promote anxiety-related behaviour and reversing the beneficial effects of TM in combination with LFD. Nevertheless, TRF introduces a significant modification in olfactory detection ability emphasised in the HFD group with TM and TRF. As HFD causes deterioration of odour recognition, odour discrimination and odour-dependent learning, TRF restores olfactory odour recognition [63]. In this context, an increase of olfactory sensitivity was observed in rats by an intracerebroventricular injection with orexin, an anorexigenic molecule imitating a fasting state [64]. The group with a dietary change to LFD and TM revealed similar olfaction improvements as in the HFD group with TM and TRF, thus also supporting the conclusion of a recovery of olfactory deficits caused by an HFD. Collectively, the increased activity pattern in the OF, the decreased anxiety-related behaviour in the EPM, and the restoration of olfactory recognition suggest that the combination of diet change to LFD and TM represents the most effective intervention against behavioural dysfunctions in obesity.

To further investigate the relationship between the interventions groups, PCA was used as an exploratory tool [43]. The observations of PCA indicated that the group with diet change to LFD with TM showed the fewest internal variance, underscoring the importance of this group. Given that the group which performed only a change to LFD partially forms a "cluster" with the previously described intervention group, there is an indication that dietary change can be considered to be more influential compared to the TRF intervention parameter against obesity. Furthermore, we used PCA as an additional tool to support previous findings, and explicitly not as a stand-alone approach.

Using machine learning methods, we aimed to strengthen the hypothesis of whether FGF21 persists as a putative biomarker for improved behaviour after weight reduction. Indeed, we identified FGF21, body weight, odour detection and the activity pattern in the OF as highly weighted features. For a reliable interpretation of the outcomes, there should be, for example, an association between the decrease in body weight and FGF21 concentration, and vice versa. This can be confirmed by the analysis of body composition in the groups that were switched to a LFD, and is in line with previous studies, although without using the correlation matrix [65]. Regarding the observed correlations, such as that between FGF21 concentration and mean velocity in the OF, these findings have no further consensus, as vertical activity and general mobility time were selected as the putative biomarkers for impaired obesity-related behavioural dysfunction. Thus, the correlation matrix was employed in this study to constrain predicted features and not vice versa. Therefore, we assume that the higher accuracy of the ML models based on the FS dataset corroborates the selected features, mainly FGF21 and body weight, as relevant biomarkers for impaired behaviour. In this context, the results underpin the hypothesis that FGF21 may serve as a putative biomarker for improved behaviour after weight reduction in obese mice.

However, the present study reveals limitations to some extent. The smell detection ability test (BPT) may have a high dropout rate and a high rate of false positive results [66]. Additionally, it was shown that obese-prone rats have an innate deficit with respect to sweet taste detection [67], which may explain the high dropout rates seen in the SPT. As the prediction of highly weighted features also included the latency time, this feature should be interpreted with caution. Another limitation of the study is the impact of the diet

used in this study. The HFD was implemented to trigger inflammatory processes in the periphery [68], as well as in the brain [11]. However, a cafeteria diet more accurately mimics an obese human diet and the associated comorbidities, such as metabolic syndrome, but does not reveal inflammatory processes to the same extent as an HFD [69]. Nevertheless, this study provides potential insights for human studies. Based on the results, we speculate that instead of time-restricted eating, moderate exercise training and especially a change in eating behaviour could be of great interest in reducing body weight and fat. Additionally, further research of FGF21 in brain tissue and meta-analysis of both human and mice studies would provide essential insights into FGF21 interaction as a predictor or biomarker for impaired obesity-related behavioural dysfunction.

5. Conclusions

The variety of methodological approaches in this study leads to a compelling argument, with a recurring emphasis on the core groups and observations. To put the puzzle together, the evidence suggests that (i) the combination of LFD and TM improves body weight, circulating FGF21 concentration and behavioural parameters; (ii) the dietary switch to LFD and LFD with TM are very likely to interrupt the vicious circle of obesity; and (iii) FGF21 can be considered as a potential biomarker for improved behaviour after weight reduction, since an improvement in behaviour is associated with a lower FGF21 concentration. Moreover, collecting analogous, non-invasive parameters in humans would allow to verify whether FGF21 functions as a biomarker for improved locomotion and olfaction detection ability after weight reduction in obese mice.

Supplementary Materials: The following are available online at https://www.mdpi.com/article/10.3390/nu13092916/s1, Table S1: Experimental parameters used for PCA, Multidimensional Heatmap and ML feature selection. Table S2: Classification report of ML algorithms. Table S3 (Excel): Correlation matrix of multidimensional heatmap with correlation values. Table S4 (Excel): PCA values. Table S5: Selected features. Graphical abstract was made with BioRender.com.

Author Contributions: Conceptualisation, A.K. and D.J.; methodology, A.K., N.P.G. and M.W.; software, A.P., D.L.B. and D.B.; validation, A.K., O.W. and N.P.G.; formal analysis, N.P.G., A.P., D.L.B., Ä.G. and D.B.; investigation, N.P.G., L.M., R.B., D.B. and K.P.; resources, B.V.; data curation, N.P.G.; writing—original draft preparation, N.P.G.; writing—review and editing, A.K., B.V., O.W., L.M., M.W., D.L.B. and N.P.G.; visualisation, N.P.G., A.K., A.P. and D.L.B.; supervision, A.K.; project administration, A.K. and N.P.G.; funding acquisition, A.K. and D.J. All authors have read and agreed to the published version of the manuscript.

Funding: This research was funded by the grant from the Deutsche Forschungsgemeinschaft, Bonn, Germany (KU3280/1-2 and JA 2872/1-2).

Institutional Review Board Statement: The study was conducted with the permission of the local Animal Research Committee (Landesamt für Landwirtschaft, Lebensmittelsicherheit und Fischerei (LALLF)) of the state Mecklenburg-Western Pomerania (LALLF M-V/TSD/7221.3-2-001/18) and all animals received humane care according to the EU Directive 2010/63/EU.

Data Availability Statement: Full data table and all coding sections were uploaded on 21 April 2021 and modified on 22 August 2021. https://github.com/IEC-2020/Intervention (accessed on 21 April 2021).

Acknowledgments: We thank Berit Blendow, Mareike Degner, Karin Gerber, Ilona Klamfuß, Chantal von Hörsten, Andrea Wilhelm and Petra Wolff for their excellent technical assistance and animal caring. We also thank Saptarshi Bej, Maximilian Hillemans, and Markus Wolfien for their contribution to the bioinformatical analysis and interpretation.

Conflicts of Interest: The authors declare no conflict of interest.

References

1. WHO. Obesity and Overweight. Available online: https://www.who.int/en/news-room/fact-sheets/detail/obesity-and-overweight (accessed on 19 March 2019).
2. Kaplan, N.M. The Deadly Quartet. *Arch. Intern. Med.* **1989**, *149*, 1514. [CrossRef] [PubMed]
3. Kharitonenkov, A.; Shiyanova, T.L.; Koester, A.; Ford, A.M.; Micanovic, R.; Galbreath, E.J.; Sandusky, G.E.; Hammond, L.J.; Moyers, J.S.; Owens, R.A.; et al. FGF-21 as a novel metabolic regulator. *J. Clin. Invest.* **2005**, *115*, 1627–1635. [CrossRef] [PubMed]
4. Coskun, T.; Bina, H.A.; Schneider, M.A.; Dunbar, J.D.; Hu, C.C.; Chen, Y.; Moller, D.E.; Kharitonenkov, A. Fibroblast growth factor 21 corrects obesity in mice. *Endocrinology* **2008**, *149*, 6018–6027. [CrossRef] [PubMed]
5. Luo, Y.; Ye, S.; Li, X.; Lu, W. Emerging Structure-Function Paradigm of Endocrine FGFs in Metabolic Diseases. *Trends Pharmacol. Sci.* **2019**, *40*, 142–153. [CrossRef]
6. Laeger, T.; Baumeier, C.; Wilhelmi, I.; Würfel, J.; Kamitz, A.; Schürmann, A. FGF21 improves glucose homeostasis in an obese diabetes-prone mouse model independent of body fat changes. *Diabetologia* **2017**, *60*, 2274–2284. [CrossRef] [PubMed]
7. Owen, B.M.; Ding, X.; Morgan, D.A.; Coate, K.C.; Bookout, A.L.; Rahmouni, K.; Kliewer, S.A.; Mangelsdorf, D.J. FGF21 acts centrally to induce sympathetic nerve activity, energy expenditure, and weight loss. *Cell Metab.* **2014**, *20*, 670–677. [CrossRef]
8. Gallego-Escuredo, J.M.; Gómez-Ambrosi, J.; Catalan, V.; Domingo, P.; Giralt, M.; Frühbeck, G.; Villarroya, F. Opposite alterations in FGF21 and FGF19 levels and disturbed expression of the receptor machinery for endocrine FGFs in obese patients. *Int. J. Obes.* **2015**, *39*, 121–129. [CrossRef] [PubMed]
9. Tanajak, P.; Pongkan, W.; Chattipakorn, S.C.; Chattipakorn, N. Increased plasma FGF21 level as an early biomarker for insulin resistance and metabolic disturbance in obese insulin-resistant rats. *Diab. Vasc. Dis. Res.* **2018**, *15*, 263–269. [CrossRef]
10. Lakhani, I.; Gong, M.; Wong, W.T.; Bazoukis, G.; Lampropoulos, K.; Wong, S.H.; Wu, W.K.K.; Wong, M.C.S.; Ong, K.-L.; Liu, T.; et al. Fibroblast growth factor 21 in cardio-metabolic disorders: A systematic review and meta-analysis. *Metabolism* **2018**, *83*, 11–17. [CrossRef]
11. Hotamisligil, G.S. Inflammation, metaflammation and immunometabolic disorders. *Nature* **2017**, *542*, 177–185. [CrossRef] [PubMed]
12. Lumeng, C.N.; Saltiel, A.R. Inflammatory links between obesity and metabolic disease. *J. Clin. Investig.* **2011**, *121*, 2111–2117. [CrossRef] [PubMed]
13. Guillemot-Legris, O.; Muccioli, G.G. Obesity-Induced Neuroinflammation: Beyond the Hypothalamus. *Trends Neurosci.* **2017**, *40*, 237–253. [CrossRef]
14. Martínez-Garza, Ú.; Torres-Oteros, D.; Yarritu-Gallego, A.; Marrero, P.F.; Haro, D.; Relat, J. Fibroblast Growth Factor 21 and the Adaptive Response to Nutritional Challenges. *Int. J. Mol. Sci.* **2019**, *20*, 4692. [CrossRef] [PubMed]
15. Díaz-Delfín, J.; Hondares, E.; Iglesias, R.; Giralt, M.; Caelles, C.; Villarroya, F. TNF-α represses β-Klotho expression and impairs FGF21 action in adipose cells: Involvement of JNK1 in the FGF21 pathway. *Endocrinology* **2012**, *153*, 4238–4245. [CrossRef]
16. Fisher, F.M.; Chui, P.C.; Antonellis, P.J.; Bina, H.A.; Kharitonenkov, A.; Flier, J.S.; Maratos-Flier, E. Obesity is a fibroblast growth factor 21 (FGF21)-resistant state. *Diabetes* **2010**, *59*, 2781–2789. [CrossRef] [PubMed]
17. Elsayed El-Swefy, S.; Husseini Atteia, H. Obesity and Neurodegeneration. In *Diet and Nutrition in Dementia and Cognitive Decline*; Elsevier: Amsterdam, The Netherlands, 2015; pp. 1097–1105.
18. Tomiga, Y.; Yoshimura, S.; Ra, S.-G.; Takahashi, Y.; Goto, R.; Kugimoto, I.; Uehara, Y.; Kawanaka, K.; Higaki, Y. Anxiety-like behaviors and hippocampal nNOS in response to diet-induced obesity combined with exercise. *J. Physiol. Sci.* **2019**, *69*, 711–722. [CrossRef]
19. Takase, K.; Tsuneoka, Y.; Oda, S.; Kuroda, M.; Funato, H. High-fat diet feeding alters olfactory-, social-, and reward-related behaviors of mice independent of obesity. *Obesity* **2016**, *24*, 886–894. [CrossRef] [PubMed]
20. Pietiläinen, K.H.; Kaprio, J.; Borg, P.; Plasqui, G.; Yki-Järvinen, H.; Kujala, U.M.; Rose, R.J.; Westerterp, K.R.; Rissanen, A. Physical inactivity and obesity: A vicious circle. *Obesity* **2008**, *16*, 409–414. [CrossRef]
21. Hatori, M.; Vollmers, C.; Zarrinpar, A.; DiTacchio, L.; Bushong, E.A.; Gill, S.; Leblanc, M.; Chaix, A.; Joens, M.; Fitzpatrick, J.A.; et al. Time-restricted feeding without reducing caloric intake prevents metabolic diseases in mice fed a high-fat diet. *Cell Metab.* **2012**, *15*, 848–860. [CrossRef] [PubMed]
22. Kruse, R.; Vienberg, S.G.; Vind, B.F.; Andersen, B.; Højlund, K. Effects of insulin and exercise training on FGF21, its receptors and target genes in obesity and type 2 diabetes. *Diabetologia* **2017**, *60*, 2042–2051. [CrossRef]
23. Geng, L.; Liao, B.; Jin, L.; Huang, Z.; Triggle, C.R.; Ding, H.; Zhang, J.; Huang, Y.; Lin, Z.; Xu, A. Exercise Alleviates Obesity-Induced Metabolic Dysfunction via Enhancing FGF21 Sensitivity in Adipose Tissues. *Cell Rep.* **2019**, *26*, 2738–2752.e4. [CrossRef]
24. Azodi, C.B.; Tang, J.; Shiu, S.-H. Opening the Black Box: Interpretable Machine Learning for Geneticists. *Trends Genet.* **2020**, *36*, 442–455. [CrossRef]
25. Dernoncourt, D.; Hanczar, B.; Zucker, J.-D. Analysis of feature selection stability on high dimension and small sample data. *Comput. Stat. Data Anal.* **2014**, *71*, 681–693. [CrossRef]
26. Xu, C.; Jackson, S.A. Machine learning and complex biological data. *Genome Biol.* **2019**, *20*, 76. [CrossRef] [PubMed]
27. Ulman, E.A. The "Original" High-Fat Diets for Diet Induced Obesity. Available online: https://www.weizmann.ac.il/vet/sites/vet/files/uploads/diet_d12451_d12492.pdf (accessed on 19 March 2019).

28. Marinho, R.; Munõz, V.R.; Pauli, L.S.; Ropelle, E.C.; de Moura, L.P.; Moraes, J.C.; Moura-Assis, A.; Cintra, D.E.; da Silva, A.S.; Ropelle, E.R.; et al. Endurance training prevents inflammation and apoptosis in hypothalamic neurons of obese mice. *J. Cell. Physiol.* **2018**, *234*, 880–890. [CrossRef] [PubMed]
29. Billat, V.L.; Sirvent, P.; Py, G.; Koralsztein, J.-P.; Mercier, J. The Concept of Maximal Lactate Steady State. *Sports Med.* **2003**, *33*, 407–426. [CrossRef] [PubMed]
30. Ferreira, J.C.B.; Rolim, N.P.L.; Bartholomeu, J.B.; Gobatto, C.A.; Kokubun, E.; Brum, P.C. Maximal lactate steady state in running mice: Effect of exercise training. *Clin. Exp. Pharmacol. Physiol. Suppl.* **2007**, *34*, 760–765. [CrossRef]
31. Chaix, A.; Zarrinpar, A.; Miu, P.; Panda, S. Time-restricted feeding is a preventative and therapeutic intervention against diverse nutritional challenges. *Cell Metab.* **2014**, *20*, 991–1005. [CrossRef]
32. Chelminski, Y.; Magnan, C.; Luquet, S.H.; Everard, A.; Meunier, N.; Gurden, H.; Martin, C. Odor-Induced Neuronal Rhythms in the Olfactory Bulb Are Profoundly Modified in ob/ob Obese Mice. *Front. Physiol.* **2017**, *8*, 2. [CrossRef]
33. Dragotto, J.; Palladino, G.; Canterini, S.; Caporali, P.; Patil, R.; Fiorenza, M.T.; Erickson, R.P. Decreased neural stem cell proliferation and olfaction in mouse models of Niemann-Pick C1 disease and the response to hydroxypropyl-β-cyclodextrin. *J. Appl. Genet.* **2019**, *60*, 357–365. [CrossRef]
34. Lehmkuhl, A.M.; Dirr, E.R.; Fleming, S.M. Olfactory Assays for Mouse Models of Neurodegenerative Disease. *J. Vis. Exp.* **2014**, *90*, e51804. [CrossRef] [PubMed]
35. Meyer, A.; Gläser, A.; Bräuer, A.U.; Wree, A.; Strotmann, J.; Rolfs, A.; Witt, M. Olfactory performance as an indicator for protective treatment effects in an animal model of neurodegeneration. *Front. Integr. Neurosci.* **2018**, *12*, 1–18. [CrossRef] [PubMed]
36. Rodgers, R.J.; Dalvi, A. Anxiety, Defence and the Elevated Plus-maze. PII: S0149-7634(96)00058-9. *Neurosci. Biobehav. Rev.* **1997**, *21*, 801–810. [CrossRef]
37. Lister, R.G. The use of a plus-maze to measure anxiety in the mouse. *Psychopharmacology* **1987**, *92*, 180–185. [CrossRef]
38. Komada, M.; Keizo, T.; Miyakawa, T. Elevated plus maze for mice. *J. Vis. Exp.* **2008**, *22*, 1088. [CrossRef]
39. Walsh, R.N.; Cummins, R.A. The Open-Field Test: A critical review. *Psychol. Bull.* **1976**, *83*, 482–504. [CrossRef]
40. Inglis, A.; Shibin, S.; Ubungen, R.; Farooq, S.; Mata, P.; Thiam, J.; Al-Mohanna, F.A.; Collison, K.S. Strain and sex-based glucocentric & behavioral differences between KK/HlJ and C57BL/6J mice. *Physiol. Behav.* **2019**, *210*, 112646. [CrossRef]
41. Seibenhener, M.L.; Wooten, M.C. Use of the Open Field Maze to Measure Locomotor and Anxiety-like Behavior in Mice. *J. Vis. Exp.* **2015**, *96*, e52434. [CrossRef]
42. Akoglu, H. User's guide to correlation coefficients. *Turk. J. Emerg. Med.* **2018**, *18*, 91–93. [CrossRef]
43. Jolliffe, I.T.; Cadima, J. Principal component analysis: A review and recent developments. *Philos. Trans. A Math. Phys. Eng. Sci.* **2016**, *374*, 20150202. [CrossRef]
44. Belanche, L.A.; González, F.F. Review and Evaluation of Feature Selection Algorithms in Synthetic Problems. *arXiv* **2011**, arXiv:1101.2320.
45. Heberle, H.; Meirelles, G.V.; da Silva, F.R.; Telles, G.P.; Minghim, R. InteractiVenn: A web-based tool for the analysis of sets through Venn diagrams. *BMC Bioinform.* **2015**, *16*, 169. [CrossRef] [PubMed]
46. Wilkinson, M.J.; Manoogian, E.N.C.; Zadourian, A.; Lo, H.; Fakhouri, S.; Shoghi, A.; Wang, X.; Fleischer, J.G.; Navlakha, S.; Panda, S.; et al. Ten-Hour Time-Restricted Eating Reduces Weight, Blood Pressure, and Atherogenic Lipids in Patients with Metabolic Syndrome. *Cell Metab.* **2020**, *31*, 92–104.e5. [CrossRef]
47. Tezze, C.; Romanello, V.; Sandri, M. FGF21 as Modulator of Metabolism in Health and Disease. *Front. Physiol.* **2019**, *10*, 419. [CrossRef] [PubMed]
48. Astrup, A. The role of dietary fat in the prevention and treatment of obesity. Efficacy and safety of low-fat diets. *Int. J. Obes. Relat. Metab. Disord.* **2001**, *25* (Suppl. S1), S46–S50. [CrossRef] [PubMed]
49. Laing, B.T.; Do, K.; Matsubara, T.; Wert, D.W.; Avery, M.J.; Langdon, E.M.; Zheng, D.; Huang, H. Voluntary exercise improves hypothalamic and metabolic function in obese mice. *J. Endocrinol.* **2016**, *229*, 109–122. [CrossRef]
50. Ringseis, R.; Mooren, F.-C.; Keller, J.; Couturier, A.; Wen, G.; Hirche, F.; Stangl, G.I.; Eder, K.; Krüger, K. Regular endurance exercise improves the diminished hepatic carnitine status in mice fed a high-fat diet. *Mol. Nutr. Food Res.* **2011**, *55* (Suppl. S2), S193–S202. [CrossRef] [PubMed]
51. Poole, D.C.; Copp, S.W.; Colburn, T.D.; Craig, J.C.; Allen, D.L.; Sturek, M.; O'Leary, D.S.; Zucker, I.H.; Musch, T.I. Guidelines for animal exercise and training protocols for cardiovascular studies. *Am. J. Physiol. Heart Circ. Physiol.* **2020**, *318*, H1100–H1138. [CrossRef]
52. Regmi, P.; Heilbronn, L.K. Time-Restricted Eating: Benefits, Mechanisms, and Challenges in Translation. *iScience* **2020**, *23*, 101161. [CrossRef]
53. Harber, M.P.; Konopka, A.R.; Undem, M.K.; Hinkley, J.M.; Minchev, K.; Kaminsky, L.A.; Trappe, T.A.; Trappe, S. Aerobic exercise training induces skeletal muscle hypertrophy and age-dependent adaptations in myofiber function in young and older men. *J. Appl. Physiol.* **2012**, *113*, 1495–1504. [CrossRef]
54. Chaix, A.; Lin, T.; Le, H.D.; Chang, M.W.; Panda, S. Time-Restricted Feeding Prevents Obesity and Metabolic Syndrome in Mice Lacking a Circadian Clock. *Cell Metab.* **2019**, *29*, 303–319.e4. [CrossRef] [PubMed]
55. Chapnik, N.; Genzer, Y.; Froy, O. Relationship between FGF21 and UCP1 levels under time-restricted feeding and high-fat diet. *J. Nutr. Biochem.* **2017**, *40*, 116–121. [CrossRef] [PubMed]

56. Hua, L.; Feng, B.; Huang, L.; Li, J.; Luo, T.; Jiang, X.; Han, X.; Che, L.; Xu, S.; Lin, Y.; et al. Time-restricted feeding improves the reproductive function of female mice via liver fibroblast growth factor 21. *Clin. Transl. Med.* **2020**, *10*, e195. [CrossRef] [PubMed]
57. Anderson, E.; Shivakumar, G. Effects of exercise and physical activity on anxiety. *Front. Psychiatry* **2013**, *4*, 27. [CrossRef] [PubMed]
58. Droste, S.K.; Gesing, A.; Ulbricht, S.; Müller, M.B.; Linthorst, A.C.E.; Reul, J.M.H.M. Effects of long-term voluntary exercise on the mouse hypothalamic-pituitary-adrenocortical axis. *Endocrinology* **2003**, *144*, 3012–3023. [CrossRef]
59. Hui, X.; Feng, T.; Liu, Q.; Gao, Y.; Xu, A. The FGF21-adiponectin axis in controlling energy and vascular homeostasis. *J. Mol. Cell Biol.* **2016**, *8*, 110–119. [CrossRef]
60. Guerrero-Vargas, N.N.; Zárate-Mozo, C.; Guzmán-Ruiz, M.A.; Cárdenas-Rivera, A.; Escobar, C. Time-restricted feeding prevents depressive-like and anxiety-like behaviors in male rats exposed to an experimental model of shift-work. *J. Neurosci. Res.* **2020**, *99*, 604–620. [CrossRef]
61. Smith, N.J.; Caldwell, J.L.; van der Merwe, M.; Sharma, S.; Butawan, M.; Puppa, M.; Bloomer, R.J. A Comparison of Dietary and Caloric Restriction Models on Body Composition, Physical Performance, and Metabolic Health in Young Mice. *Nutrients* **2019**, *11*, 350. [CrossRef]
62. Kuhla, A.; Lange, S.; Holzmann, C.; Maass, F.; Petersen, J.; Vollmar, B.; Wree, A. Lifelong caloric restriction increases working memory in mice. *PLoS ONE* **2013**, *8*, e68778. [CrossRef]
63. Lietzau, G.; Nyström, T.; Wang, Z.; Darsalia, V.; Patrone, C. Western Diet Accelerates the Impairment of Odor-Related Learning and Olfactory Memory in the Mouse. *ACS Chem. Neurosci.* **2020**, *11*, 3590–3602. [CrossRef]
64. Julliard, A.K.; Chaput, M.A.; Apelbaum, A.; Aimé, P.; Mahfouz, M.; Duchamp-Viret, P. Changes in rat olfactory detection performance induced by orexin and leptin mimicking fasting and satiation. *Behav. Brain Res.* **2007**, *183*, 123–129. [CrossRef]
65. Zhang, X.; Yeung, D.C.Y.; Karpisek, M.; Stejskal, D.; Zhou, Z.-G.; Liu, F.; Wong, R.L.C.; Chow, W.-S.; Tso, A.W.K.; Lam, K.S.L.; et al. Serum FGF21 levels are increased in obesity and are independently associated with the metabolic syndrome in humans. *Diabetes* **2008**, *57*, 1246–1253. [CrossRef] [PubMed]
66. Yang, M.; Crawley, J.N. Simple behavioral assessment of mouse olfaction. *Curr. Protoc. Neurosci.* **2009**, *48*, 8–24. [CrossRef] [PubMed]
67. Duca, F.A.; Swartz, T.D.; Covasa, M. Effect of diet on preference and intake of sucrose in obese prone and resistant rats. *PLoS ONE* **2014**, *9*, e111232. [CrossRef] [PubMed]
68. Power Guerra, N.; Müller, L.; Pilz, K.; Glatzel, A.; Jenderny, D.; Janowitz, D.; Vollmar, B.; Kuhla, A. Dietary-Induced Low-Grade Inflammation in the Liver. *Biomedicines* **2020**, *8*, 587. [CrossRef] [PubMed]
69. Lang, P.; Hasselwander, S.; Li, H.; Xia, N. Effects of different diets used in diet-induced obesity models on insulin resistance and vascular dysfunction in C57BL/6 mice. *Sci. Rep.* **2019**, *9*, 19556. [CrossRef]